UNIVERSITAT POLITÈCNICA DE VALÈNCIA

PROGRAMA DE DOCTORADO EN DISEÑO, FABRICACIÓN Y GESTIÓN DE PROYECTOS INDUSTRIALES

PROPUESTA DE INCLUSIÓN DE ESFUERZOS EN EL CONTROL DE UN BRAZO ROBOT PARA ASEGURAR EL CUMPLIMIENTO DE LA RUGOSIDAD SUPERFICIAL DURANTE OPERACIONES DE LIJADO EN DIFERENTES MATERIALES

TESIS DOCTORAL PRESENTADA POR
Rodrigo Alonso Pérez Ubeda

DIRECTORES
Dr. Santiago C. Gutiérrez Rubert
Dr. Ranko Zotovic Stanisic

Valencia, febrero de 2022

"Nunca consideres el estudio como una obligación, sino como una oportunidad para penetrar en el bello y maravilloso mundo del saber"

Albert Einstein

Non nobis, Domine, non nobis. Sed Nomine Tuo da Gloriam

Agradecimientos

En primer lugar, quiero agradecer a Dios por permitirme lograr todos mis sueños.

A mi esposa Andrea por su paciencia, consejos y amor incondicional, dándome fuerzas para seguir adelante y por acompañarme en esta aventura.

A mi familia por el gran apoyo entregado desde la lejanía, en especial a mis padres y hermana por su preocupación, apoyo, consejos y amor.

Agradezco de forma especial a mis profesores directores, Dr. Santiago Gutiérrez Rubert y Dr. Ranko Zotovic Stanisic, por su apoyo, orientación y dedicación entregada para el desarrollo de esta tesis. Su ayuda y consejos permitieron que llegara al final de este proceso.

Agradezco a todos mis compañeros de universidad, con los cuales pase momentos muy gratos de estudio y ocio, en especial a Sergio Benavent y Cesar Ayabaca.

A todos los amigos que conocí mientras vivía en València, tanto españoles como chilenos, les agradezco su compañía y buenos momentos.

Además, quiero agradecer a la institución, sus académicos y técnicos por haberme brindado todos los conocimientos y ayuda para este perfeccionamiento profesional.

Por último, agradezco a la Universidad de Antofagasta y a la Agencia Nacional de Investigación y Desarrollo de Chile por el otorgamiento de una beca de estudios en el extranjero, la cual me permitió realizar estos estudios de doctorado.

Amunt València!

Resumen

El mecanizado con brazos robots ha sido estudiado aproximadamente desde los años 90, durante este tiempo se han llevado a cabo importantes avances y descubrimientos en cuanto a su campo de aplicación. En general, los robots manipuladores tienen muchos beneficios y ventajas al ser usados en operaciones de mecanizado, tales como, flexibilidad, gran área de trabajo y facilidad de programación, entre otras, frente a las Máquinas Herramientas de Control numérico (MHCN) que necesitan de una gran inversión para trabajar piezas muy grandes o incrementar sus grados de libertad. Como desventajas, frente a las MHCN, los brazos robóticos poseen menor rigidez, lo que combinado con las altas fuerzas producidas en los procesos de mecanizado hace que aparezcan errores de precisión, desviaciones en las trayectorias, vibraciones y, por consiguiente, una mala calidad en las piezas fabricadas. Entre los brazos robots, los brazos colaborativos están en auge debido a su programación intuitiva y a sus medidas de seguridad, que les permiten trabajar en el mismo espacio que los operadores sin que estos corran riesgos. Como desventaja añadida de los robots colaborativos se encuentra la mayor flexibilidad que estos tienen en sus articulaciones, debido a que incluyen reductores del tipo Harmonic drive. El uso de un control de fuerza en procesos de mecanizado con brazos robots permite controlar y corregir en tiempo real las desviaciones generadas por la flexibilidad en las articulaciones del robot. Utilizar este método de control es beneficioso en cualquier brazo robot; sin embargo, el control interno que incluyen los robots colaborativos presenta ventajas que permiten que el control de fuerza pueda ser aplicado de una manera más eficiente. En el presente trabajo se desarrolla una propuesta real para la inclusión del control de esfuerzos en el brazo robot, así como también, se evalúa y cuantifica la capacidad de los robots industriales y colaborativos en tareas de mecanizado. La propuesta plantea cómo mejorar la utilización de un control de fuerza por bucle interior/exterior aplicado en un brazo colaborativo cuando se desconocen los pares reales de los motores del robot, así como otros parámetros internos que los fabricantes no dan a conocer. Este bucle de control interior/exterior ha sido utilizado en aplicaciones de pulido y lijado sobre diferentes materiales. Los resultados indican que el robot colaborativo es factible para realizar tales operaciones de mecanizado. Sus mejores resultados se obtienen cuando se utiliza un bucle de control interno por velocidad y un bucle de control externo de fuerza con algoritmos, Proporcional-Integral-Derivativo o Proporcional más Pre-Alimentación de la Fuerza.

Abstract

Machining with robot arms has been studied approximately since the 90s; during this time, important advances and discoveries have been made in its field of application. In general, manipulative robots have many benefits and advantages when they are used in machining operations, such as flexibility, large work area, and ease of programming, among others, compared to Numerical Control Machine Tools (NCMT) that need a great investment to work very large pieces or increase their degrees of freedom. As for disadvantages, compared to NCMT, robotic arms have lower rigidity, which, combined with the high forces produced in machining processes, causes precision errors, path deviations, vibrations, and, consequently, poor quality in the manufactured parts. Among robot arms, collaborative arms are on the rise due to their intuitive programming and safety measures, which allow them to work in the same space without risk for the operators. An added disadvantage of collaborative robots is their flexibility in their joints because they include Harmonic drive type reducers. The use of force control in machining processes with robot arms makes possible to control and correct, in real-time, the deviations generated by the flexibility in the robot's joints. The use of this control method is beneficial for any robot arm. However, the internal control included in collaborative robots has advantages that allow the force control to be applied more efficiently. In this work, a real proposal is developed to include effort control in the robot arm. The capacity of industrial and collaborative robots in machining tasks is evaluated and quantified. The proposal recommends how to improve the use of an inner/outer force control loop applied in a collaborative arm, when the real torques of the robot's motors are unknown and other internal parameters that manufacturers do not disclose. This inner/outer control loop has been used in polishing and sanding applications on different materials. The results indicate that the collaborative robot is feasible to perform such machining operations. Best results are obtained using an internal velocity control loop and external force control loop with Proportional-Integral-Derivative or Proportional plus Feed Forward.

Resum

El mecanitzat amb braços robots ha estat estudiat aproximadament des dels anys 90, durant aquest temps s'han dut a terme importants avanços i descobriments en el que fa al seu camp d'aplicació. En general, els robots manipuladors tenen molts beneficis i avantatges al ser usats en operacions de mecanitzat, com ara, flexibilitat, gran àrea de treball i facilitat de programació, entre d'altres, davant de Màquines Eines de Control Numèric (MECN) que necessiten d'una gran inversió per treballar peces molt grans o incrementar els seus graus de llibertat. Com a desavantatges, enfront de les MECN, els braços robòtics posseeixen menor rigidesa, el que combinat amb les altes forces produïdes en els processos de mecanitzat fa que apareguin errors de precisió, desviacions en les trajectòries, vibracions i, per tant, una mala qualitat en les peces fabricades. Entre els braços robots, els braços col·laboratius estan en auge a causa de la seva programació intuïtiva i a les seves mesures de seguretat, que els permeten treballar en el mateix espai que els operadors sense que aquests corrin riscos. Com desavantatge afegida als robots col·laboratius es troba la major flexibilitat que aquests tenen en les seves articulacions, a causa de que inclouen reductors del tipus Harmonic drive. L'ús d'un control de força en processos de mecanitzat amb braços robots permet controlar, i corregir, en temps real les desviacions generades per la flexibilitat en les articulacions del robot. Utilitzar aquest mètode de control és beneficiós en qualsevol braç robot, però, el control intern que inclouen els robots col·laboratius presenta avantatges que permeten que el control de força es puga aplicar d'una manera més eficient. En el present treball es desenvolupa una proposta real per a la inclusió del control d'esforços en el braç robot, així com s'avalua i quantifica la capacitat dels robots industrials i col·laboratius en tasques de mecanitzat. La proposta planteja com millorar la utilització d'un control de força per bucle interior/exterior aplicat en un braç col·laboratiu, quan es desconeixen els parells reals dels motors del robot, així com altres paràmetres interns que els fabricants no donen a conèixer. Aquest bucle de control interior/exterior ha estat utilitzat en aplicacions de polit sobre diferents materials. Els resultats indiquen que el robot col·laboratiu és factible de realitzar aquestes operacions de mecanitzat. Els seus millors resultats s'obtenen quan s'utilitza un bucle de control intern per velocitat i un bucle de control extern de força amb els algoritmes Proporcional-Integral-Derivatiu o Proporcional més Pre-alimentació de la Força.

Índice

Índice de figuras

Índice de tablas

Capítulo 1
Introducción

1.1. Antecedentes

El uso de brazos robóticos en diversos sectores industriales como la automoción, aeroespacial y el sector médico, está en continuo crecimiento. Diversos estudios [1–3] indican que el stock operativo de robots está calculado en 2.722.077 unidades aproximadamente. Desde el año 2010 la demanda de robots industriales ha aumentado considerablemente debido a la tendencia actual hacia la automatización y a las continuas innovaciones técnicas que se incorporan en los robots industriales. Además de las ya conocidas aplicaciones como *pick and place*, soldadura y pintado, en la última década los brazos robots han sido introducidos en prácticamente todas las operaciones de mecanizado [4].

Los robots están siendo utilizados para tareas de mecanizado, reemplazando a las máquinas CNC (Control Numérico Computarizado) en procesos tales como fresado, taladrado, rectificado y corte 2D. Asimismo, han sido usados para ejecutar tareas asociadas con el acabado superficial final, en aplicaciones tales como rectificado en acabado, lijado, pulido y desbarbado [5–7]. Como se puede observar, en los distintos campos de aplicación, los robots industriales tienden a remplazar a las tareas manuales, categoría en la cual podemos incluir el uso de los brazos robots

colaborativos. Esto es debido, principalmente, al hecho de que los ciclos de vida de los productos son cada vez más cortos y al incremento en las demandas de altos estándares de calidad, lo cual ha generado que se busque una alternativa frente a los procesos manuales o soluciones automatizadas poco flexibles. Sobre todo, en operaciones que son ruidosas, contaminantes e insalubres para los operadores, como son los ambientes en la industria de la automoción [8].

También aparecen como una alternativa para las máquinas CNC, frente a tareas donde se requiere un gran volumen de trabajo o cuando se van a procesar geometrías complejas.

Por ejemplo, en la industria aeroespacial y en la energética se utilizan grandes máquinas CNC multi eje para fresar piezas de gran tamaño, lo que requiere a su vez un gran tamaño de máquina, así como de altos costes operacionales [9]. Sin embargo, los robots industriales tienen una configuración idónea para procesar formas 3D complejas, además de poseer un gran volumen de trabajo, que puede ser incluso aumentado con ejes extras. Adicionalmente, los robots poseen una buena capacidad de programación, adaptabilidad y flexibilidad, con un coste de inversión menor que el requerido para una Máquina Herramienta de Control Numérico (MHCN) con el mismo volumen de trabajo [7,8]. Algunos estudios indican una reducción del 30% en el coste total, al utilizar robots en lugar de MHCN para ciertas operaciones [10].

Por otra parte, la desventaja en el uso de brazos robóticos recae principalmente en que estos presentan una menor rigidez en comparación con una máquina CNC. En general, la rigidez para un robot articulado es de 1 N/μm, lo cual es mucho menor que la rigidez de una máquina CNC estándar de 50 N/μm [8]. El factor dominante que contribuye a la deflexión del manipulador en un brazo robot es la acomodación (*compliance*) de la articulación, producto de la flexibilidad producida por la geometría y propiedades del material de la articulación, los actuadores y otros elementos de transmisión, así como de la postura del robot [11,12]. Este factor principal, combinado con las fuerzas producidas durante el proceso de corte, genera deflexiones en el efector final, con lo cual se producen errores de posición, vibraciones y, con ello, una falta de precisión dimensional y un mal acabado superficial en las piezas fabricadas [13,14].

Sin embargo, en los últimos años los robots colaborativos han ganado gran popularidad debido a su mayor flexibilidad, fácil programación, bajo coste y altos

estándares de seguridad. Pero los principales inconvenientes en este tipo de robots son, su menor capacidad y el uso de reductores en sus articulaciones del tipo *Harmonic drive.* Lo que implica que su rigidez sea menor que los robots industriales convencionales, quedando relegados a operaciones donde los esfuerzos sean menores [15–17], como es el caso de la ejecución de tareas relacionadas con el acabado superficial de piezas.

A pesar de las desventajas, tanto de los robots industriales convencionales como de los colaborativos, si ambos fueran capaces de proveer posiciones precisas, bajo situaciones de contacto, de igual manera que su conocida buena repetibilidad en vacío, el mecanizado robótico podría aportar un ahorro muy significativo para una gran cantidad de aplicaciones [18].

El mecanizado con brazos robots ha sido investigado desde diferentes puntos de vista, tales como la compensación de las fuerzas de corte, la minimización de vibraciones, la compensación de los errores de rigidez, la prevención de colisiones, el uso de la redundancia en los grados de libertad del robot, la configuración de posición de los robots y el análisis de los modelos dinámicos y de rigidez [13,19–23].

Los modelos de control para el mecanizado robótico se pueden agrupar en dos tipos:

(1) Los que tratan la generación de compensación *off-line*, donde es necesario un modelo preciso de rigidez y de fuerzas de corte para estimar las deflexiones ocurridas durante el proceso.

(2) Los que trabajan la compensación *on-line*, en la cual el uso de sensores de fuerza ha sido identificado como una herramienta clave para la programación y control en tiempo real [24–26].

Dependiendo del tipo de robot y de sus elementos auxiliares, es posible encontrar dos casos: Robots con sensores de torque (par) de un grado de libertad, en cada una de sus articulaciones, o robots con un sensor de fuerza-torque de 6 grados de libertad, ubicados en el efector final [27].

A pesar de que existe cierta limitación debido a los controles cerrados que imponen los fabricantes de robots, lo cual implica una falta de conocimiento por parte de los usuarios finales sobre los diferentes modelos de control de fuerza que podrían utilizarse, muchos investigadores consideran vital la utilización de un control de fuerza para mejorar las características del mecanizado con robots.

Específicamente, es posible encontrar trabajos sobre robots con controles únicamente de fuerza, controles de fuerza/posición y controles de impedancia, los cuales, a su vez, se utilizan con técnicas como el control adaptativo, control robusto, control inteligente o métodos clásicos de teoría de control moderna [28].

La presente tesis evalúa una propuesta de integración de control de esfuerzos en un brazo robot colaborativo para desempeñar procesos de mecanizado en materiales blandos (menos duros que el acero). A lo largo del trabajo de investigación se revisó con detalle el estado del arte en el mecanizado robótico, el uso de sensores de fuerza y torque, así como el desarrollo y aplicación de un modelo de control de fuerza con bucle interior/exterior, el cual consiste en un bucle interior de posición/velocidad, que es parte del control del robot, y un bucle externo de fuerza. La aplicación de este control de fuerza se llevó a cabo en un robot colaborativo, realizando un estudio teórico previo, apoyado con resultados de ensayos reales para suplir la falta de información sobre los parámetros de funcionamiento interno del brazo.

1.2. Hipótesis y Objetivo de la Investigación

1.2.1. Hipótesis

- Los brazos robot industriales convencionales y los colaborativos con control de fuerza son factibles de ser utilizados en operaciones de mecanizado de materiales de baja dureza, reemplazando a máquinas CNC y a ciertas tareas manuales.
- El uso de brazos robots en procesos de mecanizado sobre materiales blandos (plásticos, composites, aluminio, etc.) dota a los procesos de mayor rango de aplicación, permitiendo aumentar la rapidez del proceso con un menor coste.

1.2.2. Objetivo General

Evaluar la capacidad y factibilidad de los robots manipuladores industriales convencionales y robots colaborativos para su uso en operaciones de lijado sobre

materiales blandos (baja dureza), al proporcionar modificaciones en el control para mejorar el comportamiento y los resultados del proceso.

1.2.3. Objetivos Específicos

- Comprender los procesos de mecanizado al utilizar un brazo robot industrial y colaborativo.
- Estudiar la dinámica y el control de los brazos robot industriales, colaborativos, y proponer modificaciones adecuadas para la aplicación de un control de fuerza factible.
- Evaluar, técnica y económicamente, la aplicación de elementos sensores y métodos de control para ser integrados en los procesos de lijado con brazos robóticos.

1.2.4. Preguntas de Investigación

- ¿Es factible utilizar, técnica y económicamente, los brazos robots industriales y colaborativos para reemplazar tareas realizadas con máquinas CNC o en forma manual?
- ¿Es posible modificar el comportamiento del robot (sin acceso a sus parámetros internos) con una retroalimentación de fuerza y controlar la precisión que se alcanza?
- ¿Existen ventajas al utilizar sensores y un control de fuerza en el proceso de lijado con brazos robots?

1.3. Estructura de la Tesis

El trabajo científico que se muestra a continuación es una tesis por compendio de artículos científicos. Cada uno de los artículos que se presentan en los siguientes capítulos pueden ser leídos independientemente. Sin embargo, el conjunto de artículos conforma un trabajo completo, sobre la inclusión de esfuerzos en el control de un brazo robot para asegurar el cumplimiento de la rugosidad superficial durante operaciones de lijado en diferentes materiales. La tesis está compuesta por nueve capítulos:

1. **Introducción.**
2. **Publicación 1:** *A study on robot arm machining: Advance and future challenges.*
3. **Publicación 2:** *Design and Manufacturing of an Ultra-Low-Cost Custom Torque Sensor for Robotics.*
4. **Publicación 3:** *Study of the application of a collaborative robot for machining tasks.*
5. **Publicación 4:** *Force Control Improvement in Collaborative Robots through Theory Analysis and Experimental Endorsement.*
6. **Publicación 5:** *Behavioural study of the force control loop used in a collaborative robot for sanding materials.*
7. **Discusión de los resultados obtenidos.**
8. **Conclusiones.**
9. **Bibliografía general.**

El Capítulo 1, de introducción, consta inicialmente de un breve repaso de los antecedentes sobre el mecanizado con brazos robot, robots colaborativos y sobre control de fuerza. A continuación, se exponen las hipótesis y los objetivos de la investigación. Por último, se indica la estructura de la tesis y se describe el contenido de los capítulos posteriores.

El cuerpo principal de la tesis consta del compendio de cinco artículos científicos, en los que se mantiene el idioma de su publicación. Estos se corresponden con los capítulos del 2 al 6. En la sección 1.4 se expone un resumen sobre cada una de estas publicaciones.

En el capítulo 7 se aporta una breve discusión sobre los principales resultados obtenidos en cada artículo.

En el capítulo 8 se presentan las conclusiones de la tesis, así como el nivel de cumplimiento de los objetivos planteados y las futuras líneas de investigación asociadas al trabajo realizado.

Por último, en el capítulo 9, se muestra la bibliografía general utilizada en los capítulos 1, 7 y 8.

1.4. Resumen de las publicaciones

La primera publicación, expuesta en el capítulo 2, se titula "*A Study on Robot Arm Machining: Advance and Future Challenges*" [29]. Este trabajo fue presentado

como un artículo científico en el *29th Daaam International Symposium On Intelligent Manufacturing and Automation* de 2018. La publicación forma parte de las actas del simposio, el cual esta indexado en SCImago-SJR, cuyo factor de impacto es 0.23 en el 2018 y se ubica en el cuartil Q3 (214/484) en la categoría *Industrial and Manufacturing Engineering*. En este artículo se presenta un análisis del estado del arte sobre el mecanizado con robots, con sus respectivas ventajas y desventajas, y las diversas alternativas o soluciones con las cuales es posible mejorar los resultados en las operaciones de mecanizado. En concreto, el uso de un control de fuerza es el método seleccionado para ser implementado en el mecanizado con robots.

La segunda publicación titulada "*Design and Manufacturing of an Ultra-Low-Cost Custom Torque Sensor for Robotics*" [30], expuesta en el capítulo 3, ha sido publicada en la revista *Sensors* del año 2018. Esta revista tiene un factor de impacto de 3.031 en el JCR de 2018 y se ubica en el cuartil Q1 (15/61) en la categoría *Instruments & Instrumentation*. En este artículo se expone un novedoso diseño de sensor de torque, que permite mantener el nivel de requerimientos exigidos, con un bajo coste de fabricación. Para conseguirlo, el diseño fue validado a través de análisis matemáticos y análisis por elementos finitos, buscando determinar la mejor alternativa de desarrollo, adicionalmente se implementó un dispositivo de calibración para confirmar los resultados de las simulaciones. El uso de un sensor de torque fue una de las alternativas para implementar un control de fuerza en las aplicaciones con robots.

En el capítulo 4, se expone la tercera publicación titulada "*Study of the application of a collaborative robot for machining tasks*" [31]. Esta fue presentada inicialmente en la *8th Manufacturing Engineering Society International Conference (MESIC)* de 2019. Posteriormente, el artículo fue publicado en la revista *Procedia Manufacturing*, la cual tiene un factor de impacto de 0.516 en SCimago-SJR de 2019 y se ubica en el cuartil Q2 (108/484) en la categoría *Industrial and Manufacturing Engineering*. En esta publicación se presenta un análisis comparativo de operaciones de mecanizado realizadas con un robot industrial y un robot colaborativo. Se evidencian las ventajas y desventajas del robot colaborativo y se exponen los métodos que mejorarían el proceso de mecanizado con este tipo de robots. El robot colaborativo es el tipo de robot seleccionado para implementar un control de fuerza, debido a los beneficios que su control interno ofrece frente al control de un robot industrial no colaborativo.

"F*orce Control Improvement in Collaborative Robots through Theory Analysis and Experimental Endorsement*" [32] es el título de la cuarta publicación de la tesis, expuesta en el capítulo 5. Fue publicada en la revista *Applied Sciences* en el año 2020. Esta revista tiene un factor de impacto de 2.679 en el JCR de 2020 y se ubica en el cuartil Q2 (38/91) en la categoría *Engineering-Multidisciplinary*. En este trabajo se presenta un análisis profundo sobre el control de fuerza en brazos colaborativos. Se expone el análisis teórico y experimental del uso de un control de fuerza con bucle interior/exterior.

La quinta y última publicación, se expone en el capítulo 6, y se titula "*Behavioural Study of the Force Control Loop Used in a Collaborative Robot for Sanding Materials*" [33]. Se publicó en la revista *Materials* en 2020. Esta revista tiene un factor de impacto de 3.623 en el JCR de 2020 y se sitúa en el cuartil Q2 (152/333) en la categoría *Material Science-Multidisciplinary*. El artículo expone la aplicación del control de fuerza por bucle interior/exterior, antes desarrollado e implementado, en operaciones de lijado sobre materiales con distintas características, tales como acero, aluminio, bronce, policloruro de vinilo (PVC) y madera.

Capítulo 2

A study on robot arm machining: Advance and future challenges

29TH DAAAM INTERNATIONAL SYMPOSIUM ON INTELLIGENT MANUFACTURING AND AUTOMATION

DOI: 10.2507/29th.daaam.proceedings.134

A STUDY ON ROBOT ARM MACHINING: ADVANCE AND FUTURE CHALLENGES

Rodrigo Pérez*, Santiago C. Gutiérrez y Ranko Zotovic

Pérez, Rodrigo; Gutiérrez Rubert, Santiago Carlos & Zotovic, Ranko (2018). A Study on Robot Arm Machining: Advance and Future Challenges, Proceedings of the 29th DAAAM International Symposium, pp.0931-0940, B. Katalinic (Ed.), Published by DAAAM International, ISBN 978-3-902734- 20-4, ISSN 1726-9679, Vienna, Austria. DOI: 10.2507/29th.daaam.proceedings.134.

A study on robot arm machining: Advance and future challenges

Rodrigo Pérez [1,*], Santiago C. Gutiérrez [1] y Ranko Zotovic [2]

[1] Dept. of Mechanical and Materials Engineering, Universitat Politècnica de València, Valencia 46022, Spain.

[2] Institute of Industrial Control Systems and Computing, Universitat Politècnica de València, Valencia 46022, Spain.

* Correspondence: rodpeub@doctor.upv.es.

Abstract

Nowadays, it is not uncommon to find news and research about robotic machining applications, as milling and drilling. The flexibility, programmability and low price of robots, conversely to CNC machines, makes robotic machining an interesting opportunity for manufacturing of large parts. In this paper, the authors show the current advances on developments of robotic machining and a theoretical framework of the process, evidencing its weaknesses and strengths. Since the low stiffness of robots is their main disadvantage, the target of researchers is to improve this characteristic, and therefore avoid adverse effects like vibration, which influences the machining accuracy. The last developments can be categorized according to their research field: modelling and control of the process, robot workspace optimization, redundancy analysis, vibrating/chatter analysis and new designs and methodologies for the improvement of machining. These researches increase the efficiency and accuracy of the process with the goal to convert robots in a real alternative to CNC machines. In fact, the authors are working on the aim of proposing a characterization of several machining operations with robots, considering a force/torque control that provide the system a feedback with the improved stiffness matrix to correct errors and improve the accuracy during machining.

Keywords: machining robot arm; industrial robots; stiffness matrix; robotic accuracy.

2.1. Introduction

Machining with robotic arms is the combination of two areas or fields in engineering: machining processes and robotics. As is known, the first field uses numerical control machine tools to perform machining operations with great reliability and accuracy to make parts for various types of industries. On the other hand, industrial robots are studied to be commonly used in applications of low contact forces, such as material handling, welding, assembly, painting, etc.

The use of robotic arms in the industry is in continuous increase with an average growth of 12% per year, estimating that, in the year 2020, a total of 3,000,000 robots will be in operation [1]. In addition to its typical applications, in the last two decades, the interest in using robotic arms in machining tasks has grown, although their use in this area is still less than 5% of total sales [2]. The incorporation of robot arms for machining tasks includes many industrial sectors, from the automation and aerospace sector to medical industries. The robots have been applied for machining tasks such as milling, drilling, roughing and cutting. Also, they have been applied to solve surface finish tasks in applications as grinding, brushing, polishing and deburring [2], [3], [4].

Depending on the field of application, the robots tend to replace manual tasks, a category in which we can include collaborative robot arms. The fact that product life cycles are becoming shorter and the demand for high quality standards increases, industries look for an alternative to manual processes or inflexible automated solutions [5], especially in operations that are noisy, pollutant and unhealthy for operators as the environments of the automotive industry [6].

Robots also appear as an alternative for CNC machine tasks where a large volume of work and the development of complex geometries are required. In the aerospace and energy industry, large multi-axis CNC machines are used to mill large parts, which requires a large factory size, as well as incurring high operational costs [7]. Industrial robots are enabled to process complex 3D shapes, in addition to having a large volume of work, which can be increased with extra axes. In addition to these advantages, robots have good programmability, adaptability and flexibility with a lower investment cost in contrast to a CNC machine tool with the same

workload [4], [6]. Some studies indicated a 30% of reduction in the total cost when robots are used [8].

The disadvantage of the use of robotic arms lies mainly in that they present a lower stiffness compared to CNC machines. The stiffness for an articulated robot is 1 $N/\mu m$, which is lower than the stiffness of a standard CNC machine, 50 $N/\mu m$ [6].

This main factor, combined with the forces produced in the cutting process, generates deflections in the end effector causing position errors, vibrations, bad quality and low accuracy of the manufactured part [3]. In some cases, the end effector deflections produced by the cutting forces have reached 10 mm. Table 2.1 shows a detailed comparison of CNC machines and robotic arms for machining tasks.

Table 2.1. Comparison of CNC machines and robots for machining [4].

Indicator	CNC machine	Industrial Robot
Accuracy	-0.005 mm	-0.1 – 1.0 mm
Repeatability	-0.002 mm	-0.03 – 0.3 mm
Workspace	Limited	Large
Workspace extending	Impossible	Possible by adding extra actuated axis.
Kinematic architecture	Cartesian	Serial
Number of actuated axes	3 or 5	6+
Kinematic redundancy	Non	Yes, 1 degree of freedom at least
Complexity of trajectory	Suitable for de 3/5 axes machine	Any complex trajectory
Relation between actuated and operational space	Linear	Non-linear
Actuator feedback	Single encoder	Single or double encoders
Mechanical compliance	Relatively low	Relatively high
Compliance error compensation	Non-required	Mechanical (Gravity compensators) Algorithmic (off-line and/or on-line)
Dynamic properties	Moderate, homogeneous with theworkspace.	High, heterogeneous with the workspace.
Programming language	Standardized G-code language	Manufacture specified languages (KRL,V+, Karel, RAPID, Inform, etc.)
Manufacturing flexibility	Single or several similar operations	Any type or operation
Price	Competitive for 3 axis tools. Expensive for 5 axis tools	Competitive for 6 axis robots.

The high reduction ratio in the robot joints causes loss of friction and backlash. A small variation in the reduction ratio of the joint can induce a significant error in the accuracy of the tool centre point (TCP). The difference with the errors due to 'low stiffness' lies in that these last effects are less predictable [3].

This work focuses on the correct understanding of the phenomenon of robotic machining, to develop the guidelines of a new proposal to facing future challenges, specifically we focus on the exploration and evaluation of the latest advances in this area. This paper is organized as follows; Section 2.2 describes the robotic machining model, Section 2.3 show the last advances in the area, Section 2.4 describes the future challenges and the authors' proposal. It ends with the conclusion in section 2.5.

2.2. Main challenge: Robotic machining model

To understand the disadvantages and analyse the behaviour of the robots during a machining process, it is necessary to use an adequate and accurate mathematical model to predict the displacement of the robot structure under an applied load.

Robotic systems are designed to achieve high position accuracy. The elastic properties of its links are considered insignificant, thus the dominant factor that contributes to the deflection of the manipulator is the joint compliance. This is a product of the flexibility produced by: the geometry and the properties of the joint material, the actuators and others transmission elements and the robot posture [9], [10].

Joint compliance is the biggest problem for the deviation of the TCP. This variable is the inverse of the stiffness. Hence, to analyse the structure of the robot it is necessary to determine the value of the stiffness of each joint [11]. The factor of stiffness in machining is so important that many topics of research in robotics have been developed in this area. In general, for robots many aspects have been discussed, such as, modelling the stiffness of serial and parallel robots, identification of stiffness parameters and analysis of stiffness characteristics [10].

Pashkevich, A. et al, [12] in their studies performed an analysis of existing stiffness models, which can be seen in Table 2.2. As can be analysed, if there are more assumptions, there will be an increase in the complexity of the joint model.

According to the analysed literature, the commonly used models correspond to the cartesian stiffness matrices proposed by Salisbury and Chen & Kao [13].

To determine the Cartesian stiffness matrix, the models used the principle of virtual work, which allows making certain assumptions about the static case. Under this principle, the work must be the same in any set of coordinates, that is, the work in Cartesian coordinates must be the same as the work in the joint coordinates.

Table 2.2. Summary of related works for the Cartesian stiffness matrix [12].

Publications	Model & assumptions	Stiffness matrix
Salisbury (1980)	Serial manipulator, elasticity in actuators.	$K_c = J_\theta^{-T} \cdot K_\theta \cdot J_\theta^{-1}$
Zhang et al. (2004)	Serial kinematic chain without passive joint, elasticity in virtual joints.	$K_c = \left(\sum_i J_{\theta i} \cdot K_{\theta i}^{-1} \cdot J_{\theta i}^T \right)^{-1}$
Pashkevich et al. (2009)	Serial kinematic chain with passive joint, elasticity in virtual joints.	$\begin{bmatrix} K_c & * \\ * & * \end{bmatrix} = \begin{bmatrix} J_\theta \cdot K_\theta^{-1} \cdot J_\theta^T & J_q \\ J_q^T & 0 \end{bmatrix}^{-1}$
Chen & Kao (2000)	Serial or parallel manipulator with external loading (non-over constrained).	$K_c = J_\theta^{-T} \cdot (K_\theta - K_F) \cdot J_\theta^{-1}$
K_c – Cartesian stiffness at the end effector (6×6) K_θ – Joint stiffness of the virtual springs $(n_\theta \times n_\theta)$ J_θ – Jacobian of the virtual springs $(6 \times n_\theta)$		J_q – Jacobian of the passive joints $(6 \times n_\theta)$ K_F – Stiffness matrix induced by external loading $(n_\theta \times n_\theta)$ θ_i – Position of robot joint i.

Therefore, by mathematically developing the equality of virtual work, the expression for the Cartesian stiffness matrix is given by,

$$K_x = J(Q)^{-T} \cdot K_q \cdot J(Q)^{-1} \quad \textbf{(2.1)}$$

Where K_q corresponds to the joint stiffness matrix and $J(Q)$ the Jacobian matrix of the robot. As it can be seen, this expression corresponds to the model exposed by Salisbury, but this formulation is valid only when the robot is in a quasistatic configuration, without external loads or when the Jacobian matrix is constant through the robot's workspace, (e.g., cartesian robot) [7]. Through the Conservative Congruence Transformation (CCT), Chen, et al. [13], added an extra term known as

K_g or K_f, which considers changes in geometry under the presence of external charges $\boldsymbol{F}$. Therefore, we have,

$$K_x = J(Q)^{-T} \cdot \left(K_q - K_g\right) \cdot J(Q)^{-1} \tag{2.2}$$

Where K_g is defined by,

$$K_g = \underbrace{\left[\frac{\partial [J(Q)]^{-T}}{\partial \theta_1} F \quad \frac{\partial [J(Q)]^{-T}}{\partial \theta_2} F \cdots \frac{\partial [J(Q)]^{-T}}{\partial \theta_{n-1}} F \quad \frac{\partial [J(Q)]^{-T}}{\partial \theta_n} F\right]}_{nxn} \tag{2.3}$$

This extended definition of stiffness considers the loads of external forces on the end effector. It is not commonly used since many studies consider their negligible value when the robot is in work zone with optimized stiffness.

For an articulated arm, the Cartesian stiffness matrix is not a diagonal matrix and depends on the configuration of the robot. This indicates that, firstly, the force and the deformation in the Cartesian space are coupled. Force applied in one direction generates a deformation in all possible directions. Secondly, the stiffness is a function of the robot's kinematics through the Jacobian, $J(Q)$, which changes significantly in the robot workspace and according to the position the robot has.

With the assumption that the joint stiffness is constant and that the changes of position can be modelled, the Cartesian stiffness could be calculated. Therefore, the deformation of the TCP under the action of an external force could be estimated as,

$$\Delta X = J(Q)^{-T} \cdot (K_q - K_g) \cdot J(Q)^{-1} \cdot F \tag{2.4}$$

Some authors use the Compliance matrix for the definition of the previous equation, avoided calculation errors in the determination of the inverse Jacobian.

In general, the main difficulty of the implementation of this model is that the determination of joint stiffness is considered constant and must be achieved experimentally. Therefore, there are several methodologies that can be observed in the works of Zhang, H. et al. [6]; Abele, E. et al. [11]; Dumas, C. et al. [14] and Olofsson, B. et al. [15].

2.3. Advances in robotic machining

Robotic machining has been limited to soft materials such as plastics and/or aluminium and the use of conservative feed speeds to avoid excessive cutting forces in the process. To deal with these problems, various researches have been made with the aim of overcoming them. Chen, Y. et al, [2] studied the researches carried out until 2013, and classified them into categories according to the line of work, such as development of robotic machining systems, machining path planning, vibration/chatter analysis and dynamics.

Almost contemporarily, two projects under the European Union financing have been developed to enhance the machining with industrial robots, the first project called, "COMET" ("Plug-and-produce Components and Methods for adaptive control of industrial robots enabling cost effective, high precision manufacturing in factories of the future") wanted to reinforce the knowledge and methodologies for the implementation of robotic machining. They developed aspects such as kinematic and dynamic robot modelling, auto programming software, trajectory tracking and high dynamic composition mechanisms. Its objective was to reduce the errors produced in machining through an adaptive control of the process. The second project called "HEPHESTOS": "Hard Material Small-Batch Industrial Machining Robot", had as main objective the development of new technologies for the robotic machining of hard materials to provide a standard for planning machining, programming and control in real time. Both projects introduced important advances in the area.

More current studies, as the one conducted by Klimchik, A. et al. [4], have defined the last advances in the following aspects; (1) Improve stiffness of the manipulator, either by increasing the section or using advanced materials. (2) Use gravity mechanical compensators to reduce compliance errors. (3) The use of second encoders placed on the motor shaft to compensate errors. (4) The application of off-line error compensation techniques to modify the input path in the controller.

In general, a robotic machining cell is an integrated manufacturing system that consists of an industrial robot of 5 or more axes, a spindle for cutting tools and a compatible software for programming multiple trajectories. In addition, depending on the application, auxiliary elements can be added, such as a seventh sliding axis, rotating tables, force/torque sensors and vision systems that will increase the

functionality and flexibility of the cell. Next, a review of the state of art about last advances and studies regarding robotic machining are shown to obtain a better conception of the models and architectures used.

2.3.1. Control of the machining process

The control models for robotic machining can usually be differentiated into two types; (1) generation of off-line compensation, where a precise model of stiffness and cutting forces is necessary to estimate the deflections occurred during the process and (2) compensation on-line, where the use of force/torque sensors are the key tool for programming and control in real time [16], [17]. Specifically, we will find force controls, force/position controls and impedance controls. These control types are used with adaptive, robust, intelligent or classical control methods or techniques [18].

Pan, Z. and Zhang, H. [6], [9], in their research focused on improving the quality and efficiency of robotic machining through two methods; compensate the deformation of the robot and maximize the material removal rate. To achieve this, firstly, they used the conventional stiffness model and a force sensor to perform a real-time compensation of the programmed trajectory. In Figure 2.1, the compensation principle can be appreciated.

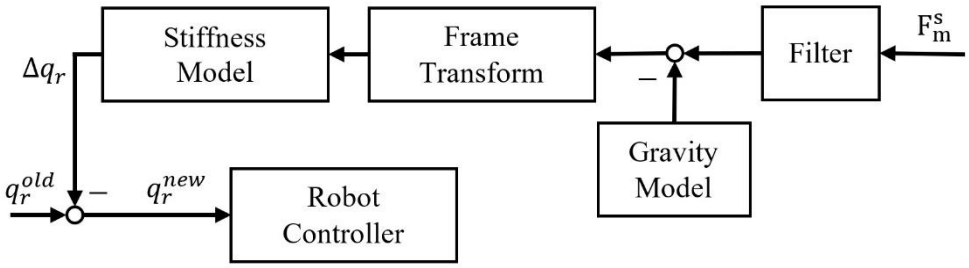

Figure 2.1. (a) Principle of real time deformation compensation. ($\boldsymbol{F_m^s}$: sensing force, $\boldsymbol{q_r}$, joint position) [6], [9].

Secondly, its purpose was to maximize the material removal rate (MRR), which is given by the following relationship,

$$MRR = w \cdot d \cdot f \tag{2.5}$$

Where w is the width of cut (mm), d the depth of cut (mm) and f the cut feed in (mm/min). The width and depth of cut are kept constant therefore a conservative value is usually given for the cut feed to avoid damage to the spindle. To maximize this rate, they used an adaptive type control. But, as it is complicated to measure the material removal rate directly, they regulated this value through force measurement of the sensor at the end effector. Adjusting adaptively the cut feed to regulate the force allowed to extend the life of the tool and increase the productivity of the process. The experimental results of the controls in real time allowed them to reduce the work cycle from between 30% and 50% and improved the surface quality with a superficial accuracy from 0.9 mm to 0.3 mm. In a subsequent research [19] the authors applied different types of control for the material removal rate, including a PI (Proportional and Integral), adaptive and fuzzy control. The adaptive control being the one that delivered better results from the point of view of the stability of the system.

In Tyapin, I. et al. [16] we found a comparison of two models for calculation of offline force, the first only considers the influence of the depth of cut and the second considers the influence of the depth and width of cut as parameters. Their results indicated that the second model is more accurate to identify deviations from the process.

Other more current methodologies have been found in the work of Sörmo, O. et al [20] and Chen, S. & Zhang, T. [21], who developed an adaptive force control model. Also, in the work of Cano P. et al [22], who developed an iterative learning control, and in the work of Ilyukhin, Y. et al. [23], who developed an adaptive control, but they used signals of the currents in the windings of motors to provide information about the loads acting on the drives.

Cen, L. et al. [7], have proposed a model that allows a better understanding of the dynamic effects produced in the milling forces. Their model differs from the others, because they do not use static cut models that are only valid for the features of CNC machines. Based on the Sutherland and DeVor studies, the instantaneous milling force is a function of the instantaneous thickness of the chip, which in turn

is affected by the flexibility of the machining system. Therefore, an iterative calculation of the balance of the dynamics of the chip load without cutting at each instant of time is required. This theory plus the use of the improved stiffness model allowed the creation of an algorithm to calculate the instantaneous dynamic force.

The comparison of the dynamic model with the experiments showed a reduction from 50% to 75% in the calculation errors of forces. Similar research can be found in the work of Klimchik, A. et al. [24], but they used the stiffness model proposed by Pashkevich, A. et al, [12]. In the case of drilling process control, we found the works of Garnier, S. et al. [25] and Gomes, D. et al. [18], both emphasized that the control of the process should be carried out in three phases; the first contact or indent phase, the material removal phase and the final contact phase. The first work realized a theoretical model estimating the force of each phase and thus compensating the trajectory. The second work realized a force control in real time that diminished the sliding produced in the first contact, but even so, it cannot avoid deflections in other directions. The results showed are very interesting, since demonstrate the reliability of using the improved stiffness model that consider the dynamics parameters. The application of this model could allow a more accurate online force control to compensation in real time.

2.3.2. Planning and programming trajectories in machining.

To handle the lack of standardization in robot programming, producers have offered solutions in software such as, Kuka CAMRob, Motoman Standard CNC G-Code Converter, FANUC Roboguide, etc., to transfer trajectories into the robot program. Other external companies have also offered some specific programs such as Robotmaster, PowerMill, etc. [26]. However, the use of external software implies an extra cost. In the literature we can find with certain methods to program and plan the trajectory of the robot. Pan & Zhang [9], proposed a simple and quick method to program the trajectory of machining. They only used the flex pendant of the robot and marked several guide points through trajectory of the TCP. Then a robot self-learning process linked such points and finally a post processor filtered and reduced the data to generate a program. Some efforts have also focused on generating an approach to standardize robotic machining, as in Huynh H. et al. [27] who simulated the machining process using a simplified multibody model, or Zivanovic, S. et al.

[28] who proposed an approach for the application of new standards in machining operations through the use of industrial robots. The methodology developed in accordance with the ISO 10303-238 standard was proposed for the execution of programming, simulation and robot machining process.

2.3.3. Redundancy.

As mentioned above, the behaviour of the robot varies in the workspace, since both its kinematics and dynamics depend on the position. Each posture has its own state of stable conditions and along the trajectory the robot arm can have infinite number of configurations, therefore the researchers take advantage of this redundancy to improve the machining.

A robot is redundant when the degrees of freedom (DOF) of the end effector are less than the degrees of freedom of the joint space. This redundancy increases the accessible volume and the ability of the robot to avoid obstacles. In the literature, three types of redundancy were defined:

- Structural redundancy: Joint space dimension m is larger than the operational space dimension n.
- Kinematic redundancy: Joint space dimension m is larger than the task realized degree t.
- Functional redundancy: Operational space dimension n is larger than the task realized degree t.

Mousavi, S. et al. [29], experimentally evaluated the use of functional redundancy for one and two degrees of freedom. Their experiments showed that using a degree of freedom allowed them to obtain more stable areas where productivity can be doubled. On the other hand, adding a second degree of freedom in redundancy could increase productivity by 40% or conversely it could be diminished. In Figure 2.2, stability can be observed for 1-DOF (rotation angle of six axis).

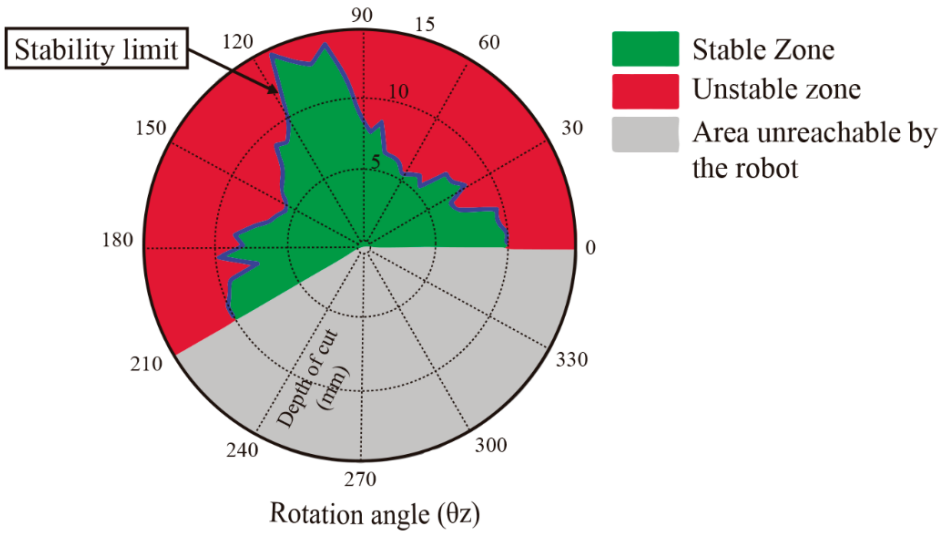

Figure 2.2. Stability as function of the redundancy of 1-dof [29].

In subsequent research [30], the use of a degree of redundancy was optimized by using a model to adaptively control posture throughout machining. The experiments demonstrated the benefit of using a functional redundancy control to improve stability, achieving improved accuracy from 11 to 2.5 μm for the same cutting conditions. The importance of these studies is that the use of redundancy allows movement from unstable to stable areas without changing the cutting conditions and thus ensure the machining result. The disadvantage is that they do not consider the dynamic effects of machining.

2.3.4. Posture optimization in robots

The redundancy of robots allows the improvement of dexterity and thus raises their performance. In this sense, many researchers created and analysed indices to evaluate the effectiveness of the robot's posture during machining operations.

Some known performance indices are:

- 'Number condition' of the Jacobian matrix is the upper limit of the relative amplification of rounding error when solving a system of linear equations to measure the distance to singularities.

- 'Manipulability' is the absolute value of the determinant of the Jacobian matrix. It was stated that a good manipulability index indicated a point in the workspace "far away" from the singularities.
- 'Velocity ratio' measures the robot's ability to move in a given direction.
- 'Force transmission ratio' represents the robot's ability to balance a given load.
- 'Joint-force index' is defined as the ratio between the maximum static force in any joint and the external load.

However, other authors have created other indices to optimize the position of the robot, as is the case of Zargarbashi, S. et al. [31] who defined the new index known as 'Robot Transmission Ratio' (RTR), which is the absolute value of the cosine of the angle between the vector of torque and the joint-rate vectors. Its objective is trying to quantify the effectiveness of the actuator force in producing a prescribed robot posture. Maximizing this index allows minimizing the magnitudes of the torque and position vectors, which lets the engines to work in accordance with their capacities.

Caro, S. et al. [8] made a methodology to determine the best place in the workspace to perform the machining operation. They define a criterion of quality of the machining which is expressed in terms of the displacement of the tool, the objective of optimization is to minimize this index. The theoretical results showed that the optimal workspace is associated with the best redundancy scheme.

Guo, Y. et al. [10], defined another index which is based on measuring the stiffness of the robot in certain positions. They studied the "translational compliance sub-matrix", which expresses the relationship between the translational displacements of the end effector and the applied force. The experiments carried out maximizing the index in drilling tasks demonstrated a uniform finish and lower deflections of the tool, which indicated a greater resistance of the robot to the machining forces.

The previous works have been focused on obtaining methods to select the orientation for a specific position of machining, but to obtain the optimal machining position it is necessary to optimize the global workspace of the robot. Lin

Lin, Y. et al. [32] proposed a posture optimization methodology, which is based on evaluating three indexes in maps of the robot's workspace: kinematics, stiffness

and deformation. With this, the best machining performance can be determined. In Figure 2.3, the optimized posture can be appreciated following the previous methodology, this allows the decrease of the deviations from 0.61 to 0.25 mm.

Despite the good results in the optimization indexes, it can be observed that none consider the dynamics effects of the process, they are only based on kinematic and static criteria, so the consideration of dynamic models such as the one presented in Cen, L. et al. [7] could improve the results in the optimization of the workspace of the robot.

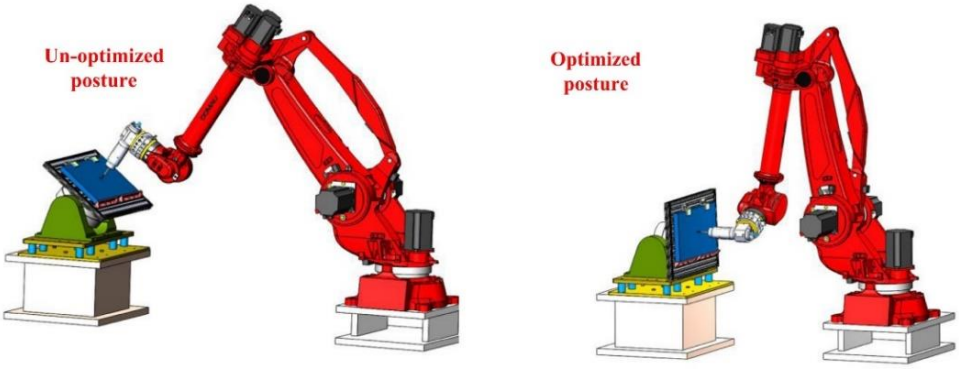

Figure. 2.3. The placement of workspace with respect to robot [32].

2.3.5. Vibration/chatter analysis

One of the biggest obstacles to defend the use of robots in machining processes are the vibrations that are generated during the process. The natural frequency usually takes values from 10 to 20 Hz, lower value than CNC machines, so taking into consideration that the cutting forces in the machining are periodic and sometimes have unpredictable variations, the occurrence of phenomena of vibration or chatter it is not surprising [3].

As main sources of these vibrations, two phenomenon have been identified; regenerative chatter and mode coupling chatter, the first is due to the variation in the forces and depth of cut and the second is due to the vibration of the mass system in all its degrees of freedom with different amplitude and phase [5]. These adverse effects damage the surface, which is compounded by poor dimensional accuracy,

the tool life is reduced and can even cause damage in the machine. Several investigations have been developed to reduce or eliminate this problem.

Pan, Z. et al [5], in their studies, discovered that when the chatter occurs, the amplitude of the cutting force increases drastically, and the chatter frequency can be observed through the Fast Fourier Transform from the sensor data. While they studied the process with different directions of advances and depths of cut, they observed the presence of a low frequency vibration (10 Hz) when the depth of cut was only 2 mm moving in minus Z direction. This frequency corresponds to the natural frequency of the base of the robot, so when the vibration occurs it occurs throughout the structure. This vibration does not change with the variation of cutting parameters or the location of the work surface, but it varies according to the location in the robot workspace and the direction of movement.

It is known that using high spindle speeds theoretically reduces vibrations for any depth of cut. But experiments showed the opposite, so the authors, exposed the mode coupling chatter as the biggest factor of this vibration. Pan, et al. [5] proposed a model of two degrees of freedom, which allowed the analyses of the behaviour of the robot. Their model corresponded to the experimental results and the main factors were the configuration of the robot and the depth of cut. As recommendations, they proposed to use specific tools to control the direction of the cutting forces, in addition to using robot positions and trajectories that minimize the angle between the resultant cutting force and the maximum direction of the robot's main stiffness.

The drawback of this model is that it cannot be applied to different types of cutting operations continuously, since the range of motion and flexibility of the robot is affected. Cen, L. et al, [33] presented a model to avoid mode coupling chatter, but based it on the improved stiffness model. This model avoided having to change cut feed direction or the orientation of the piece. This new model allowed definition of the cutting parameters to obtain a greater stiffness when altering the direction of maximum stiffness, as shown in Figure 2.4. The experimental results of the model showed a reduction greater than 45% in the resultant force and a reduction of the mode coupling vibrations occurred when increasing the advance speed.

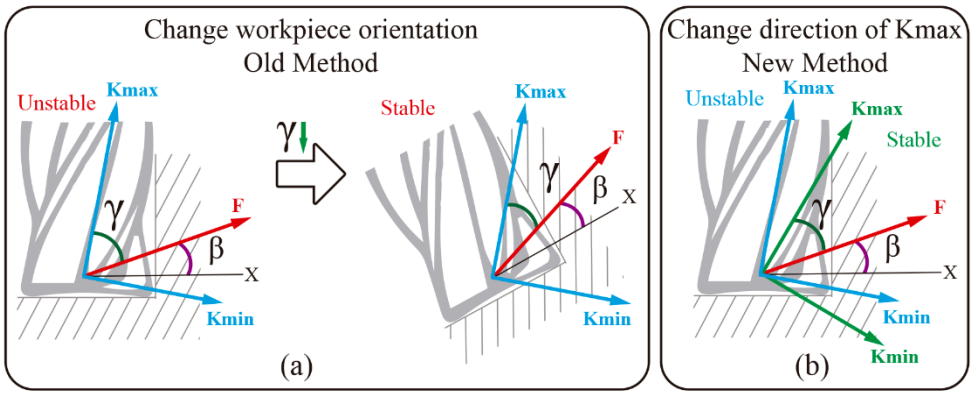

Figure 2.4. Comparison between Pan et al. and Cen et al. chatter avoidance methods: (a) Old method, (b) New method [33]. F: force, K: stiffness, β: angle between X-axis and force, γ: angle between force and maximum stiffness

Other authors such as Vieler, H. et al. [34], proposed a vibration reduction methodology through the use of secondary encoders. These encoders measure the output position of the engine, which allows to generate an offset and, this way, an error compensation is achieved. The amplitude of the deviation was reduced from 0.75 mm to 0.25 mm. Although this model reduces certain effects, it has the problem of not considering the dynamic effects in the definition of the stiffness.

2.3.6. Devices and methodologies

Sörnmo, O. et al. [35] and Mohammad, A. et al. [36], developed a system known as a macro-mini manipulator, which consists of a robot arm as macro manipulator that allows the exercise of the main movements of the process and the mini manipulator which consists of a device specifically designed to perform the respective improvement. In the case of the work carried out for Sörnmo, O. et al., the micro manipulator, in which the spindle is mounted, had a mechanism operated by piezo-actuator that allowed the compensation of the deflections in three directions, through strain gauges and capacitive sensors that measured the Spindle position. The experimental results of this system achieved precisions in milling of ±12 μm. On the other hand, the work presented in Mohammad A. et al., the mini manipulator

controlled the force applied in the polishing processes with which it reduced the inertial effects that caused unwanted vibrations.

Möller, C. et al. [37], used secondary encoders to improve the quality of machining in the aerospace industry. The use of secondary encoders and an adaptive control allowed improvements of the effective stiffness and repeatability of machining operations. They tested this model experimentally through the evaluation of repeatability with circular movements increasing accuracy twofold over the case without encoders.

Tian, F. et al. [38], presented a specific solution to solve the problems of polishing on curved surfaces, their objective was to control the polishing forces through a platform with flexible abrasive tool, which in conjunction with the control of the robot allows polished mirror quality. On the other hand, Barnfather, J.D. et al. [39], investigated the compensation of dimensional errors through data from a cloud of points using optical scanners. They showed an efficient method that can perform an inspection of the cloud of points, which were aligned with the cutting coordinates and was used to compensate the trajectory. Their results improved dimensional errors by 96%.

Finally, the work of Denkena, B. et al. [40] focused on a new robot design that had enough stiffness to withstand the forces of machining. After evaluating several designs, they concluded that a mixture of robot arm with conventional machine is the best combination to face the machining tasks. All these proposals are good for a specific case, but they do not solve the general problem of robotic machining.

2.4. Future Works

Analysing the advances obtained in robotic machining, it has not yet been possible to unify a procedure or methodology that can be used for more than one machining operations. We believe that the cutting force and robot stiffness modelling can be improved by using as a basis the proposal of Cen L. et al.

The problem of programming robot arms for machining processes continues, even though, certain attempts have been made to normalize the language. Also, there is no complete development of special equipment for robotic machining, as there could be the creation of specific spindles or sensors with low weight.

The study of the advances in the area is the first step to direct the future work. The authors want to evaluate the capacity and feasibility of industrial robot arms and collaborative robot arms for their use in machining operations with soft materials by proposing modifications in their control to convert it into an adaptive control and improve its behaviour in machining operations. The objective of our work will be (1) Characterize the machining processes with industrial and collaborative robot arm, (2) Study the dynamics and control of robot arms and propose the appropriate modifications to convert them into an adaptive control and (3) Evaluate technically and economically the application of sensor elements and control methods to be integrated into machining processes with robotic arms.

2.5. Conclusions

Robotic machining has several specific problems and multiple heterogeneous contributions by different authors. The aim of this article has been to clarify the concepts and understand better the problems. We have proposed a review of the theoretical background, as well as the state of art about recent research and developments related to robotic machining. Despite the great advances of the last decade, there is still a long way to go until robotic machining is widely used in industry.

The advances reviewed show us that robots have the full capacity to be improved to deal with these new operations. Not only can the new robot designs be improved by having a better understanding of the process. these advances could give a second life to the robots that are in multiple companies performing their typical tasks. If the industrial robots were able to provide accurate positions under contact situations in the same way as their well-known good repeatability, robotic machining could be a very significant improvement for many applications.

The best way to control the accuracy of the machining operations performed by robot arms seems to use a method that considers the torque generated. The control system for the robot arm needs to have feedback of the dynamic to prevent damages in their joints and engines and to achieve the required accuracy.

The authors suggest studying certain areas of robot machining that have not been developed completely (modelling and programming of robotic machining), as

well as the proposal to evaluate and demonstrate the feasibility of the process with the aim of this being applied to multiple machining operations. Possibly, the main contribution of this article is to restructure a field which has so many different problems and varies approaches to the solutions.

2.6. References

1. Robotics, W. Executive Summary World Robotics 2017 Industrial Robots. *World Robot. Rep.* **2017**, 15–24.
2. Chen, Y.; Dong, F. Robot machining: recent development and future research issues. *Int. J. Adv. Manuf. Technol.* **2013**, *66*, 1489–1497, doi:10.1007/s00170-012-4433-4.
3. Iglesias, I.; Sebastián, M. a.; Ares, J.E. Overview of the State of Robotic Machining: Current Situation and Future Potential. *Procedia Eng.* **2015**, *132*, 911–917, doi:10.1016/j.proeng.2015.12.577.
4. Klimchik, A.; Ambiehl, A.; Garnier, S.; Furet, B.; Pashkevich, A. Efficiency evaluation of robots in machining applications using industrial performance measure. *Robot. Comput. Integr. Manuf.* **2017**, *48*, 12–29, doi:10.1016/j.rcim.2016.12.005.
5. Pan, Z.; Zhang, H.; Zhu, Z.; Wang, J. Chatter analysis of robotic machining process. *J. Mater. Process. Technol.* **2006**, *173*, 301–309, doi:10.1016/j.jmatprotec.2005.11.033.
6. Hui Zhang; Jianjun Wang; Zhang, G.; Zhongxue Gan; Zengxi Pan; Hongliang Cui; Zhenqi Zhu Machining with flexible manipulator: toward improving robotic machining performance. In Proceedings of the Proceedings, 2005 IEEE/ASME International Conference on Advanced Intelligent Mechatronics.; IEEE, 2005; pp. 1127–1132.
7. Cen, L.; Melkote, S.N. Effect of Robot Dynamics on the Machining Forces in Robotic Milling. *Procedia Manuf.* **2017**, *10*, 486–496, doi:10.1016/j.promfg.2017.07.034.
8. Caro, S.; Dumas, C.; Garnier, S.; Furet, B. Workpiece placement optimization for machining operations with a KUKA KR270-2 robot. In Proceedings of the

2013 IEEE International Conference on Robotics and Automation; IEEE, 2013; pp. 2921–2926.

9. Pan, Z.; Zhang, H. Robotic machining from programming to process control: a complete solution by force control. *Ind. Robot An Int. J.* **2008**, *35*, 400–409, doi:10.1108/01439910810893572.
10. Guo, Y.; Dong, H.; Ke, Y. Stiffness-oriented posture optimization in robotic machining applications. *Robot. Comput. Integr. Manuf.* **2015**, *35*, 69–76, doi:10.1016/j.rcim.2015.02.006.
11. Abele, E.; Weigold, M.; Rothenbücher, S. Modeling and identification of an industrial robot for machining applications. *CIRP Ann. - Manuf. Technol.* **2007**, *56*, 387–390, doi:10.1016/j.cirp.2007.05.090.
12. Pashkevich, A.; Klimchik, A.; Chablat, D. Enhanced stiffness modelling of manipulators with passive joints. *Mech. Mach. Theory* **2011**, *46*, 662–679, doi:10.1016/j.mechmachtheory.2010.12.008.
13. Chen, S.F.; Kao, I. Conservative congruence transformation for joint and Cartesian stiffness matrices of robotic hands and fingers. *Int. J. Rob. Res.* **2000**, *19*, 835–847, doi:10.1177/02783640022067201.
14. Dumas, C.; Caro, S.; Garnier, S.; Furet, B. Joint stiffness identification of six-revolute industrial serial robots. *Robot. Comput. Integr. Manuf.* **2011**, *27*, 881–888, doi:10.1016/j.rcim.2011.02.003.
15. Olofsson, B. Topics in Machining with Industrial Robot Manipulators and Optimal Motion Control, Department of Automatic Control, Lund University, 2015.
16. Tyapin, I.; Hovland, G.; Kosonen, P.; Linna, T. Identification of a static tool force model for robotic face milling. In Proceedings of the 2014 IEEE/ASME 10th International Conference on Mechatronic and Embedded Systems and Applications (MESA); IEEE, 2014; pp. 1–6.
17. Lehmann, C.; Halbauer, M.; Euhus, D.; Overbeck, D. Milling with industrial robots: Strategies to reduce and compensate process force induced accuracy influences. In Proceedings of the Proceedings of 2012 IEEE 17th International Conference on Emerging Technologies & Factory Automation (ETFA 2012); IEEE, 2012; pp. 1–4.

18. Rosa, D.G.G.; Feiteira, J.F.S.; Lopes, A.M.; de Abreu, P.A.F. Analysis and implementation of a force control strategy for drilling operations with an industrial robot. *J. Brazilian Soc. Mech. Sci. Eng.* **2017**, *39*, 4749–4756, doi:10.1007/s40430-017-0913-7.
19. Zhang, H.; Pan, Z. Robotic machining: material removal rate control with a flexible manipulator. In Proceedings of the 2008 IEEE Conference on Robotics, Automation and Mechatronics; IEEE, 2008; pp. 30–35.
20. Sörnmo, O.; Olofsson, B.; Robertsson, A.; Johansson, R. Increasing Time-Efficiency and Accuracy of Robotic Machining Processes Using Model-Based Adaptive Force Control. *IFAC Proc. Vol.* **2012**, *45*, 543–548, doi:10.3182/20120905-3-HR-2030.00065.
21. Chen, S.; Zhang, T. Force control approaches research for robotic machining based on particle swarm optimization and adaptive iteration algorithms. *Ind. Robot An Int. J.* **2018**, *45*, 141–151, doi:10.1108/IR-03-2017-0045.
22. Marchal, P.C.; Sörnmo, O.; Olofsson, B.; Robertsson, A.; Ortega, J.G.; Johansson, R. Iterative Learning Control for Machining with Industrial Robots. *IFAC Proc. Vol.* **2014**, *47*, 9327–9333, doi:10.3182/20140824-6-ZA-1003.00550.
23. Ilyukhin, Y.V.; Poduraev, Y.V.; Tatarintseva, A.V. Nonlinear Adaptive Correction of Continuous Path Speed of the Tool for High Efficiency Robotic Machining. *Procedia Eng.* **2015**, *100*, 994–1002, doi:10.1016/j.proeng.2015.01.459.
24. Klimchik, A.; Bondarenko, D.; Pashkevich, A.; Briot, S.; Furet, B. Compliance error compensation in robotic-based milling. In Proceedings of the Lecture Notes in Electrical Engineering; Springer, Cham, 2014; Vol. 283, pp. 197–216.
25. Garnier, S.; Subrin, K.; Waiyagan, K. Modelling of Robotic Drilling. *Procedia CIRP* **2017**, *58*, 416–421, doi:10.1016/j.procir.2017.03.246.
26. Brunete, A.; Gambao, E.; Koskinen, J.; Heikkilä, T.; Kaldestad, K.B.; Tyapin, I.; Hovland, G.; Surdilovic, D.; Hernando, M.; Bottero, A.; et al. Hard material small-batch industrial machining robot. *Robot. Comput. Integr. Manuf.* **2017**, *7*, 59–1, doi:10.1016/j.rcim.2017.11.004.
27. Huynh, H.N.; Verlinden, O.; Riviere-Lorphevre, E. Robotic Machining Simulation using a Simplified Multibody Model. In *Annals of DAAAM and Proceedings of the International DAAAM Symposium*; 2017; pp. 0885–0894 ISBN 9783902734112.

28. Zivanovic, S.; Slavkovic, N.; Milutinovic, D. An approach for applying STEP-NC in robot machining. *Robot. Comput. Integr. Manuf.* **2018**, *49*, 361–373, doi:10.1016/j.rcim.2017.08.009.
29. Mousavi, S.; Gagnol, V.; Bouzgarrou, B.C.; Ray, P. Control of a Multi Degrees Functional Redundancies Robotic Cell for Optimization of the Machining Stability. *Procedia CIRP* **2017**, *58*, 269–274, doi:10.1016/j.procir.2017.04.004.
30. Mousavi, S.; Gagnol, V.; Bouzgarrou, B.C.; Ray, P. Stability optimization in robotic milling through the control of functional redundancies. *Robot. Comput. Integr. Manuf.* **2018**, *50*, 181–192, doi:10.1016/j.rcim.2017.09.004.
31. Zargarbashi, S.H.H.; Khan, W.; Angeles, J. Posture optimization in robot-assisted machining operations. *Mech. Mach. Theory* **2012**, *51*, 74–86, doi:10.1016/j.mechmachtheory.2011.11.017.
32. Lin, Y.; Zhao, H.; Ding, H. Posture optimization methodology of 6R industrial robots for machining using performance evaluation indexes. *Robot. Comput. Integr. Manuf.* **2017**, *48*, 59–72, doi:10.1016/j.rcim.2017.02.002.
33. Cen, L.; Melkote, S.N. CCT-based mode coupling chatter avoidance in robotic milling. *J. Manuf. Process.* **2017**, *29*, 50–61, doi:10.1016/j.jmapro.2017.06.010.
34. Vieler, H.; Karim, A.; Lechler, A. Drive based damping for robots with secondary encoders. *Robot. Comput. Integr. Manuf.* **2017**, *47*, 117–122, doi:10.1016/j.rcim.2017.03.007.
35. Olof, S.; Schneider, U.; Robertsson, A.; Puzik, A.; Johansson, R. High-Accuracy Milling with Industrial Robots using a Piezo-Actuated High-Dynamic Compensation Mechanism. *COMET* **2013**.
36. Mohammad, A.E.K.; Hong, J.; Wang, D. Design of a force-controlled end-effector with low-inertia effect for robotic polishing using macro-mini robot approach. *Robot. Comput. Integr. Manuf.* **2018**, *49*, 54–65, doi:10.1016/j.rcim.2017.05.011.
37. Möller, C.; Schmidt, H.C.; Koch, P.; Böhlmann, C.; Kothe, S.-M.; Wollnack, J.; Hintze, W. Machining of large scaled CFRP-Parts with mobile CNC-based robotic system in aerospace industry. *Procedia Manuf.* **2017**, *14*, 17–29, doi:10.1016/j.promfg.2017.11.003.

38. Tian, F.; Lv, C.; Li, Z.; Liu, G. Modeling and control of robotic automatic polishing for curved surfaces. *CIRP J. Manuf. Sci. Technol.* **2016**, *14*, 55–64, doi:10.1016/j.cirpj.2016.05.010.
39. Barnfather, J.D.; Abram, T. Efficient compensation of dimensional errors in robotic machining using imperfect point cloud part inspection data. *Measurement* **2018**, *117*, 176–185, doi:10.1016/j.measurement.2017.12.021.
40. Denkena, B.; Bergmann, B.; Lepper, T. Design and optimization of a machining robot. *Procedia Manuf.* **2017**, *14*, 89–96, doi:10.1016/j.promfg.2017.11.010.

Capítulo 3

Design and Manufacturing of an Ultra-Low-Cost Custom Torque Sensor for Robotics

sensors

MDPI

Article

Design and Manufacturing of an Ultra-Low-Cost Custom Torque Sensor for Robotics

Rodrigo Pérez Ubeda [1,*], Santiago C. Gutiérrez Rubert [1], Ranko Zotovic Stanisic [2] and Ángel Perles Ivars [3]

[1] Department of Mechanical and Materials Engineering, Universitat Politècnica de València, Valencia 46022, Spain; scgutier@mcm.upv.es
[2] Department of Systems Engineering and Automation, Universitat Politècnica de València, Valencia 46022, Spain; rzotovic@isa.upv.es
[3] Department of Computer Systems and Computation, Universitat Politècnica de València, Valencia 46022, Spain; aperles@disca.upv.es
* Correspondence: rodpeub@doctor.upv.es; Tel.: +34-96-387-7622

Received: 23 April 2018; Accepted: 30 May 2018; Published: 1 June 2018

check for updates

Pérez Ubeda, R., Gutiérrez Rubert, S. C., Zotovic Stanisic, R., & Perles Ivars, Á. (2018). Design and Manufacturing of an Ultra-Low-Cost Custom Torque Sensor for Robotics. Sensors, 18(6), 1786. https://doi.org/10.3390/s18061786

Design and Manufacturing of an Ultra-Low-Cost Custom Torque Sensor for Robotics

Rodrigo Pérez Ubeda [1,*], Santiago C. Gutiérrez Rubert [1], Ranko Zotovic Stanisic [2] and Ángel Perles Ivars [3]

[1] Department of Mechanical and Materials Engineering, Universitat Politècnica de València, Valencia 46022, Spain.
[2] Department of Systems Engineering and Automation, Universitat Politècnica de València, Valencia 46022, Spain.
[3] Department of Computer Systems and Computation, Universitat Politècnica de València, Valencia 46022, Spain.
[*] Correspondence: rodpeub@doctor.upv.es.

Abstract

This article describes a new, very low-cost torque sensor. It was designed to obtain a geometric shape suitable for very affordable manufacturing by machining. The torque sensor was developed under the principle of measurement by strain gauges. It has been designed in order to make manufacturing operations as simple as possible. Optimization was achieved through finite element analysis. Three test sensors for 1, 5, and 20 Nm were designed and machined. Calibration of the three sensors has been carried out obtaining excellent results. An analysis of the dimensional quality of the product and associated costs demonstrates that manufacturing is possible with very simple machining operations, standard tools, and economic equipment.

Keywords: torque sensor; design of sensors; manufacturing of low-cost sensors.

3.1. Introduction

Robot arms have been used in industry for more than five decades in applications such as automotive, electronics, and shipbuilding [1,2]. The "classic" robot arms are not oriented for interaction with humans. Nevertheless, the new generations of robots, like collaborative [3], lightweight, exoskeletons, do make controlled contact with humans. This requires modifications in their design in order to include devices that allow for this. For these applications, it is very useful to be able to measure forces and torques. The possibility to measure and control these variables increases the applicability of robots, enabling improved operation and performance while enhancing the safety of their respective activities [2–5]. In addition, providing precise torque values is a key factor for dynamic decoupling and control of the force-movement of robotic arms [6].

Thus, measurement and estimation of force and torque are key components of a collaborative robot. The expansion of robotic applications, the growth of new demands, and the high cost of commercial sensors have brought an active development of force and torque sensors, with different configurations and applications [1,7].

Commercial six degrees of freedom (6-DOF) force/torque sensors may cost more than €4000 [8,9], and those for torque only (one degree of freedom) are between €1400 and €3000 [10,11]. However, the use of the latter ends up being more expensive since more units are needed in the robot.

While current sensors offer good characteristics, they are not simple to manufacture, an issue that has yet to be addressed despite having been considered as one of the primary design requirements detailed by Hirzinger, G. et al. [12] in their first work on force/torque sensors.

An analysis of the costs of the other components that do not comprise the elastic element indicates that these are very economic, with a general cost of less than €100. This indicates that the process of manufacturing complex geometries for elastic elements raises the production costs of the sensor. Due to this reason, the objective of this project was to develop a uniaxial sensor, designed via favourable geometry, from the point of view of manufacture by machining in order to reduce costs as much as possible while maintaining the performance.

In general, two types of sensors may be found inside a robot—those that are located at the end effector (Figure 3.1a), which are complex sensors comprising six force and torque components, and those located in the joints of the robot (Figure 3.1b), which are purely torsional sensors [2]. The latter, being integrated in the joints, enable application of advanced control methods for joint torque control, vibration damping, and stiffness control [13]. Torque sensors are widely used in arms intended for assistance for the disabled [14] and since customized, economical designs are required, custom manufacturing is necessary in order to obtain the desired characteristics.

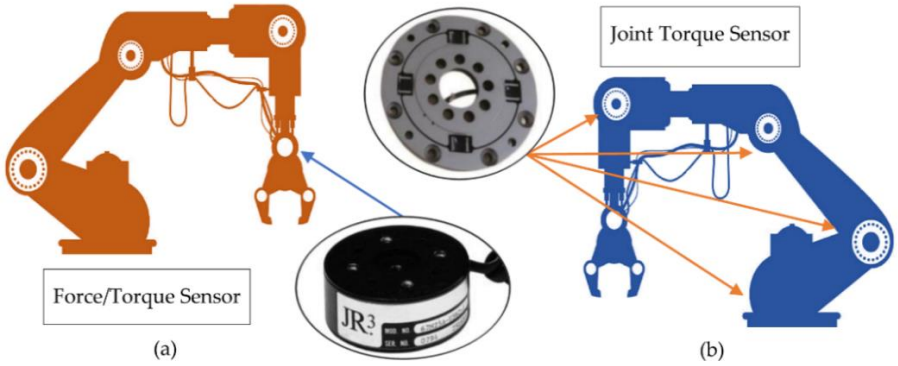

Figure 3.1. Use of sensors in a robotic arm, (a) single force and torque sensor located in the manipulator, (b) torque sensors arranged in each joint of the robot arm.

From the point of view of application, force/torque sensors are used in industry to control the interaction force between the robot and the environment for tasks such as polishing, deburring, engraving, etc.

Force/torque sensors are usually comprised of six components (6-DOF) and require relatively complex geometries, which complicates manufacturing and results in increased costs. On the other hand, their main limitation is that they detect force/torque in the end effector.

In contrast, a lightweight and collaborative robot must be able to react if any of its links come intocontact with an unexpected object. For this reason, it is necessary that each joint is equipped with itsown sensor. However, these may be torque sensors with one degree of freedom and may be designedwith much simpler and more economical geometries.

As an example, some force/torque and torque-only sensors are shown in Figure 3.2. The work ofMa, J. and Song, A. [15] (Figure 3.2a) represents the typical 6-DOF force/torque, consisting of an elastic bodycontaining crossbeams.

Sun, Y. et al. [4] developed a 6-DOF sensor for a spatial robot used in the Chinese space station.Its elastic body with crossbeams is shown in Figure 3.2b. It has slim beams not completely solid, with cavities, as main feature. This allows to concentrate the stresses to obtain better sensitivity.

Liang, Q. et al. [16] proposed the design of a sensor based on a more complex geometry called E-type membrane, or EE (Figure 3.2c). This sensor enables the measurement of the six components of force and torque with a low degree of coupling, but with the great disadvantage of requiring a laborious and complex design and, therefore, high manufacturing cost.

Wu, B. and Cai, P. [17] developed a more complex 6-DOF sensor by assembling three different parts. They called this design "Sliding structure". The sensor may be appreciated in Figure 3.2d. It has two independent elastic elements, assembled to the external ring through a top and a bottom cover. A better decoupling is obtained by dividing the measurement between two elastic elements.

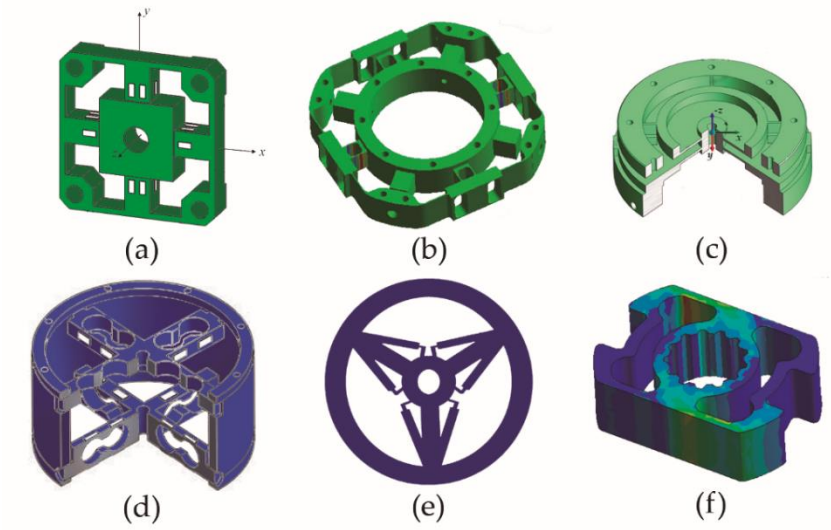

Figure 3.2. Types of force/torque sensor structures: (a) Crossbeam, (b) Crossbeam modified, (c) Body E-type membrane (EE) (d) Sliding structure, (e) Four-bar linkage shape, (f) Square cube.

Zhang, H. et al. [2] proposed a design of a torque sensor based on the crossbeams type, but with a four-bar link shape (see Figure 3.2e). It has high sensitivity without loss of stiffness. Despite these good features, their design is very complex to manufacture causing an increase of the price.

Figure 3.2f represents another example of geometry used for a torque sensor, such as that detailed by Khan, H. et al. [18], presenting a design called Square Cube that greatly facilitates the installation of strain gauges. However, it increases the complexity of the elastic element, as well as the manufacturing costs.

The previous examples show how the geometry of the elastic body is becoming more and more complex in order to obtain a better performance of the sensor. This article proposes a simple geometry uniaxial sensor allowing for the reduction of manufacturing costs.

The article is structured as follows: Section 3.2 presents the design methodology, materials, and analysis of design and manufacturing requirements; Section 3.3 shows the results and discussion of the design and manufacture of the sensor, corresponding calibration, and cost analysis; finally, the conclusions are presented in Section 3.4.

3.2. Design Methodology

The elastic element is the most expensive part, having to comply with the specifications of torque and dimensions required for the target application. For that reason and before this manufacturing, its behaviour was validated through finite element analysis in SolidWorks Simulation (Computer Aided Engineering, CAE, application).

To obtain an economic sensor, complex geometries which require elaborate cutting operations and special tools must be avoided since they increase manufacturing time and require numerical control programs for machine tools capable of achieving this level of complexity.

Bearing in mind the ease of machining and understanding that the value of dimensional and geometric tolerances directly influences this concept, small variations have been introduced into the 3D models used in the CAE simulations in order to test how these variations affect the end functionality of the sensor. These

include variations in dimension, position of elements, and geometrics (flatness, parallelism, coaxiality, etc.). In this way, it is possible to establish the level of precision required during the manufacturing process.

3.2.1. Selection of material for elastic element

The material with which the elastic element of the sensor will be manufactured must comply with a series of characteristics, such as easy machining by chip removal, high sensitivity to applied torque, linear response deformation, low density, and fairly isotropic and homogeneous behaviour.

For the elastic element, aluminium or steel alloys are usually used. An analysis of the characteristics of these materials indicates that the advantages of aluminium are better machinability and lower weight. In contrast, the advantages of steel are greater Young's modulus and elastic limit.

In the articles referenced [1,2,19,20], different authors have used different aluminium alloys. After evaluating several proposals, it was decided to use 7075-T6 aluminium alloy. Table 3.1 shows its main properties.

This aluminium alloy has very good characteristics such as modulus of elasticity, high elastic limit, and very easy machining, comparable to the characteristics of some steels, which allows support of high tension and deformation levels while maintaining a good safety factor against overload.

Table 3.1. Mechanical Properties: Aluminium 7075-T6

Property	Density (g/cm3)	Young's Modulus (MPa)	Poisson's Ratio	Yield Strength Sy (MPa)	Ultimate Strength Su (MPa)
Value	2.80	71.7	0.33	503	572

Although the aluminium is more expensive than steel, the price difference is negligible for such small lightweight sensors. Finally, aluminium has been chosen as it presents a good combination of benefits and price.

Since one of the goals is to obtain a parametric design valid for sensors of various sizes (this report details testing for 1, 5, and 20 Nm), a maximum diameter of 65 mm and thickness of 10 mm were used as initial requirements. These dimensions are in strict accordance with available standard dimensions of raw

materials—in this case, for cylindrical bars. Once again, this results in a reduction of costs. In addition, these values correspond to those acceptable for the real requirements of a collaborative robot arm prototype in which the sensors will be applied. It should be noted that the proposed method is valid for any other dimension or torque requirements.

3.2.2. Analysis of design requirements

In the search for a single simple design for the elastic element of the sensor, the most common geometries were analysed within the sensors that use strain gauges. Zhang, H. et al. [2] and Aghili, F. et al. [21] studied the most common types of elastic elements used in torque sensors, which may be seen in Figure 3.3.

The Solid and Hollow Cylinders (Figure 3.3 a, b) are simple, rigid structures. However, they are sensitive to no torsional components. Thus, designs have evolved to other types of more complex geometries that minimize this effect while greatly increasing sensor sensitivity.

The most common type of elastic element is similar to the Hub-Sprocket (Figure 3.3 c) but with the inclusion of four beams or crossbars in its central body. This variant of the Hub-Sprocket is known as the Maltese Cross.

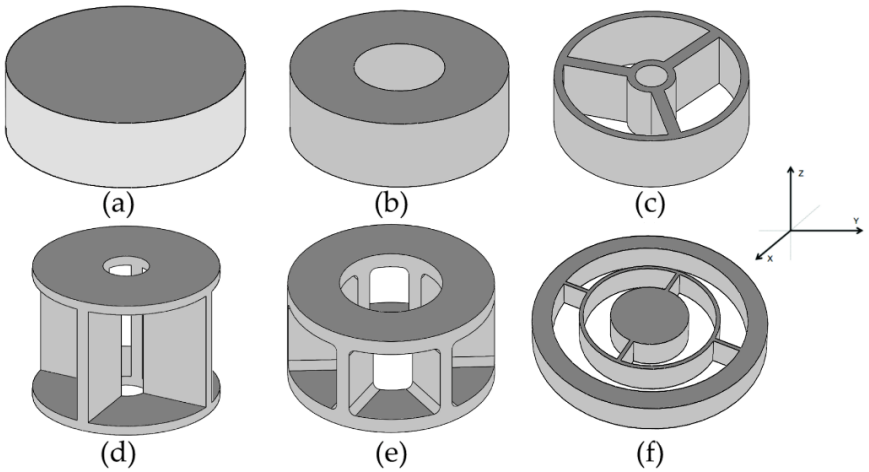

Figure 3.3. Types of torque sensor structures with gauges: (a) Solid Cylinder, (b) Hollow Cylinder, (c) Hub-Sprocket (d) Hollow Cruciform, (e) Hollow Hexaform, (f) Spoke Topology. [2].

Ma, J. and Song, A. [15]; Kim, G.-S. et al. [22], and Kim, Y.G. et al. [23] designed three- and six-component sensors using crossbeam geometry. These sensors have good rigidity but low isotropy and a high degree of coupling, which is why other researchers modified their characteristics to improve performance [19]. Although the Hub-Sprocket topology sensor has lower performance compared to more complex ones, such as the "E-type membrane", its torque measurement is better since it enables greater sensitivity. This makes it one of the most commonly used geometries to measure torque component Mz (see Figure 3.4a) and it is favoured even more considering that its geometry is not one of the most complex, thus enabling easier manufacture.

The Hollow Cruciform design (Figure 3.3d) is used in commercial torque sensors. This sensor has good sensitivity, but the stiffness is low and no torsional torques are high. The Hollow Hexaform sensor (Figure 3.3e) is similar in its basic geometry to the Hollow Cruciform. However, due to the increased number of wing pairs and the shorter height, the Hollow Hexaform sensor is stiffer and more sensitive. Finally, torque sensors with Spoke Topology (Figure 3.3f) provide high sensitivity but the lack of stiffness introduces a joint angle error.

Considering the characteristics observed, it was concluded that the development of a single simple geometry for the design of the sensor using the Hub-Sprocket typology could reduce manufacturing costs, thus obtaining an economic, lightweight, customized torque sensor (for a specified torque with required dimensions) that facilitates proper performance.

3.2.3. Selection and arrangement of strain gauges

The Hub-Sprocket topology with four beams was selected, in which four gauges will be installed. Two gauges will be placed in one of the four beams (in each of its side walls) and the other two in the beam diametrically opposite. With this configuration, in each pair of gauges, one will work under compression and the other under tension. In this way, gain is multiplied by two and nonlinearity is reduced.

The Hub-Sprocket type geometry is characterized by deformation of its beams. Deformation acts in the same way as in a recessed beam (Figure 3.4a), enabling use of uniaxial gauges to measure torque, as shown in Figure 3.4b. Since there are four

beams, two will be used to attach the four gauges, forming a complete Wheatstone bridge, which facilitates the best measurements [24].

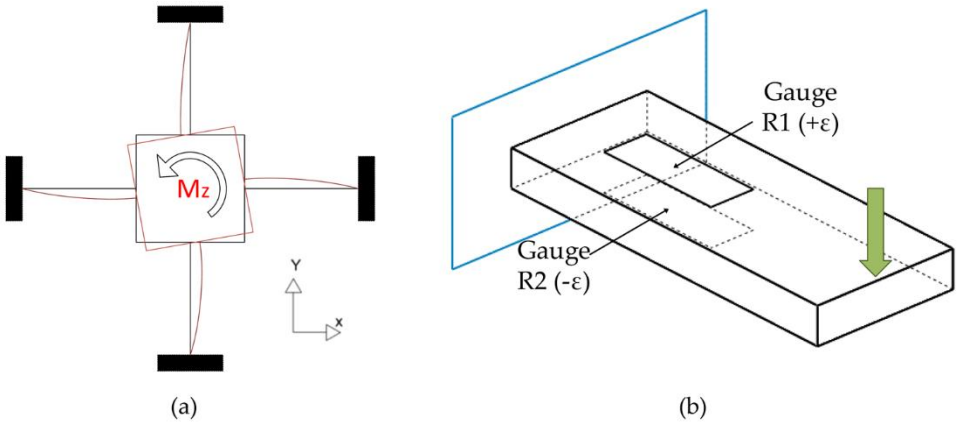

Figure 3.4. Hub-Sprocket Geometry: (a) Beam deformation; (b) Attachment of gauges

The strain gauges used are models KFH-6-120-C1-11L1M2R and KFH-6-350-C1-11L1M2R, supplied by the company Omega [25], whose characteristics are summarized in Table 3.2. These uniaxial gauges have a cost of €8 per unit and good performance.

Table 3.2. Strain gauge specifications.

Parameters	Contents
Gauge Factor	2 ± 1%
Gauge Resistance	120 ± 0.35 % / 350 ± 0.35% Ω
Gauge Size	6 x 2 mm
Minimum Radius of Curvature	10 mm

The arrangement of the four gauges corresponds to that of a complete Wheatstone bridge, as shown in Figure 3.5.

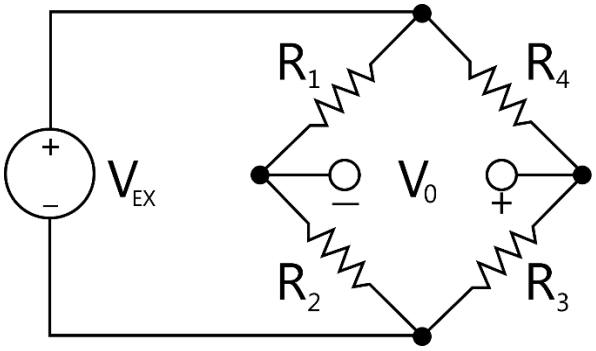

Figure 3.5. Complete Wheatstone bridge.

The equation that defines the Wheatstone bridge output [24] is,

$$\boldsymbol{V_0 = \left[\frac{R_3 - \Delta R_3}{R_3 - \Delta R_3 + R_4 + \Delta R_4} - \frac{R_2 + \Delta R_2}{R_1 - \Delta R_1 + R_2 + \Delta R_2}\right] V_{EX}} \quad \textbf{(3.1)}$$

where V_{EX} is input voltage and R_i the resistances of the gauges. In an ideal sensor, all gauges are equal, the dimensions of the elastic element are perfect, and each gauge is placed at the site of maximum deformation of the element. In this case, all the values are symmetric and therefore $R_1 = R_2 = R_3 = R_4 = R$ and $\Delta R_1 = \Delta R_2 = \Delta R_3 = \Delta R_4 = \Delta R = R \cdot GF \cdot \varepsilon_m$. Where R is the resistance of the gauge, GF is the gauge factor and ε_m is the measured strain. The bridge output voltage obtained in this case is,

$$\boldsymbol{V_0 = \left[-\frac{\Delta R}{R}\right] V_{EX} = -GF \cdot \varepsilon_m \cdot V_{EX}} \quad \textbf{(3.2)}$$

Due to dimensional errors and the location of the gauges, the variations obtained by each will be different, so that $\Delta R_1 \neq \Delta R_2 \neq \Delta R_3 \neq \Delta R_4$. In this case, the formula (1), expressed in accordance with strains, results as,

$$\boldsymbol{V_0 = \left[\underbrace{\frac{1}{2 + GF(\varepsilon_4 - \varepsilon_3)}}_{\text{A}} - \underbrace{\frac{GF}{2 + GF(\varepsilon_4 - \varepsilon_3)} \cdot \varepsilon_3}_{\text{B}} - \underbrace{\frac{1}{2 + GF(\varepsilon_2 - \varepsilon_1)}}_{\text{C}} - \underbrace{\frac{GF}{2 + GF(\varepsilon_2 - \varepsilon_1)} \cdot \varepsilon_2}_{\text{D}}\right] V_{EX}} \quad \textbf{(3.3)}$$

This expression has four addends, A, B, C and D, with a difference of strains in the denominator. Since the strains in this study are of the order of thousandths, their difference will not generate important errors in linearity, as any difference would be of thousandths, thus when dividing 1 by this value, no significant numerical

variation will result for the factors, A, B, C and D. The values from Figure 3.10 (see section 3.2) are substituted into equation (3) and reach approximately 0.499 for factors A and C, which would be annulled analytically, and 0.999 for factors B and D—the latter being a common factor for the difference in strain ($\varepsilon_3 - \varepsilon_2$). As will be seen in later analyses, the greater effect on the bridge output result is influenced by this difference in strain. In the following sections, the influence of manufacturing variations on these strains shall be analysed.

3.2.4. Manufacturing requirements and functional verification

Since the elastic element is metallic and given that its construction will be unitary, or of very few equal elements, machining is the most viable option. However, it is usually an expensive process, since it is possible to generate almost any geometry coordinating simultaneously the movements of several axes of the machine. To reduce costs and avoid the use of expensive equipment, geometries are restricted to those that can be obtained with a single degree of freedom, i.e., cut feed movement of the tool along a single axis.

Only those machining operations will be used in which the cut feed is along the Z axis of the machine, according to ISO-841, as in the case of drilling, reaming, threading, etc. Considering these restrictions, Figure 3.6 shows some of the geometric alternatives considered for the design of a 1 Nm sensor, with their corresponding finite element analyses to determine the value of deformations resulting in each of the proposals.

The analysis showed stresses (Figure 3.6, upper blue image) and strains (Figure 3.6, lower image) when loading the sensor through four central holes of small diameter, where it is connected to the joint axis, with a torque of 1 Nm along the Z axis. The body of the sensor is tied to the device, i.e. robot arm, using its 8 outermost holes of small diameter. The lower part of Figure 3.6 shows the maximum stresses obtained from each geometry when applying the resulting torque and the micro strains.

As can be seen in the results of Figure 3.6, design alternative (d) had the greatest strains when a torque of 1 Nm was applied. The main characteristic of this alternative is the hollowing of the structure by means of four drills with a diameter of 23.5 mm, which comprise the four crossbeams (Hub-Sprocket geometry). Gauges

shall be installed in areas of maximum deformation: red for tension and blue for compression. The way to pass the required wires will be through the central hole. The curved area, where the gauges will be attached, is compatible with the minimum radius of curvature allowed by the gauges, according to their specifications (Table 3.2).

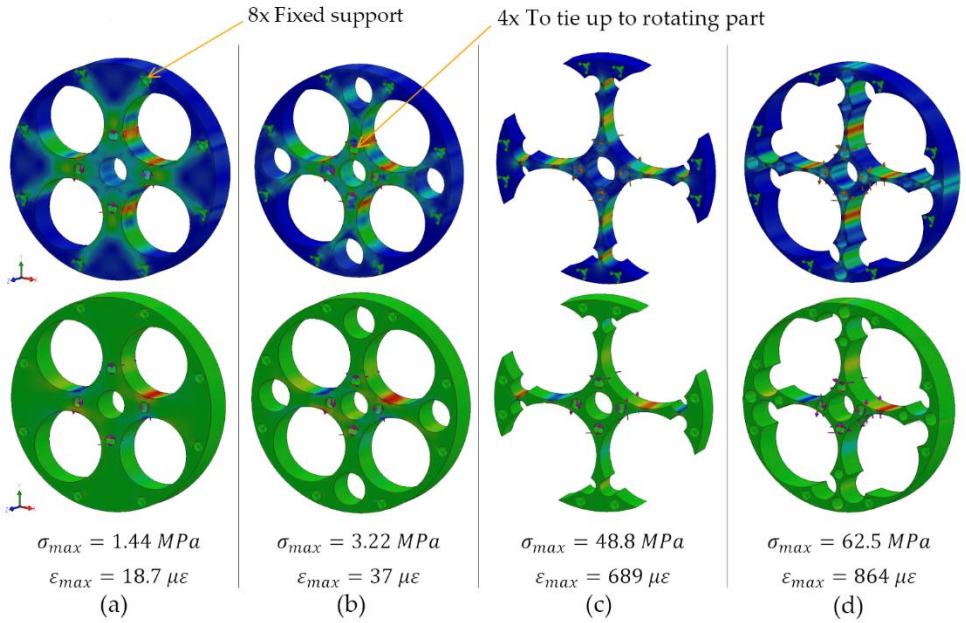

Figure 3.6. Example of different geometries, (a–d) with the results of CAE analysis.

3.2.5. Analytical model

Next, an analytical model of the proposed design is included for a better understanding of the simulation results.

The proposed design is a variation of an elastic body with crossbeams. As the elastic body is symmetric about the X and Y axes, the analysis focused only on one crossbeam.

Under the effect of a moment, Mz, the curved crossbeam will deform, as shown in Figure 3.4. That means, the curved crossbeam is under a load of flexion along it. Due to the ties, the external ring of the elastic body is rigid, so the curved crossbeam is embedded by its right end. In its left end, where the torque is applied, the curved

crossbeam is free to rotate around the Z axis, but it does not have the freedom to shift since its union to the central node prevents shift. Thus, it is considered like a crossbeam embedded at one end and supported on the other end, as it is shown in Figure 3.7.

Crossbeams are commonly undetermined static structures. Therefore, it is necessary to use the principle of overlapping in order to determinate their reactions to external loads.

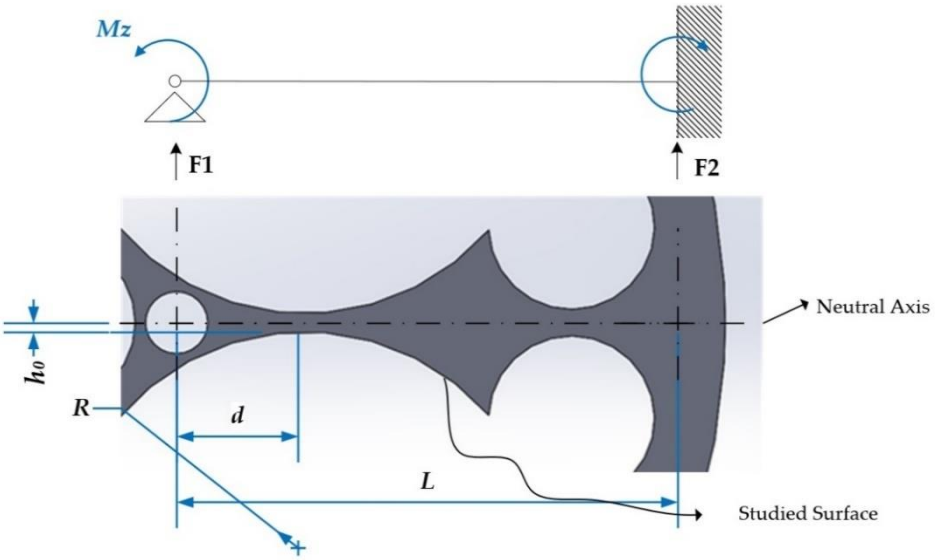

Figure 3.7. Mechanical model of an elastic body under Mz.

Once the reactions are defined, the bending moment, $M_f(x)$, acting on the curved crossbeam can be determined. This bending moment depends on the x location along the curved crossbeam. The stress, σ_x, and the strain, ε_x, on the surface of the curved crossbeam under the action of a torque (M_z) can be obtained as follows:

$$\boldsymbol{\sigma_x = \frac{M_f(x) \cdot C(x)}{I(x)} = \frac{3 \cdot M_z \cdot (3 \cdot x + L - 3 \cdot d)}{16 \cdot b \cdot L} \cdot \frac{1}{\left(h_0 + R - \sqrt{R^2 - x^2}\right)}} \quad \textbf{(3.4)}$$

$$\boldsymbol{\varepsilon_x = \frac{M_f(x) \cdot C_s(x)}{E \cdot I(x)} = \frac{3 \cdot M_z \cdot (3 \cdot x + L - 3 \cdot d)}{16 \cdot E \cdot b \cdot L} \cdot \frac{1}{\left(h_0 + R - \sqrt{R^2 - x^2}\right)}} \quad \textbf{(3.5)}$$

where $I(x)$ is the moment of inertia of the cross section and $C(x)$ is the distance from the neutral axis of the curved crossbeam to the studied surface. Both variables are related with the curved geometry of the surface. "b" is the thickness of the sensor, L is the crossbeam length, R is the radius of the circumference that define the studied surface, d is the distance from the center of the circumference to the end of the crossbeam, E is the material elasticity module, and h_0 is the minimum height of the crossbeam. Figure 3.8 presents two of the cases analysed by finite elements.

The first curve $\varepsilon_1(x)$, shown in blue in the Figure 3.8, corresponds with the sensor that has only big size holes, as in Figure 3.6 A, where can be seen in red and blue the compression (down part of the blue curve) and tension (up part of the blue curve) effects on the same face of the crossbeam. The second curve $\varepsilon_2(x)$, shown in black in Figure 3.8, represents the case similar to Figure 3.6 D, that include other small size holes in order to increase the length of the crossbeam and thus the strain on the narrower zone.

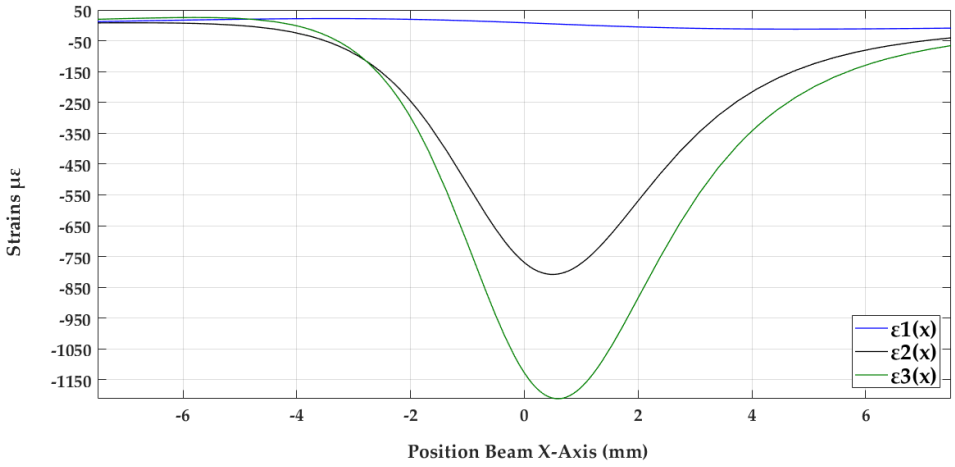

Figure 3.8. Behaviour strain of the elastic bodies with geometries A and D.

The last curve, $\varepsilon_3(x)$, shown in green in Figure 3.8, represents an optimizing of the geometry Figure 3.6 (d). The optimized design is achieved decreasing the parameter b, and increasing the parameter R of the proposed sensor.

3.3. Results and discussion

Following the steps of the point above, the results obtained from the manufacture of three sensors and the steps carried out to achieve them are displayed below.

3.3.1. Design optimization

The way to increase deformations to the desired value of 1000 με, an acceptable value measured via gauges, was achieved through small design modifications, such as reducing its thickness to 6 mm and verifying its influence using new simulations. The use of finite elements allow to obtain the optimized design.

During this process, the objective was to homogenize and standardize the size of drills and positions, reducing the number of required tools, while ensuring market viability. For example, a hole of diameter 10.43 mm should be modified to 10.5 mm to facilitate the purchase of the tool at a reduced price.

Figure 3.9 shows the final design of the elastic element of the 1 Nm torque sensor and results after analysis.

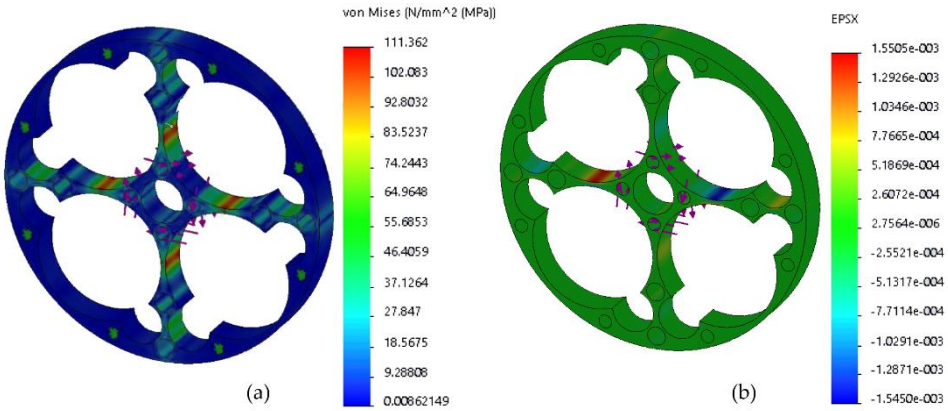

Figure 3.9. Finite element analysis: (a) Stress analysis; (b) Strain analysis.

The analysis yielded a maximum deformation of 1550.5 $\mu\varepsilon$ and a maximum Von-Mises stress equal to 111.362 MPa. This value exceeds the 1000 $\mu\varepsilon$ desirable, but as the strain gauge tends to average the measurement and considering that its length is greater than the area of maximum strain, it will measure high and medium strain

zones, so in the calibration process the value will be slightly reduced, being equally acceptable.

To evaluate the degree of coupling of the sensor, other finite element analyses are carried out considering different load directions. This will have a maximum coupling error of 10% if forces of 800 N are generated along the direction of the X or Y axis.

An analysis of the transverse sensitivity of the sensor, through deformations in the Z direction, indicated that the geometry design is beneficial, as the sensitivity decreases compared with that expected with a geometry composed of flat beams.

Finally, the analysis for the other sensors can be easily made by changing parameters in the initial design. Table 3.3 presents the maximum strain for the developed sensors.

Table 3.3. Strain of the sensors.

Torque Sensor	Maximum Strain
1 Nm	1550 με
5 Nm	2293 με
20 Nm	2384 με

3.3.2. Analysis of deviations in manufacturing

As a prior analysis to the manufacture of the elastic element, the possible effects on production with a drilling machine have been considered, since this device is very economical, albeit not very precise. For this reason, several variations were provided in the 3D model of the final design, with the intention of observing, through finite element analysis, the impact of these deviations on the result of strains and torque measurement.

On the other hand, possible measurement errors are classified into three types according to the resulting effects: offset, gain, and nonlinearity. If not excessive, offset errors are easy to correct, using software for example, and are mainly due to the electronic or mechanical setup of the sensor. Gain errors can be adjusted by weighting with external resistors to the bridge through the amplification system. The most serious error is non-linearity, because it cannot be easily corrected after the measurements.

Following, possible machining deviations are analysed because they could change strains and therefore induce measurement errors. It is important to emphasize that variations in strain ε_3 and ε_2 will have considerable influence when linearly is increasing or decreasing the final output of the voltage, equation (3.3). As an example, Figure 3.10 shows the result of the deformation analysis in the direction of the X axis, before the variations in size or position of the 8 mm drill, 23.5 mm drill, and the sensor width.

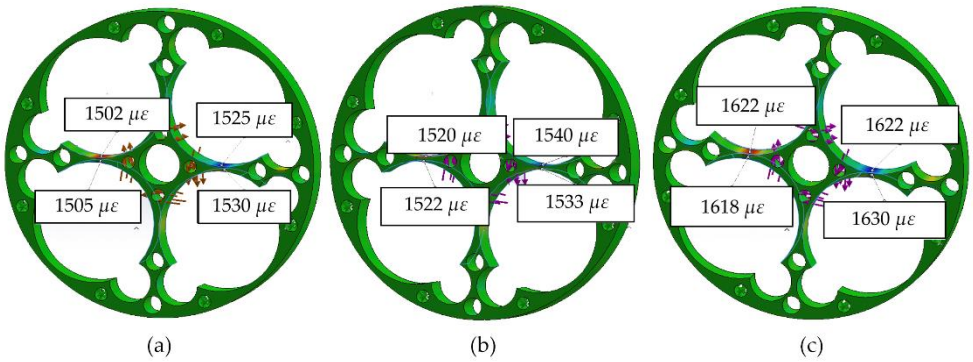

Figure 3.10. Strain variation in accordance with tolerance: (a) Location, (b) Size and (c) Flatness.

The comparing of the theoretical voltage output of the Wheatstone bridge with the ideal design is showed in Table 3.4. In conclusion, the relation voltage/torque may slightly change the offset and/or the slope, but they keep very good linearity, corroborating the good properties of the selected material.

Table 3.4. Voltage variation in accordance with manufacturing deviation.

Case	Machining deviation	Nominal dimension	Voltage output variation
Figure 3.10 (a)	Offset of +0.5 mm	Hole of Ø 8 mm located in the beams	-2%
Figure 3.10 (b)	Increase +0.5 mm in Ø	Big Hole of Ø 23.5	-1%
Figure 3.10 (c)	1° of surface inclination	Flatness (differences in thickness)	+4%

Through these results, it can be corroborated that the use of imprecise coarse operations with equipment, such as a drill for boring holes and a conventional saw for cutting thickness, has a very small effect on the results of measurement of the torque. Nevertheless, manufacturing tolerances will have to comply with the accepted limits to avoid those fluctuations and to guarantee the right assembly of the sensor.

3.3.3. Dynamic properties of the sensor

The identification of dynamic properties of the sensor was made with a finite elements model in SolidWorks Simulation.

A modal analysis was performed to obtain the dynamic response of the sensor to different input frequencies. The analysis was made in the condition of real work. The first six resonance frequencies are shown in Table 3.5.

Table 3.5. Resonance Frequencies

Mode	**1**	**2**	**3**	**4**	**5**	**6**
Responding Frequency (Hz)	5214.4	5668.9	12752	12773	13478	13589

In addition, a harmonic analysis was performed to identify and predict the dynamic behaviour of the sensor subject to harmonically varying loads. In Figure 3.11, the diagrams of the elastic deformation can be appreciated to verify if the design can withstand high frequency input torques without resonance.

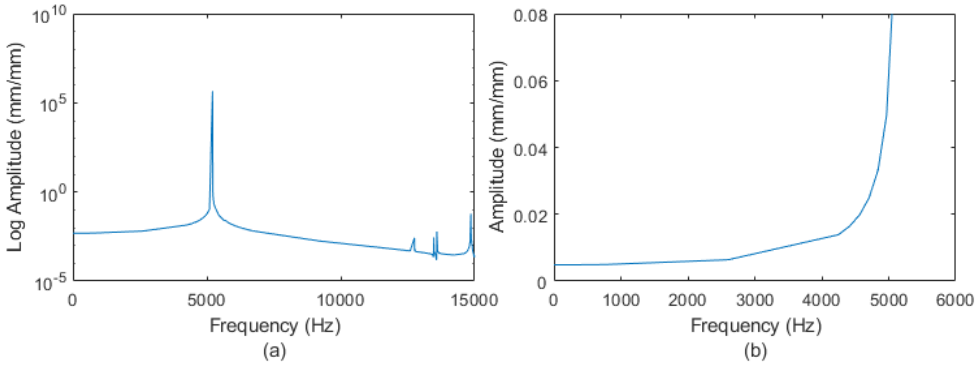

Figure 3.11. Harmonic response of the diagrams under the measuring of torque Mz.

Figure 3.11 (a) displays the frequency response and the first six resonance frequencies. Figure 3.11 (b) shows the frequency range between 0 and 5200 Hz, from which it can be concluded that the sensor bandwidth is between 0 to 2000 Hz. In this range, we can obtain a good precision of the results. For higher frequencies up to 4000 Hz, the sensor could be used if it is calibrated in depth. After this zone, control problems could appear due to the approach of the resonance frequency.

The simulation of a step input of 20 Nm was performed and the results before filtering are represented in Figure 3.12. It can be seen that the establishment time is 2 ms.

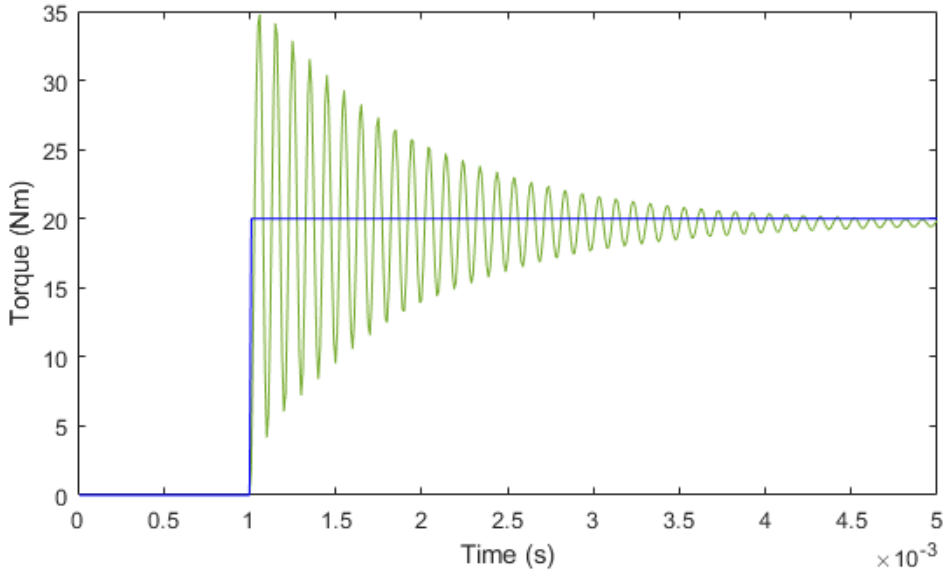

Figure 3.12. Time response of the sensor a step input de 20 Nm.

3.3.4. Manufacturing process

As the objective of the work is to reduce the manufacturing cost of the sensor, low-cost manufacturing operations, sawing, and drilling were tested. For this, basic equipment (or variations thereof) was used, as well as other equipment in order to improve the position of drilled holes.

These are:

- Conventional saw for metals (SABI-SM).

- Conventional column drill without manual control of the displacement of the bench where part is attached (INCO-3Z).
- Conventional column drill with manual control of the displacement of the bench where part is attached (Optium BF 20 Vario).
- Milling machine with position control in its bench (Kondia 500).

The base material was a 7075-T6 cylindrical billet with a diameter of 65 mm. A 6 mm thick section was cut from the billet using a manual saw. Sawing is a very economical and simple operation, and although it is not a precise method to obtain a flat face, this lack of precision has no effect, since the surface is mostly eliminated by drilling operations, as may be seen in the sensors shown in Figure 3.6.

For the most economical way to manufacture the sensor, a conventional drilling machine without position control would be used. However, lack of precise control in the positioning of drilling centres causes breakage in the resulting walls, as these are designed to be very thin due to the high sensor-sensitivity requirement.

As a second economical manufacturing alternative, a drill with position control in the bedplate was used (Figure 3.13 (a)), enabling manufacturing that prevents breakages but with a slightly increased cost. This type of machine may be found in most laboratories, or in the case of subcontracting the service, it has a very low machine hourly rate.

As a final alternative, and without discarding the idea of quick, simple operations, if greater automation is preferred, a CNC machine (computerized numerical control) may be used or subcontracted. Due to the type of operations to be carried out, it is not even necessary to prepare an NC program; the "Teach in" mode may be used directly to drill holes. This last alternative also has the advantage of a reduction of total production time and therefore costs; however, the higher hourly rate for this type of machine causes the final cost to increase slightly.

Testing of the milling process was satisfactory. Manufacturing times were low, and as the design and manufacture of the sensor were parameterized, the geometries for the other sensors were quickly obtained. The modifications were verified through finite element analysis and the manufacture of the 5 and 20 Nm sensors was carried out easily.

Figure 3.13 (a) shows a small manual control bench, the manufacturing process using a CNC milling machine with simple operations (Figure 3.13 (b)), and the result obtained for two of the three sensors (Figure 3.13 (c) and (d)).

A postprocess dimensional check on the three sensors showed that in no case are subsequent reaming operations required to improve the surface and dimensional finish of the holes, which has a favourable effect on cost. The final weight of the elastic elements is 17.34, 29.14, and 31.10 gr for the 1, 5, and 20 Nm sensors, respectively, proving that they fulfil the requirement of being lightweight.

Figure 3.13. Improvements in manufacturing (a) Manual control bench; (b) CNC milling machine; (c) Sensor 1 Nm; (d) Sensor 20 Nm.

3.3.5. Calibration procedure

To obtain the behaviour curve of the sensor, voltage vs. torque, a calibration process is required. In this process, a discrete set of weights will be applied to the sensor in order to obtain, through an electronic circuit, the corresponding variations in voltage. This procedure must be precise, economical, and easy to reproduce.

3.3.5.1. Calibration bench

Figure 3.14 shows the calibration bench developed to produce exclusively pure torque in order to ensure that only deformation resulting from the torque is detected by the strain gauges. This bench enabled static calibration of the sensor and was comprised of a main structure and an electronic calibration system.

The main structure was comprised of a metal base that supported the sensor and a lever and pulley symmetric system, which allowed two forces to be applied in opposite directions in order to generate pure torque, as outlined in Figure 3.14.

The electronic calibration system consisted of a signal amplifier, data acquisition system, and personal computer. The gauges were configured on a Wheatstone bridge, the output of which was routed to a Texas Instruments INA125P instrumentation amplifier. The calibration circuit supplied the Wheatstone bridge with a reference voltage of 2.5 V and 5 V for the bridges using gauges of 120 Ω and 350 Ω, respectively. This different voltage was due to the fact that, in the case of the sensor with gauges of 120 Ω, the INA125P was not capable of supplying the required current to provide a reference voltage of 5 V. In the case of gauges of 350 Ω, it did not present this effect. The bridge output signal, in mV, was amplified by the INA125P, with an average gain of 607 and 333 for the 1 and 20 Nm sensors, respectively, and routed to the acquisition system.

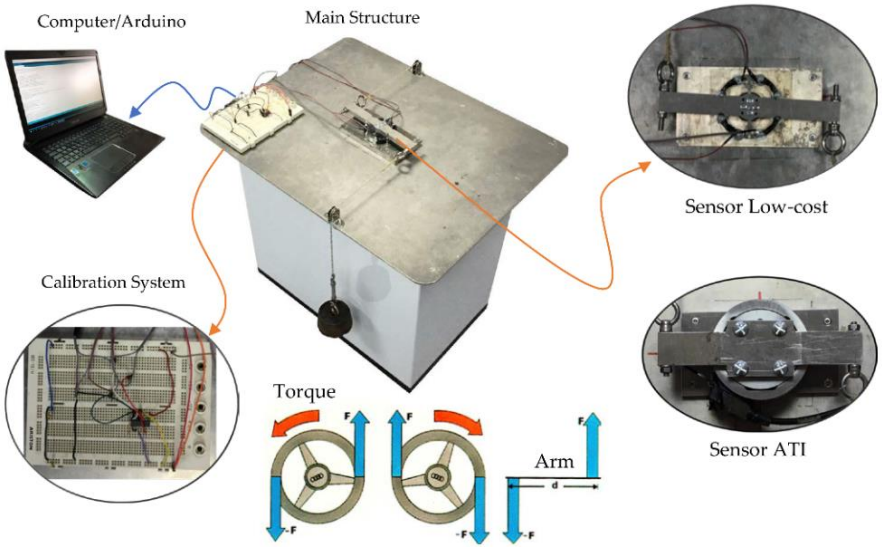

Figure 3.14. Calibration Bench.

The INA125P circuit was selected because it is an amplifier specially designed for Wheatstone bridges, containing an internal voltage stabilizer (voltage fluctuations are a potential source of error) and being of low cost. As will be seen later, the results were quite satisfactory. For the acquisition system, a simple Arduino Uno board was selected that incorporates a Microchip/Atmel ATmega328P microcontroller with a 10-bit AD converter. The Arduino board performed

conversions continuously and transmitted them through the USB output to a personal computer. The calibration bench was verified through of a commercial sensor ATI-Delta SI-330-30 (Figure 3.14). A maximum error of 0.23% F.S. was obtained in the torque measurement.

3.3.5.2. Calibration procedure

Prior to calibration, the gauges were carefully attached to the elastic element. Afterwards, the complete sensor was installed in the calibration bench. The Wheatstone bridge circuit, amplification system, and Arduino Uno controller are connected, as shown in Figure 3.15.

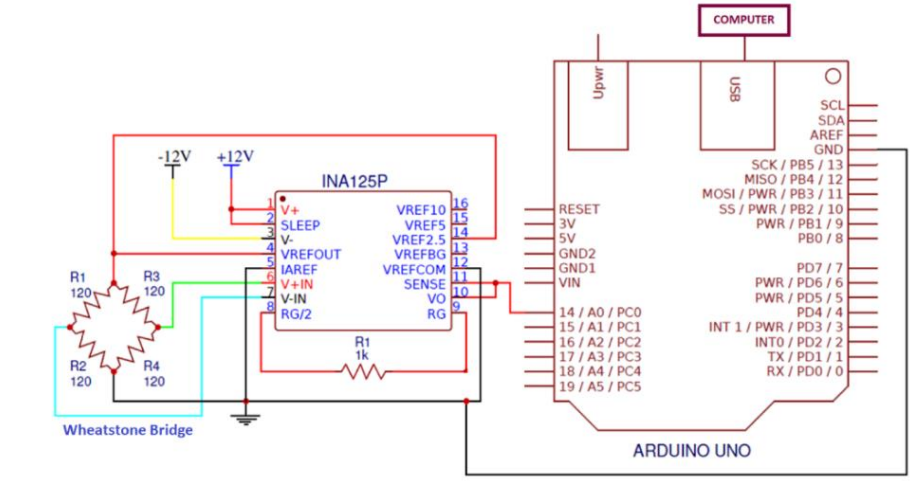

Figure 3.15. Calibration circuit.

Once the connections had been established, calibration was carried out by changing the weights supported by the sensor and capturing the output variations. For example, Figures 3.16 shows the graphs of the output voltage of the Wheatstone bridge versus applied torque for the 1 and 20 Nm sensors.

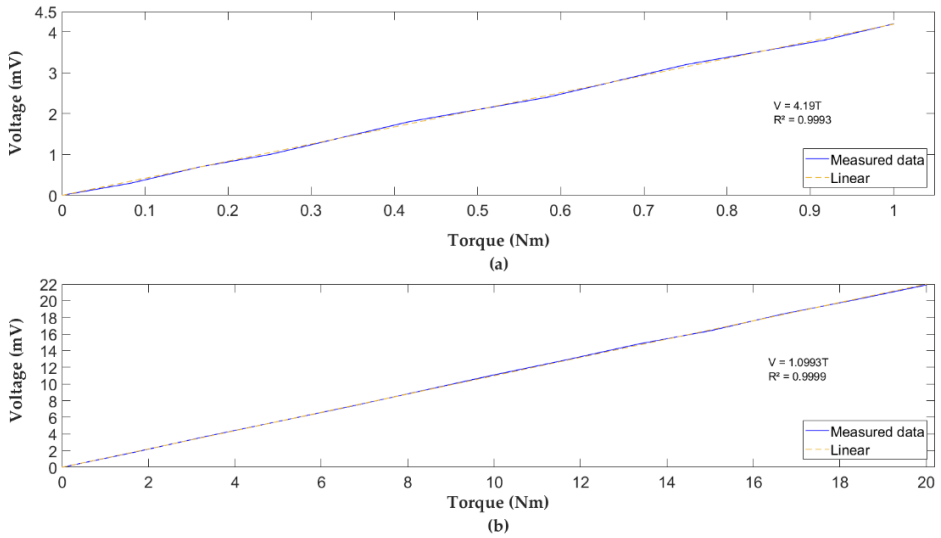

Figure 3.16. Graph bridge output voltage vs. applied torque: (a) 1 Nm Sensor, (b) 20 Nm.

For the 1 Nm sensor, loads of 0 to 0.6 Kg were applied with an increment of 0.05 Kg. In the case of the 20 Nm sensor, loads of 0 to 12 Kg were applied, with increments of 1 Kg. Both sensors had very good linearity (linear regression coefficient R2 near to 1). Obtaining the calibration line for both sensors enabled comparison of the calculated and applied torque. The results of the calibration of the sensors presented excellent results. These are shown in Table 3.6. It can be seen that the 1 Nm sensor has a linearity and measurement error more than the 20 Nm sensors. Instead, it has more sensitivity, better resolution, and better torsional stiffness.

Table 3.6. Calibration results

Sensor	Linearity Error (%F.S.)	Meas. Error (%F.S.)	Strain με	Sensitivity (mV/Nm)	Resolution (Nm)	Hysteresis Error (%F.S.)	Torsional Stiffness (10^6 Nm)
1 Nm	1.27	1.92	1004	4.19	0.002	3.54	3.57
20 Nm	0.61	1	2207	1.09	0.02	4.64	2.15

Table 3.7 allows one to compare the values of sensitivity and torsional stiffness with respect to a Hub-Sprocket sensor (four flat beams) with similar dimensions and

features. The geometry of curved beams presents a better performance for the sensor of 1 Nm and quite similar for the 20 Nm.

Table 3.7. Sensitivity and torsional rigidity for sensor type Hub-Sprocket.

Sensor	Sensitivity (mV/Nm)	Torsional Stiffness (10^6 Nm)
1 Nm	2.85	4.14
20 Nm	0.99	2.56

Although the calibration process is economical and enables good results, it is very susceptible to typical variations, such as electronic assembly sensitivity, mechanical friction of the pulley system at low weights, etc. Therefore, it is advisable to use proper components in order to prevent these problems.

3.3.6. Manufacturing costs

The cost analysis for the manufacture of the sensor, by drilling, milling and an external CNC company [26], are shown in Table 3.8.

Table 3.8. Manufacturing costs per machine type.

Concept	Labour costs	Total machinery costs	Total Cost
Drilling Sensor	€4.00	€20.00	€24.00
Milling Sensor	€10.00	€52.50	€62.50
CNC Milling sensor	External Manufacturing		€165.23

Labour costs correspond to the preparation of the machine tool. Machinery costs correspond to manufacturing costs, machining time, and tools used. It should be noted that the first two processes incur design costs, equal and constant for both, and therefore are not included in the calculation.

It should be taken into account that the manufacturing cost may vary depending on the country and many other factors. The prices shown are real in our context but indicative in other cases. On the other hand, the production of the type of sensors presented in this article is oriented to prototype or small series. In the case of a large series, an automatized production will lower the cost.

A sensor designed with a similar size Hub-Sprocket was developed in our facilities with a real cost of €183.6, which reinforces our hypothesis that simple operations reduce the manufacturing cost.

The cost of milling is twice the cost of drilling. Nevertheless, both costs in this proposal are low compared to that of commercial sensors. Development of the sensor is economical, thus manufacture by milling may be defined as "low cost" and manufacture by drilling as "ultra-low cost".

The total cost of the sensor, including manufactured parts, gauges, amplification electronics, and digital microcontroller system would be below €100.

3.4. Conclusions

Very important part of the cost is related to manufacturing (machining). Therefore, a more affordable and simpler form of production has been sought. All torque sensors currently available on the market have flat beams (Hub-Sprocket type) or complex geometries requiring more laborious operations. However, in this proposal, curved crossbeams were chosen in order to facilitate machine manufacture.

Drilling is much more affordable than milling. Thus, if the geometry of the sensor is adapted to be achievable with a drill, standard tools should be used to reduce costs drastically. However, for geometries with very thin wall thicknesses, positioning control is required, normally on the X and Y axes where drilling operations are carried out. In these cases, inclusion of a manual position control would suffice.

Finite element analysis of admissible geometric variations was crucial for the selection of machining equipment and operations that truly facilitated a considerable reduction of costs.

Moreover, the proposed calibration method enables manufactured sensors to be characterized and conditioned for operation in an easily reproducible manner.

It should also be noted that development of future sensors shall not exceed the values shown, since having parameterized the design, modification of dimensions and manufacturing of new elastic elements for different loads will be a much faster process.

The extension of the low-cost solution to multiaxis sensors could be possible only if the sensor was made by an assembled structure of parts and each part was made by simple machining operations. This would allow to reduce the cost compared to monolithic sensors with very complex geometries.

Summarizing, a torque sensor has been developed at a cost lower than those commercially available and with fully operational results. That way, any laboratory or research centre with simple machines can develop their own customized sensor to be used in their prototypes or small series, with a more affordable price.

In case the sensors are going to be commercialized, other associated costs should be kept in mind, such as costs related to packaging, advertisement, software, profit, etc. They are outside the scope of this article.

Author Contributions: Although in the full reviews all the authors have taken part, Ranko Zotovic Stanisic has been focused in the real use of the sensors in robot arms and the quality of calibration results. Santiago Gutiérrez Rubert worked in the influences of geometric variations at the machining process and type of operations to be used. Ángel Perles Ivars took part in the computer simulations and interpretation of the results. Rodrigo Pérez Ubeda acted as the link among different knowledge fields in order to achieve the implementation of real prototypes.

Funding: The authors are grateful for the financial support of the Spanish Ministry of Economy and European Union, grant DPI2016-81002-R (AEI/FEDER, UE).

Conflicts of Interest: The authors declare no conflict of interest.

3.5. References

1. Kang, M.-K.; Lee, S.; Kim, J.-H. Shape optimization of a mechanically decoupled six-axis force/torque sensor. *Sens. Actuators A Phys.* **2014**, 209, 41–51.
2. Zhang, H.-X.; Ryoo, Y.-J.; Byun, K.-S. Development of Torque Sensor with High Sensitivity for Joint of Robot Manipulator Using 4-Bar Linkage Shape. *Sensors* **2016**, 16, 991.

3. Jung, B.; Kim, B.; Koo, J.C.; Choi, H.R.; Moon, H. Joint Torque Sensor Embedded in Harmonic Drive Using Order Tracking Method for Robotic Application. *IEEE/ASME Trans. Mechatron*. **2017**, 22, 1594–1599.
4. Sun, Y.; Liu, Y.; Zou, T.; Jin, M.; Liu, H. Design and optimization of a novel six-axis force/torque sensor for space robot. *Measurement* **2015**, 65, 135–148.
5. Weng, S.; Xia, Z.; Deng, H.; Gan, Y.; Xiong, J. Design of an overload protection device for six-axis force/torque sensors. In Proceedings of the 2016 IEEE International Conference on Real-Time Computing and Robotics, RCAR 2016, Angkor Wat, Cambodia, 6–10 June 2016; pp. 239–242.
6. Kashiri, N.; Malzahn, J.; Tsagarakis, N.G. On the Sensor Design of Torque Controlled Actuators: A Comparison Study of Strain Gauge and Encoder-Based Principles. *IEEE Robot. Autom. Lett*. **2017**, 2, 1186–1194.
7. Sun, Y.-X.; Cao, H.-B.; Li, M.; Lin, R.-H.; Pan, H.-Q.; Shuang, F.; Gao, L.-F.; Ge, Y.-J. Design and calibration of a torque sensor based on sectional redundant measurements. In Proceedings of the 2015 IEEE International Conference on Information and Automation, Lijiang, China, 8–10 August 2015; pp. 262–267.
8. HBMshop. Available online: https://b2bstore.hbm.com/myHBM/ipc/applyConfiguration/(layout=7.0124_152_86_87_93_94_98_110_95_131&cScrollCharGroupName=%24BASE_GROUP&uiarea=2&xcm=hbm_ b2boccasionalcrm)/.do (accessed on 24 October 2017).
9. Futek MTA400-FSH01877 Tri-Axial Load Cell. Available online: https://shop.elkome.com/en/mta400- fsh01877-tri-axial-load-cell.html (accessed on 24 October 2017).
10. Futek TFF400-FSH02592 Reaction Torque Sensor. Available online: https://shop.elkome.com/en/tff400fsh02592-reaction-torque-sensor.html (accessed on 24 October 2017).
11. Honeywell Model 2102—National Instruments. Available online: http://sine.ni.com/nips/cds/view/p/ lang/es/nid/211865 (accessed on 24 October 2017).
12. Hirzinger, G.; Dietrich, J. Multisensory robots and sensor-based path generation. In Proceedings of the 1986 IEEE International Conference on Robotics and Automation, San Francisco, CA, USA, 7–10 April 1986; Volume 3, pp. 1992–2001.

13. Hirzinger, G.; Albu-Schaffer, A.; Hahnle, M.; Schaefer, I.; Sporer, N. On a new generation of torque controlled light-weight robots. In Proceedings of the 2001 ICRA IEEE International Conference on Robotics and Automation (Cat. No.01CH37164), Seoul, Korea, 21–26 May 2001; Volume 4, pp. 3356–3363.
14. Kinova Robotics. Specifications Actuators. Available online: https://www.kinovarobotics.com/sites/ default/files/Actuator_KA58-KA75_TechSpecs_EN_Web.pdf (accessed on 11 November 2017).
15. Ma, J.; Song, A. Fast Estimation of Strains for Cross-Beams Six-Axis Force/Torque Sensors by Mechanical Modeling. *Sensors* **2013**, 13, 6669–6686.
16. Liang, Q.; Zhang, D.; Coppola, G.; Mao, J.; Sun, W.; Wang, Y.; Ge, Y. Design and Analysis of a Sensor System for Cutting Force Measurement in Machining Processes. *Sensors* **2016**, 16, 70.
17. Wu, B.; Cai, P. Decoupling analysis of a sliding structure six-axis force/torque sensor. *Meas. Sci. Rev*. **2013**, 13, 187–193.
18. Khan, H.; D'Imperio, M.; Cannella, F.; Caldwell, D.; Cuschieri, A.; Semini, C. Towards Scalable Strain Gauge-Based Joint Torque Sensors. *Sensors* **2017**, 17, 1905.
19. Sheng, A.; Liu, H.L.T. A novel six-component force sensor of good measurement isotropy and sensitivities. *Sens. Actuators A Phys*. **2002**, 100, 223–230.
20. Liang, Q.; Zhang, D.; Song, Q.; Ge, Y.; Cao, H.; Ge, Y. Design and fabrication of a six-dimensional wrist force/torque sensor based on E-type membranes compared to cross beams. *Measurement* **2010**, 43, 1702–1719.
21. Aghili, F.; Buehler, M.; Hollerbach, J.M. Design of a Hollow Hexaform Torque Sensor for Robot Joints. *Int. J. Robot. Res*. **2001**, 20, 967–976.
22. Kim, G.-S.; Kang, D.-I.; Rhee, S.-H.; Um, K.-W. Design and fabrication of a three-component force/moment sensor using plate-beams. *Meas. Sci. Technol*. **1999**, 10, 295–301.
23. Kim, Y.G.; Kwak, J.H.; Hong, D.H.; An, J. Miniaturized force-torque sensor built in a robot end-effector for delicate tool-tip gripping control. *Elektron. Elektrotech*. **2014**, 20, 3–7.
24. National Instruments Measuring Strain with Strain Gages. Available online: http://www.ni.com/white- paper/3642/en/ (accessed on 7 November 2017).

25. Pre-wired Strain Gauges. Available online: https://es.omega.com/pptst/KFH.html (accessed on 24 October 2017).
26. Proto Labs Ltd. Protolabs. Available online: https://uploads.protolabs.co.uk/es/PartUpload-MultiPart.aspx?LinkFrom=FC (accessed on 24 April 2017).

Capítulo 4

Study of the application of a collaborative robot for machining tasks

Available online at www.sciencedirect.com

ScienceDirect

Procedia Manufacturing 41 (2019) 867–874

Procedia MANUFACTURING

www.elsevier.com/locate/procedia

8th Manufacturing Engineering Society International Conference

Study of the application of a collaborative robot for machining tasks

R. Perez-Ubeda[a]*, S.C. Gutierrez[a], R. Zotovic[b], J. Lluch-Cerezo[a]

[a]*Dept. of Mechanical and Materials Engineering, Universitat Politècnica de València, Cami de Vera S/N, Valencia, 46022, Spain*
[b]*Dept. of Systems and Automation Engineering, Universitat Politècnica de València, Cami de Vera S/N, Valencia, 46022, Spain*

Perez-Ubeda, R., Gutiérrez, S. C., Zotovic, R., & Lluch-Cerezo, J. (2019). Study of the application of a collaborative robot for machining tasks. Procedia Manufacturing, 41, 867–874. https://doi.org/10.1016/j.promfg.2019.10.009

Study of the application of a collaborative robot for machining tasks

R. Perez-Ubeda[a]*, S.C. Gutierrez[a], R. Zotovic[b], J. Lluch-Cerezo[a]

[a] Dept. of Mechanical and Materials Engineering, Universitat Politècnica de València, Valencia, 46022, Spain

[b] Dept. of Systems and Automation Engineering, Universitat Politècnica de València, Valencia, 46022, Spain

* Correspondence: rodpeub@doctor.upv.es.

Abstract

The importance of collaborative robots is increasing very fast in the industry. They have several advantages over the 'classical' robot arms: they may work side-by-side with humans, their environment needs less adaptation, they may be easily transported, etc. Their joints are more elastic than those in classical robots. For this reason, they are less suited for machining. In this work, a collaborative robot, a sensor of 6 Degree of Freedom (DOF) and a spindle with flex-shaft attachment are used to perform milling operations on soft materials. An inner/outer loop control is being developed to control the movements and the cutting forces. The experiments have been designed to evaluate the capability of the robot with milling operations with different parameters. An analysis of the dimensions and the finished surface will be carried out. The contribution of this article is to determine the possibilities and limitations of the collaborative robots in machining applications, with external control of forces.

Keywords: Robotic machining; elastic robots; co-bots; force control.

4.1. Introduction

It is known that in the last years, industrial robots have been used in many manufacturing applications, such as welding, painting, metrology, assembly, and

machining. The prediction of the International Federation of Robotics, IFR [1], is that by 2020 more than 1.4 million new industrial robots will be installed in factories around the world. The last trend in this area is the use of collaborative robots in industry [2]. Car companies will replace old-style industrial robots with a combination of humans and collaboratives robots (co-bots) assisting humans to gain needed flexibility

The field of co-bots has been expanded significantly over the past ten years. A collaborative robot is a robot, which can safely work directly alongside human workers to complete a task. The significant benefits of these new co-bots are their flexibility, safety, ability to be rapidly deployed, and ease of training. These robots along with the benefits of Industry 4.0 will allow a deep change in future manufacturing and production processes. In the academic world, smart robotics applications are being developed and tested every day where collaborative robots can directly cooperate with the human operators connected through an efficient communication network [3].

In the field of machining applications, robotic arms can be applied for tasks such as milling, drilling, cutting, grinding, brushing, polishing, and deburring. Depending on the field of application, the robots tend to replace manual tasks especially in operations that are noisy, pollutant and unhealthy for operators [4]. Also, they appear as an alternative for CNC machine tasks where a large volume of work and the development of complex geometries are required. In addition to these advantages, robots have good programmability, adaptability, and flexibility with a lower investment cost in contrast to a CNC machine tool with the same workload [5]. The disadvantage of the use of robotic arms lies mainly in that they present a lower stiffness compared to CNC machines. The stiffness for an articulated robot is 1 $N/\mu m$, which is lower than the stiffness of a standard CNC machine, 50 $N/\mu m$. This factor combined with the forces produced in the cutting process generates deflections in the end-effector causing position errors, vibrations, bad quality and low accuracy of the manufactured part. In some cases, the end-effector deflections produced by the cutting forces have reached 10 mm [6].

The high productivity, flexibility, and quality of co-bots together with low cost and high levels of safety make them a very good alternative in machining tasks [7]. However, the disadvantages of these robots, from the point of view of

manufacturing, is that their stiffness is even lower than that of a traditional robot. Therefore, these have been used more in tasks of pick and place, machine tending and quality inspection. Their stiffness is lower due to their joints usually contain harmonic drives, which have a great reduction and low weight, but add more elasticity to the articulation of the robot. This elasticity produces that dynamic and control models of the robot arm which are more complex [8].

To reduce the effects on classical robots, many investigations have been carried out using various methodologies and procedures. One of the most used process control methodologies, which consists of using loops of motion control or force, to compensate deviations due to low joint stiffness [9]. Various models have already been developed and evaluated for milling and drilling processes; however, due to the non-linear relationship and other uncertainties of the robotic machining system, there are differences between the ideal model and the current model. To introduce such a deviation, it is necessary to introduce advanced control schemes to adjust the parameters in accordance with the machining status. Due to this, advanced control approaches have been made, including adaptive control, fuzzy logic control and neural network control. Approaches to force/position control have also been proposed [10]. The latter can be used to see its effect on machining with a collaborative robot. Control of interaction between a robot manipulator and the environment is crucial for successful execution of tasks, like the machining where the robot's end-effector has to manipulate a cutting tool to perform some operation on a surface.

During the interaction, the environment sets constraints on the geometric paths can be followed by the end-effector. (constrained motion). The use of a pure motion control strategy for controlling is a candidate to fail. This control can be used only if the tasks were accurately planned; therefore, it requires an accurate model of the kinematics and dynamics of the robots and the environment (geometry and mechanical features); the last is difficult to obtain.

In practice, the contact force is the variable that describes the state of interaction in the most complete way. Interaction control strategies can be grouped into two categories: those performing indirect force control and those performing direct force control. The first achieve force control via motion control without explicit closure of

a force feedback loop. The last, offer the possibility of controlling the contact force to the desired value, thanks to the closure of a force feedback loop [11].

Within the direct force control loops we can find the inner/outer loop, either by using the movement control loop by position or by speed, as can be seen in Figure 4.1(a) and 4.1(b), respectively.

In the figure, f_d denote the desired force reference, C_F and K_F are control force matrix whose elements give the control actions to perform along with the operational space directions of interest, M_d is a mass matrix, K_P and K_D are the matrices of the inner loop PD (proportional-derivative) control, K is the passive stiffness, x_e and f_e are the 'pose' (position and orientation) and force of the end-effector, and x_F is a suitable reference to be related to a force error, whose relation with the force error can be expressed as,

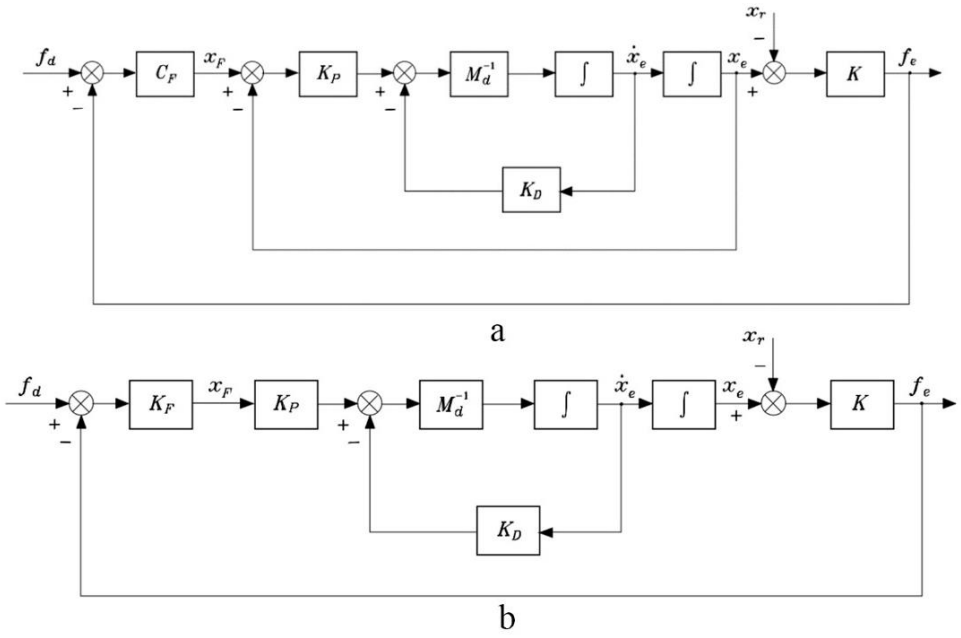

Figure 4.1. (a) Block scheme of force control with inner position loop; (b) Block scheme of force control with inner velocity loop.

$$\boldsymbol{x_F = C_F(f_d - f_e)} \tag{4.1}$$

The equation (4.1), C_F matrix performs the external control loop with PID (proportional-integrative-derivative)-type controls. However, given the high propensity to noise of the force sensor, the classical derivative control action is not applicable in the outer loop. Two alternatives are usually used [12]. The first is to pass the force error through a low pass filter, where 'a' is the cut-off frequency of the filter itself. In this case, the expression of the control action in the Laplace domain would be:

$$\boldsymbol{x_F = f_d + (K_P + K_D s)\left(f_d - \frac{a}{s+a} f_e\right)} \quad \textbf{(4.2)}$$

The second possibility is to use the speed instead of the derivative of the force to dampen the system,

$$\boldsymbol{x_F = f_d + f_P(f_d - f_e) - K_d \dot{x}} \quad \textbf{(4.3)}$$

The previous examples show how the control force is possible to be implemented in a robotic system. This article proposes an analysis of the effects on the dimensions and the finishing surface of the parts machined with collaborative robots. Also, it is a preliminary study of the cutting forces to determine the possibilities and limitations of implementing a force control as shown above.

The article is structured as follows: Section 4.2 presents the methodology, materials, and experiments; Section 4.3 shows the results and discussion of the robotic machining, and finally, the conclusions are presented in Section 4.4.

4.2. Methodology

The design of the experiment consists in perform slot and step operations to study the effects of the parameters of cut, such as depth of cut, cut speed, feed speed and the position of the robot. To study the effect of less stiffness present in collaborative robots, milling operations are carried out on two robots with different characteristics. Table 4.1 shows the main characteristics of these.

The machining cell with a robotic arm is made up of robot plus force sensors, specifically for the case of the Mitsubishi robot, an ATI Delta force sensor is used for the UR3 robot, OnRobot HEX-EB165, both sensors have 6 degrees of freedom.

Table 4.1. Robot specifications.

Robot	Axis	Max load (N)	Reach (mm)	Speed End-effector (m/s)
Mitsubishi RV-2AJ	5	20	480	2.1
Universal Robot UR3	6	30	500	1

The same spindle was used, composed by a Dremel model FortiFlex which has a flexible head which was installed in the end-effector of each robot through a coupling of writer's manufacture. In Figure 4.2, both workbenches can be seen. The 6-DOF sensor ATI has been mounted on the worktable, and the OnRobot sensor has been mounted on the end-effector. The sensors relate to the robots trough of an interface with LABVIEW, and the sensor measures the contact force between the end-effector and the workpiece. This sensor allows measurement of the machining force in the plane of work. Therefore, the goal of control is to achieve the desired force.

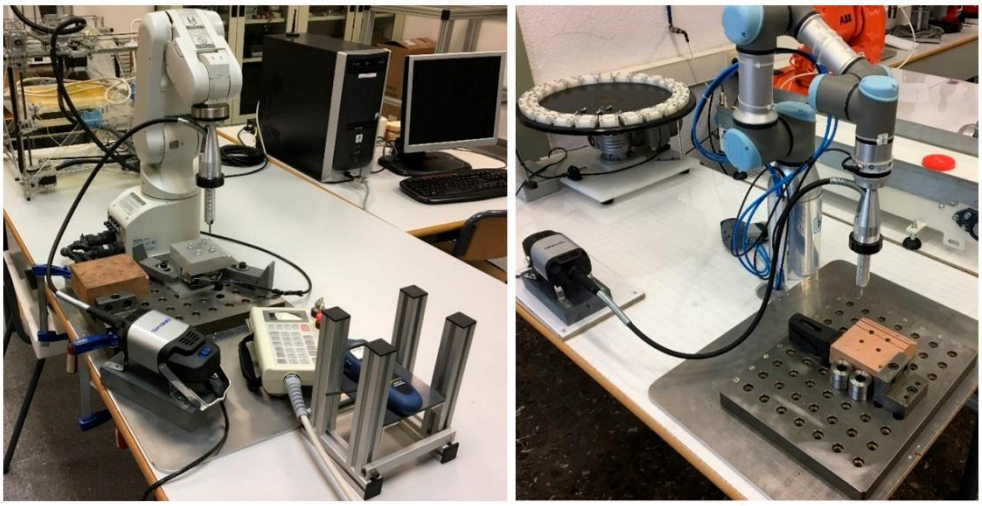

a b

Figure 4.2. (a) Machining cell with Mitsubishi robot; (b) Machining cell with UR3 robot.

The milling operations consisted of slots and steps on rough material 100 mm in length. The cutting tool used was a flat mill with 4 mm diameter, and two-edged,

the conditions of cut are 19600 rpm and a feed speed of 4080 mm/min. The other conditions of cut are shown in Table 4.2.

Table 4.2. Experiments parameters.

N°	Robot	Material	Operation	Depth of cut (mm)	Width of cut (mm)
1	Mitsubishi RV-A2J	Aluminium	Step	1	4
2	Mitsubishi RV-A2J	Resin	Slot	1	4
3	Universal Robot UR3	Resin	Step	0.5	2
4	Universal Robot UR3	Resin	Step	1	2
5	Universal Robot UR3	Resin	Step	2	2
6	Universal Robot UR3	Resin	Step	1	4
7	Universal Robot UR3	Resin	Step	2	4
8	Universal Robot UR3	Resin	Slot	0.5	4
9	Universal Robot UR3	Resin	Slot	1	4
10	Universal Robot UR3	Resin	Slot	2	4

It should be noted that to obtain the real spinning revolution of the spindle; a digital tachometer PCE-DT-65 was used. This measure is necessary to verify the revolutions executed by the Dremel since it does not have direct control to designate it.

For correct programming of the robots and to ensure the dimensions in the final piece, a 'Digigraph 3D-taster' probe and a 'Tschorn Standard Zero Presetter' comparator were used to accurately locate the zero origin of the piece and the lengths of the tools. After machining, the dimensional tolerances were analysed with a comparator clock 'Standard G' and Surface Roughness Tester 'Mitutoyo SJ-201'. To take advantage of the material, the sequence of operations was carried out in the form of a staircase with each step representing different cutting conditions. This also allows having the same reference (side face of the piece) to make subsequent measurements.

4.3. Results and discussion

4.3.1. Machining with robots

The results of the experimental machining without force control can be seen in Figure 4.3, in part (a), the results for milling in aluminium by the Mitsubishi robot are shown.

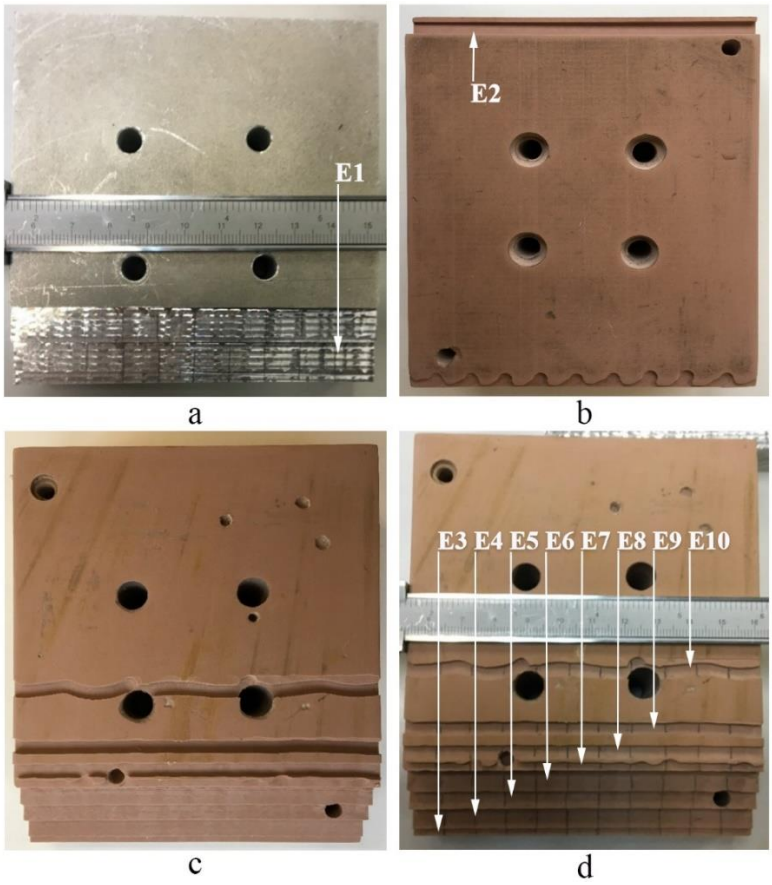

Figure 4.3. (a) Machined aluminium part; (b) Machined resin part face a; (c) Machined resin part face b; (d) Machined resin part with experiments.

It can be observed with the naked eye that there is a poor finish, mainly due to a small advance and the effect of the cutting forces on the robot arm, which could be

seen visually as a resistance of the arm to follow its movement, which generates a shallow grid. In the case of the performance of the Mitsubishi robot with the resin, slot Figure 4.3(b), a good finish can be observed for the same cutting conditions. In Figure 4.3(b), in the lower part you can see the effect of milling with the elastic robot UR3. As it can be observed for the same conditions of cut, 2 mm of depth of pass and a width of the diameter. The machining is completely affected by the low stiffness of its joints, generating these waves because the movement control will proceed to recover the indicated displacement. Here it is demonstrated how soft materials such as resins already affect the performance of the process.

In Figure 4.3 (c) and (d), one can see the rest of the experiments made with the collaborative robot in resin. As can be seen, as the cutting conditions increase, the instability of the process increases to such an extreme, as in experience E10, where the tool deviates completely.

In Figure 4.4, a graph with a dimensional analysis of the milled pieces is shown.

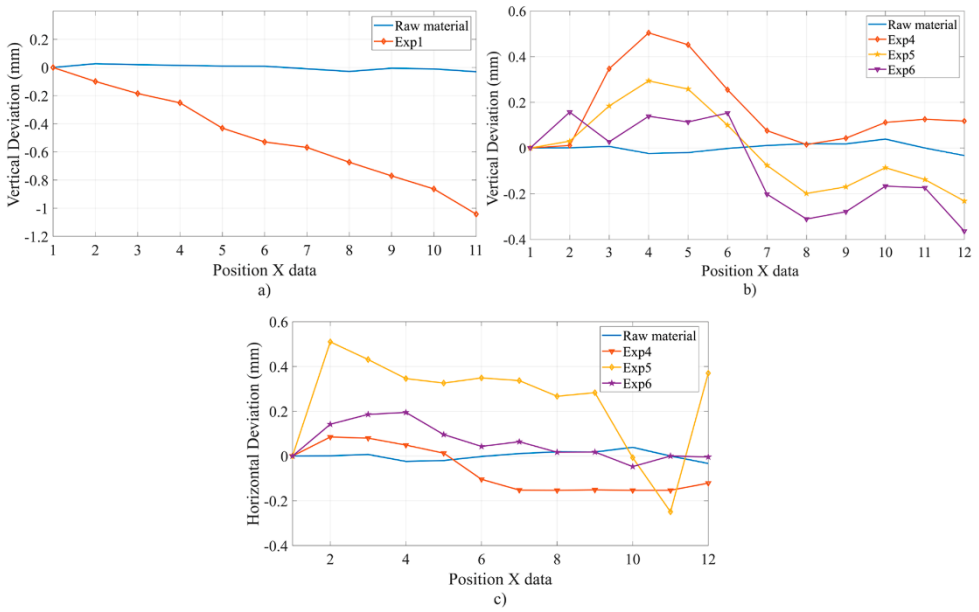

Figure 4.4. (a) Vertical deviation in aluminium; (b) Vertical deviation in resin; (c) Horizontal deviation in resin.

The vertical deviation indicates the deviation generated in the depth of cut concerning the plane of cut, on the other hand, the horizontal deviation is the deviation of the path contained in that plane of cut concerning the programmed one.

In the case of the Mitsubishi robot, Figure 4.4(a), an increase of the vertical deviation is observed as the position in the direction of the cutting feed increased. This increase is constant, and its variations with respect to the trend line are small, this is explained by the fact that the robot is more rigid than the collaborative one, but its maximum deviation is due to the fact that the 5-axis design does not allow adjustment to the orientation of the tool centre point, with which a work plane different from that of the piece is obtained.

Table 4.3. Roughness results.

Surface	R_a (μm)	R_y (μm)	R_z (μm)	R_q (μm)
Resin raw	2,85	24,76	17,72	3,65
Exp 3	3,81	30,82	23,56	4,93
Exp 4	3,81	26,52	22,31	4,74
Exp 7	6,51	76,53	42,38	8,33
Aluminium raw	2,47	15,94	13,65	3,09
Exp 1	1,49	10,49	8,20	1,86

In Table 4.3, the results obtained with the roughness tester are attached. The samples are not filtered, the cut-off length is 0.8 mm, and the evaluation length is five times cut-off length.

Despite the reduced appearance of machining in aluminium, the result of milling is better than workpiece raw. In the case of the collaborative robot, the increase in roughness is not as pronounced as the dimensional tolerances.

4.3.2. Cutting forces

In order to be able to carry out an inner/outer loop control, it is necessary to know the force profiles of the machining operations carried out. As can be seen in Figure 4.5, the machining presents much instability. This is mainly due to the low stiffness of the wrist joints, which, if they are not included in the control loop, would generate perturbations in the force measured by the sensor.

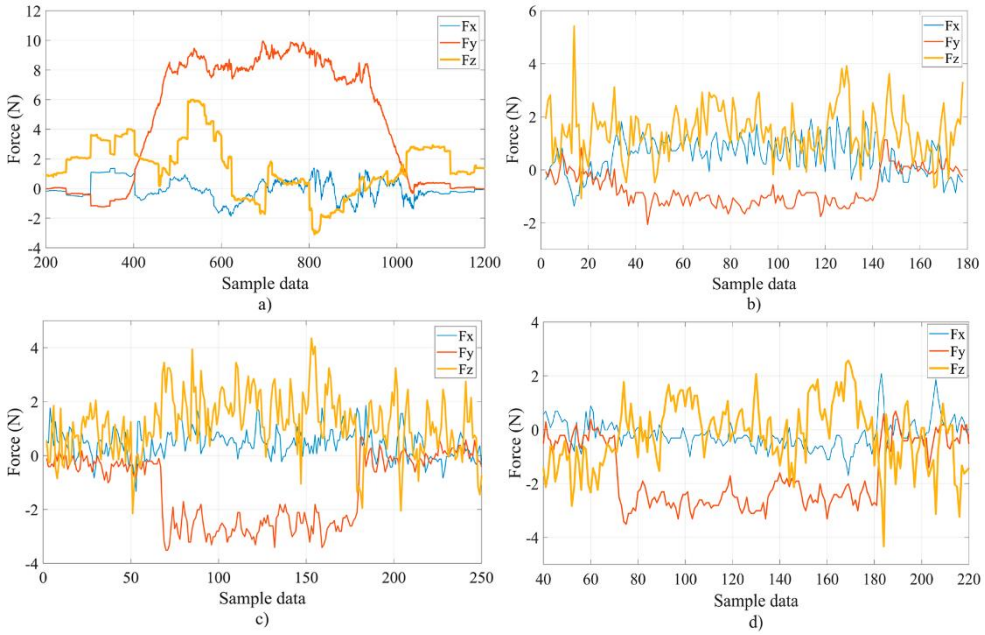

Figure 4.5. Machining forces (a) Experiment 1; (b) Experiment 4; (c) Experiment 6; (d) Experiment 9.

The collaborative robot UR3 has many advantages to implement a force control because its inner control allows read easily the position and velocity variables in joints and end-effector reference frame. We implemented a control inner/outer loop, as in the equation (3), trough the command script '*speedL*.' When performing tests with force control, the instability in the measurements significantly affected the control loop, generating errors that were not compensated. So, it is necessary to go deeper into the robot machining model to make the control more precise. A first alternative is to include the elasticity of the joints in the control loop through a correct definition of the matrices of stiffness in joint and task space. This implies modifying the dynamic model of the robot to consider it as an elastic no lineal model, with which the effects due to flexibility could be diminished.

4.4. Conclusions

Given the results obtained, the lack of stiffness of the collaborative robot arms makes it difficult to achieve machining operations with controlled dimensional and finishing requirements. However, the reduction system that collaborative robots incorporate in their joints allows a greater adjustment to reach them, compared with rigid robot arms.

In the collaborative, the stiffness can be determined individually, in each joint, depending on the configuration adopted by the arm and the cutting conditions used (cut feed, spindle speed, step depth, and overlap).

As has been verified in the preliminary tests carried out to evaluate the use of a collaborative robot in the performance of machining operations, its control must be completed with an external loop. It will capture instantaneous efforts in real-time, which will serve to modify the Cartesian deflection using the matrix of stiffness of the arm. In this way, it will be possible to act dynamically on the trajectory carried out in order to meet objectives.

To achieve this, a precise mathematical model is needed according to the actual behaviour of the arm's hardware (depending on the type of installed gearboxes, machining operation, tools, etc.), which allows expansion of the stiffness matrix tested it against variations, in part from its variables, measured externally.

Acknowledgments

The authors are grateful for the financial support of the Spanish Ministry of Economy and European Union, grant DPI2016-81002-R (AEI/FEDER, UE).

This work was funded by the CONICYT PFCHA/DOCTORADO BECAS CHILE/2017 – 72180157.

4.5. References

1. International Federation of Robotics IFR forecast: 1.7 million new robots to transform the world´s factories by 2020 Available online: https://ifr.org/ifr-press-releases/news/ifr-forecast-1.7-million-new-robots-to-transform-the-worlds-factories-by-20 (accessed on Feb 15, 2019).

2. Robotic Industries Association (RIA) Top 6 Future Trends in Robotic Automation Available online: https://www.robotics.org/blog-article.cfm/Top-6-Future-Trends-in-Robotic-Automation/101 (accessed on May 6, 2019).
3. Grau, A.; Indri, M.; Lo Bello, L.; Sauter, T. Industrial robotics in factory automation: From the early stage to the Internet of Things. In Proceedings of the Proceedings IECON 2017 - 43rd Annual Conference of the IEEE Industrial Electronics Society; 2017; Vol. 2017-Janua, pp. 6159–6164.
4. Hui Zhang; Jianjun Wang; Zhang, G.; Zhongxue Gan; Zengxi Pan; Hongliang Cui; Zhenqi Zhu Machining with flexible manipulator: toward improving robotic machining performance. In Proceedings of the Proceedings, 2005 IEEE/ASME International Conference on Advanced Intelligent Mechatronics.; IEEE, 2005; pp. 1127–1132.
5. Klimchik, A.; Ambiehl, A.; Garnier, S.; Furet, B.; Pashkevich, A. Efficiency evaluation of robots in machining applications using industrial performance measure. *Robot. Comput. Integr. Manuf.* **2017**, *48*, 12–29, doi:10.1016/j.rcim.2016.12.005.
6. Iglesias, I.; Sebastián, M. a.; Ares, J.E. Overview of the State of Robotic Machining: Current Situation and Future Potential. *Procedia Eng.* **2015**, *132*, 911–917, doi:10.1016/j.proeng.2015.12.577.
7. Robots, U. An introduction to common collaborative robot applications Available online: https://info.universal-robots.com/common-collaborative-robot-applications (accessed on Sep 23, 2018).
8. De Luca, A. Flexible Robots. In *Encyclopedia of Systems and Control*; Springer London: London, 2013; pp. 1–10 ISBN 978-1-4471-5102-9.
9. Perez, R.; Gutierrez Rubert, S.C.; Zotovic, R. A Study on Robot Arm Machining: Advance and Future Challenges. In *29TH DAAAM INTERNATIONAL SYMPOSIUM ON INTELLIGENT MANUFACTURING AND AUTOMATION*; 2018; pp. 0931–0940.
10. Chen, S.; Zhang, T. Force control approaches research for robotic machining based on particle swarm optimization and adaptive iteration algorithms. *Ind. Robot An Int. J.* **2018**, *45*, 141–151, doi:10.1108/IR-03-2017-0045.

11. Siciliano, B.; Sciavicco, L.; Villani, L.; Oriolo, G. *Robotics*; Advanced Textbooks in Control and Signal Processing; Springer London: London, 2009; ISBN 978-1-84628-641-4.
12. Zotovic, R.; José, P.; Gil, G.; Redolar, M.C. Control de Fuerza y de Impacto de un Robot con Cambio de Período de Muestreo. In Proceedings of the XXV Jornadas de Automática; 2014.

Capítulo 5

Force Control Improvement in Collaborative Robots through Theory Analysis and Experimental Endorsement

applied sciences

MDPI

Article

Force Control Improvement in Collaborative Robots through Theory Analysis and Experimental Endorsement

Rodrigo Pérez-Ubeda [1,*], Ranko Zotovic-Stanisic [2] and Santiago C. Gutiérrez [1]

[1] Department of Mechanical and Materials Engineering, Universitat Politècnica de València, 46022 Valencia, Spain; scgutier@mcm.upv.es

[2] Institute of Industrial Control Systems and Computing (ai2), Universitat Politècnica de València, 46022 Valencia, Spain; rzotovic@isa.upv.es

* Correspondence: rodpeub@doctor.upv.es; Tel.: +34-96-387-76-22

Received: 4 June 2020; Accepted: 22 June 2020; Published: 24 June 2020

check for updates

Pérez-Ubeda, R., Zotovic-Stanisic, R., & Gutiérrez, S. C. (2020). Force Control Improvement in Collaborative Robots through Theory Analysis and Experimental Endorsement. Applied Sciences, 10(12), 4329. https://doi.org/10.3390/app10124329.

Force Control Improvement in Collaborative Robots through Theory Analysis and Experimental Endorsement

Rodrigo Pérez-Ubeda [1]*, Ranko Zotovic-Stanisic [2], and Santiago C. Gutiérrez [1]

[1] Department of Mechanical and Materials Engineering, Universitat Politècnica de València, 46022 Valencia, Spain.

[2] Institute of Industrial Control Systems and Computing (ai2), Universitat Politècnica de València, 46022 Valencia, Spain.

* Correspondence: rodpeub@doctor.upv.es.

Abstract

Due to the elasticity of their joints, collaborative robots are seldom used in applications with force control. Besides, the industrial robot controllers are closed and do not allow the user to access the motor torques and other parameters, hindering the possibility of carrying out a customized control. A good alternative to achieve a custom force control is sending the output of the force regulator to the robot controller through motion commands (inner/outer loop control). There are different types of motion commands (e.g., position or velocity). They may be implemented in different ways (Jacobian inverse vs. Jacobian transpose), but this information is usually not available for the user. This article is dedicated to the analysis of the effect of different inner loops and their combination with several external controllers. Two of the most determinant factors found are the type of the inner loop and the stiffness matrix. The theoretical deductions have been experimentally verified on a collaborative robot UR3, allowing us to choose the best behaviour in a polishing operation according to pre-established criteria.

Keywords: force control; collaborative robot; inner/outer loop; elastic robot; polishing operation

5.1. Introduction

In the next few years, a significant increase in the number of industrial robots is expected. The prediction of the International Federation of Robotics (IFR) [1] is that between 2020 and 2022, nearly two million new industrial robots will be installed in factories around the world. However, despite this high demand, the robots are not useful for many manufacturing tasks today—in particular, those found in small and medium enterprises. A goal for the next generation of smart factory floors is to bring humans and robots closer together, working efficiently and collaborating safely [2].

Commonly, industrial robots are used in applications of low contact forces, such as material handling, welding, assembly, and painting. Nevertheless, in the last few years, industrial robots have been used in many applications of high interaction, such as milling, drilling, threading, and cutting. Also, they have been used to perform surface finish tasks such as grinding, brushing, polishing, and deburring [3].

On the other hand, the use of collaborative robots (cobots) has increased in recent years. The high productivity, flexibility, and quality of cobots, together with their low cost and high levels of safety, making them a perfect alternative in interaction tasks. However, the disadvantages of these robots are their lower stiffness compared with traditional ones. Their stiffness is lower because their joints usually contain harmonic drives. These have a safe and reliable power transmission with high reduction and low weight. However, they add more elasticity to the joints of the robot. The high force produced in the contact, combined with the low stiffness, generates deflections in the end effector, causing position errors and vibrations [4,5].

In the last few decades, many studies have been carried out in the area of force control using robots with elastic joints. One of the first relevant works [6] uses a corrective control for the singular perturbation model and the integral manifold technique to develop an inner/outer control. Where the inner loop is linearizing feedback control, and the outer loop can be implemented with the typical rigid robot force controls, as impedance control or hybrid position/force control. In the articles of Ren, T. et al. [7] and Ajoudani, A. et al. [8], the authors use the joint elastic torques to decouple the joint actuators and perform an impedance force control. The works in Magrini, E. et al. [9], Ahmad, S. [10] and Goldsmith, P. et al. [11] use a torque-

controlled system to make a hybrid position/force control. Finally, a sliding mode control, adaptive control, and robust control have also been used as a solution to force control [12–15]. These techniques, in general, assume that the dynamic models of elastic joint robots are precisely known. Also, they assume the user can access the torques of the motors, which is not usually the case in commercial robots. Besides, the desired trajectory must be derivable at least four times, and the acceleration of the robot must be measured. However, in many commercial robots, the acceleration and the dynamic parameters cannot be obtained.

Other researchers have developed force controllers without knowledge of dynamics, such as the works found in Ma, Z. et al. [16] and Huang, L. et al. [17]. Nevertheless, the robot control with elastic joints requires measurements of the whole state of the system as the motor side angles, the link side angles, and the torque of the joints. These measures are difficult to get them in a commercial robot.

Commonly, commercial manipulators do not allow direct access to the actuator torques; therefore, a torque-based control cannot be used. However, most commercial manipulators have built-in position controllers. Some also have the possibility of velocity regulation. In these cases, it is possible to achieve a force control by using inner/outer controllers that consists of an inner position/velocity loop plus an outer force control loop. The external loop provides a reference position/velocity to the inner loop. Examples of inner/outer force control loops on rigid manipulators can be found in the works of Chiaverini, S. et al. [18], Winkler, A. and Suchy, J. [19], De Schutter, J. et al. [20] and Neranon, P. and Bicker, R. [21].

An advantage of the inner/outer loop is that this control does not need to know the dynamic parameters of the robot [20]. The errors in the dynamic model can be modelled as force disturbances. Some researches apply the inner/outer algorithm directly to the robot motion control. This has the advantage of executing the task relatively straightforward [22–24], while others develop a macro-mini manipulator, where the robot is the macro manipulator, and a special end-effector is the mini manipulator or active device [25–27].

As collaborative robots are lighter and cheaper, the use of mini manipulators does not appear to be an available alternative. The mini manipulator requires the development of another and specific mini controller to each process. This method requires actuators, power amplifiers, active control devices, and algorithms. They

are expensive and relatively difficult to implement. Besides, a specific device generates less stiffness and raise weight in the end effector [28].

According to the above, this article proposes the analysis and experimentation of a force control with an inner motion loop on collaborative robot arms. The methodology implemented allows us to demonstrate the possibility for cobots to perform a force control, although the internal parameters of the robot remain unknown. This work proves the application of these control in a polishing operation. Additionally, the analysis proposed considers the effect of the stiffness in the robot when it is used in force tasks with an inner/outer control loop.

This article is structured as follows. Section 5.2 presents the dynamic model for robots with elastic joints. Section 5.3 describes the inner/outer control loops with their advantages and drawbacks. Then, Section 5.4 shows an analysis of the possible inner loops and how the inner loops can affect the response of the force control. Section 5.5 shows the methodology, experimental platform, techniques used, and task planning. Section 5.6 exposes the results and discussion of the experiments performed with a commercial collaborative robot. In this section, the inner position loop and the velocity loop are compared. Besides, different algorithms for outer loops are contrasted. The best inner/outer loop is applied in a polishing task. Finally, Section 5.7 collects the conclusions.

5.2. Description of Dynamic model for a robot with elastic joints

Under the assumptions in Zollo, L. et al. [29], the dynamic model of a robot with elastic joints can be expressed as

$$\boldsymbol{M}(\boldsymbol{q})\ddot{\boldsymbol{q}} + \boldsymbol{C}(\boldsymbol{q},\dot{\boldsymbol{q}}) + \boldsymbol{G}(\boldsymbol{q}) + \boldsymbol{K_q}(\boldsymbol{q}-\boldsymbol{\theta}) + \boldsymbol{F_q}\dot{\boldsymbol{q}} + \boldsymbol{D}\left(\dot{\boldsymbol{q}}-\dot{\boldsymbol{\theta}}\right) = -\boldsymbol{J}^{\boldsymbol{T}}(\boldsymbol{q})\boldsymbol{f} \qquad \textbf{(5.1)}$$

$$\boldsymbol{B}\ddot{\boldsymbol{\theta}} + \boldsymbol{K_q}(\boldsymbol{\theta}-\boldsymbol{q}) + \boldsymbol{F_\theta}\dot{\boldsymbol{\theta}} + \boldsymbol{D}\left(\dot{\boldsymbol{\theta}}-\dot{\boldsymbol{q}}\right) = \boldsymbol{\tau} \qquad \textbf{(5.2)}$$

where $\boldsymbol{q}$, $\dot{\boldsymbol{q}}$, and $\ddot{\boldsymbol{q}}$ are the $(n \times 1)$ vectors of position, velocity, and acceleration of links, respectively. $\boldsymbol{\theta}$, $\dot{\boldsymbol{\theta}}$, and $\ddot{\boldsymbol{\theta}}$ are the $(n \times 1)$ vectors of positions, velocities, and accelerations of motors. $\boldsymbol{M}(\boldsymbol{q})$ is the $(n \times n)$ robot link inertia matrix, $\boldsymbol{C}(\boldsymbol{q},\dot{\boldsymbol{q}})$ is the $(n \times 1)$ vector of centrifugal and Coriolis torques, $\boldsymbol{K_q}$ is the $(n \times n)$ diagonal matrix of joint stiffness coefficients, $\boldsymbol{G}(\boldsymbol{q})$ is $(n \times 1)$ vector of gravitational torque, and $\boldsymbol{B}$ is

a $(n \times n)$ constant diagonal matrix, including the rotor inertia in the gear ratios. $\boldsymbol{F_q}$, $\boldsymbol{F_\theta}$, and $\boldsymbol{D}$ contain, in this order, the viscous coefficient in the link side, the viscous coefficient in the motor side, and the damping of the elastic springs at the joints. $\boldsymbol{\tau}$ is the $(n \times 1)$ input vector of driving torques, $\boldsymbol{f}$ is the $(n \times 1)$ vector of contact force exerted by the end effector on the environment, and $\boldsymbol{J(q)}$ is the Jacobian matrix that relates joint velocities $\dot{\boldsymbol{q}}$ with the vector of end-effector velocities, $\dot{\boldsymbol{x}}$. The Jacobian is assumed to be non-singular. The transpose of the matrix, $\boldsymbol{J^T(q)}$, also relates the end effector force with the joint torques.

$$\dot{\boldsymbol{x}} = \boldsymbol{J(q)}\dot{\boldsymbol{q}} \tag{5.3}$$

$$\boldsymbol{\tau} = \boldsymbol{J^T(q)f} \tag{5.4}$$

For analysis purposes, the environment is modelled as a frictionless and elastically compliant plane, which is very common in force control [18,29,30]. One contact point is considered, and the contact force is expressed as

$$\boldsymbol{f} = \boldsymbol{K_e}(\boldsymbol{x} - \boldsymbol{x_e}) \tag{5.5}$$

where $\boldsymbol{x}$ is the end-effector position, $\boldsymbol{x_e}$ is the position at the contact point, and $\boldsymbol{K_e}$ is the constant symmetric stiffness matrix of the environment.

5.3. Inner/outer control loops

Among the main benefits of the force control with inner/outer loops are that the dynamics and kinematics of the robot are included through the inner loop. In addition, this control is easy to implement because only the outer control loop must be regulated. Also, sometimes, this control strategy is the only possible way to perform a custom force control.

On the other hand, the inner/outer loop has some disadvantages. There are limitations in the robot command set—for example, some robots do not have velocity commands. There is a lack of information about the inner loop, control type, and control parameters. There is no possibility to access the input of the torques directly, which makes it impossible to implement a force control in a robot that applies inverse dynamic methods [6,9,31].

The stiffness of the environment is a very important factor in the performance of the interaction tasks. Therefore, it is necessary to know this parameter to have better force control.

The sampling period of the inner loop, established initially for position control, could be too slow for force control. Some functions necessary for control (e.g., the Jacobian matrix) cannot be implemented using the set of commands. Due to the sampling period, if the external loop is implemented through an external computer, there will be communication delays.

The general block schemes of the typical configurations of inner/outer loops, with an inner position loop and an inner velocity loop, are shown in Figure 5.1. The force of environment $\boldsymbol{f_e}$ measured with the force sensor is compared with the desired force $\boldsymbol{f_d}$. After that comparison, force error $\boldsymbol{e_f}$ is generated. This error is used by the force controller to produce the reference of absolute position $\boldsymbol{x_f}$ (Figure 5.1(a)), incremental position $\Delta\boldsymbol{x_f}$ (Figure 5.1(b)), or velocity $\dot{\boldsymbol{x}}_{\boldsymbol{f}}$ (Figure 5.1(c)).

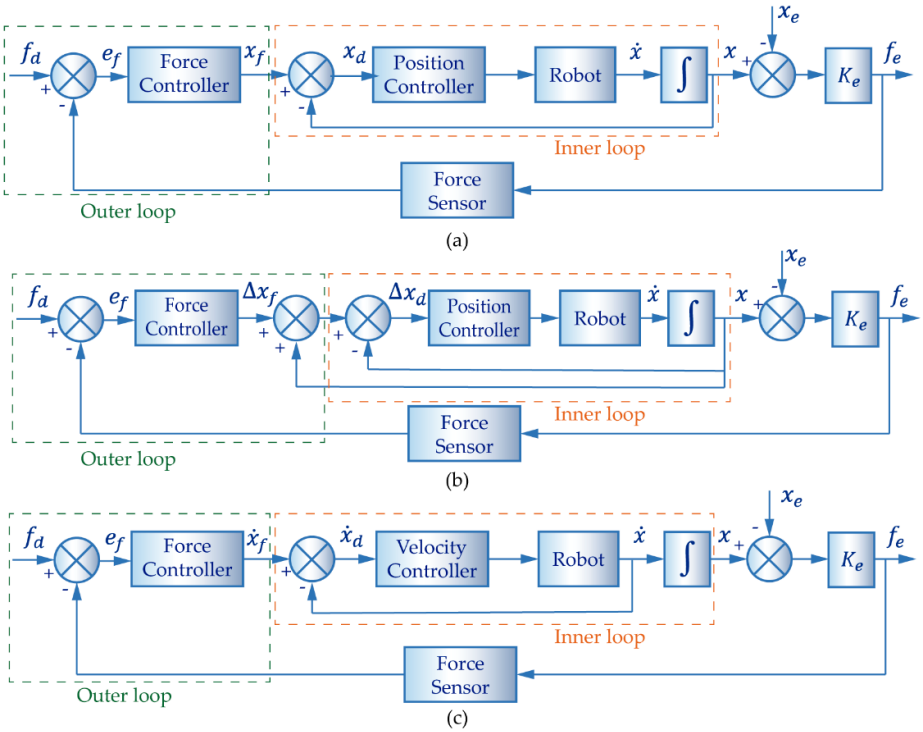

Figure 5.1. Force control with inner motion loops (a) with inner absolute position loop, (b) with inner incremental position loop, and (c) with inner velocity loop.

In the three schemes, it has been assumed that the internal controller compensates nonlinearities of the process. In the diagrams, the only difference between position and velocity lies in the integrator, which is not included in the inner loop for the velocity controller. However, there are crucial differences not reflected in the graphs.

The parameters of the controllers can differ for position and velocity control. Thus, it could be necessary to implement different external loops depending on the inner controller. Also, the stiffness matrix is not the same in the three cases.

The external force loops are not limited by the set of motion commands of the robot. In recent decades, many authors proposed several types of general algorithms for outer loops. Table 5.1 shows some of the most relevant, where $\boldsymbol{u}$ is the control action applied over the inner loop, $\boldsymbol{f_d}$ and $\boldsymbol{f}$ are the reference and measured force, respectively. $\dot{\boldsymbol{f}}_{\boldsymbol{d}}$ and $\dot{\boldsymbol{f}}$ are the reference and measured derivative force, respectively. $\boldsymbol{K_{pf}}$, $\boldsymbol{K_{df}}$, and $\boldsymbol{K_{if}}$ are the gain matrices of the proportional, derivative, and integral control, in this order. $\boldsymbol{K_{vf}}$ is the gain matrix of the velocity feedback damping, $\dot{\boldsymbol{x}}$ is the cartesian velocity, and $\boldsymbol{FF}$ is the feedforward action.

Table 5.1. Typical control action for outer force loops.

Algorithm	Control Action	
Proportional Derivative—PD	$\boldsymbol{u} = \boldsymbol{K_{pf}}(\boldsymbol{f_d} - \boldsymbol{f}) + \boldsymbol{K_{df}}(\dot{\boldsymbol{f}}_{\boldsymbol{d}} - \dot{\boldsymbol{f}})$	**(5.6)**
Proportional with Velocity feedback—PV	$\boldsymbol{u} = \boldsymbol{K_{pf}}(\boldsymbol{f_d} - \boldsymbol{f}) - \boldsymbol{K_{vf}}\dot{\boldsymbol{x}}$	**(5.7)**
Proportional—Integrative—Derivate—PID	$\boldsymbol{u} = \boldsymbol{K_{pf}}(\boldsymbol{f_d} - \boldsymbol{f}) + \boldsymbol{K_{df}}(\dot{\boldsymbol{f}}_{\boldsymbol{d}} - \dot{\boldsymbol{f}}) + \boldsymbol{K_{if}}\int(\boldsymbol{f_d} - \boldsymbol{f})dt$	**(5.8)**
Proportional—Integral with Velocity feedback—PIV	$\boldsymbol{u} = \boldsymbol{K_{pf}}(\boldsymbol{f_d} - \boldsymbol{f}) - \boldsymbol{K_{vf}}\dot{\boldsymbol{x}} + \boldsymbol{K_{if}}\int(\boldsymbol{f_d} - \boldsymbol{f})dt$	**(5.9)**
Proportional with Feedforward—P + FF	$\boldsymbol{u} = \boldsymbol{FF} + \boldsymbol{K_{pf}}(\boldsymbol{f_d} - \boldsymbol{f})$	**(5.10)**

As can be read in Neranon, P. and Bicker, R. [21], PD and PID controls are usually replaced by a PV or PIV controls due to the high noise produced by the force sensor, which makes the use of a derivative control impracticable.

As it is known from control theory, the integral control action guarantees zero error if the system is stable. However, it brings some problems like potential stability loss, wind-up, and slow convergence. Additionally, in force control, if the sampling period is slow, the integrator does not eliminate the error, as it will be demonstrated in the experimental part of this paper. For these reasons, the use of an integrator should be considered for every case.

One of the main problems in force control is the change from free to constrained movement. This transition phase, also called impact, is probably the most critical part of the task. This difficulty could lead to the need for the use of different regulators in each phase. In Zotovic, R. and Valera, A. [32], a single valid controller for force control and impact control is proposed. First, the controller is set to perform speed control in free movements and force control in constrained movements. It avoids the need to switch regulators and their associated problems. Second, they proposed switching off the proportional constant and the feedforward to attenuate the impact. Therefore, the stability of the system is improved through a better dissipation of energy.

In Siciliano, B. et al. [33], researchers studied two cases of external loops for different inner loops. For an inner position loop, the authors proposed an external PV force controller. For an internal velocity loop, the authors proposed just a proportional, P, force control for the outer loop. The authors deduced that a proportional regulator of external force, with a proportional regulator for the inner velocity loop, reaches the reference force in a finite time. However, this does not happen with the inner regulator by position. For this reason, it is necessary to add an integrator in the force loop. It is known that this reduces bandwidth and stability margin.

5.4. Analysis of inner motion loops

The inner loops are implemented inside robot controllers. In most commercial robots, the details, such as dynamics parameters, gains, and algorithms of the inner

controller, are not available for users. However, today, most of the robot controllers compensate for the nonlinear dynamics or, at least, the effect of gravity. The force control tasks are usually performed at very low velocities and accelerations. Thus, the inertia, centrifugal, and Coriolis forces have less influence than gravity force.

As stated previously, the inner control may be a position loop or a velocity loop. Several authors have used different forms of inner loops. All of them had to use Cartesian commands. Some used absolute position commands [21,34]. Zeng, G. and Hemami, A. [35] used position increments instead of absolute positions, and in the works of Magrini, E. et al. [9] and Han, D. et al. [30], the authors used inner velocity loops. It should be emphasized that some robot controllers do not have cartesian velocity commands, so this option is not always available.

An essential feature for the force control in a robot is the cartesian stiffness matrix. This matrix determines the deviation of the robot from the nominal trajectory, under the effect of external forces.

The expression for this matrix depends on several factors. First, it is influenced by the location of the position/velocity sensor for the feedback of the inner loop. It may be located on the motor (a typical configuration for rigid robots) or on the link (for the elastic ones). The cartesian stiffness matrix is not equal in all the working range of the robot. It may be essential to know the expression for the stiffness matrix to deduce where to perform the task, what will be the errors, etc.

Another important factor is how the inner loop coordinate transformation is performed. The force control must be programmed in cartesian space. However, the motors are controlled in joint space. Thus, cartesian coordinates must be transformed into joint coordinates. This can be implemented in two ways, through the Jacobian inverse method or the Jacobian transpose method. Thus, the control action of the inner position loop can be computed with these two methods by the robot controller [33]. In the first case, the first step is to compute the cartesian position error and use the Jacobian inverse to transform it into joint coordinate errors. Then, the control action is carried out. In the second case, the regulator is applied directly to the cartesian position error. The result is multiplied by the Jacobian transpose to obtain the input torques of the motors. These two possible configurations, called Jacobian inverse control and Jacobian transpose control, can be seen in Figure 5.2.

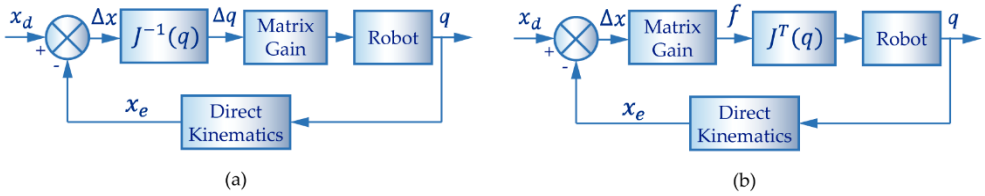

Figure 5.2. Block schemes of operational space control (a) with Jacobian inverse and (b) with Jacobian transpose.

In Section 5.4.1, the cartesian stiffness matrix is analysed depending on the location of the position/velocity sensor, and the type of inner loop. Section 4.2 will study the effect of different combinations of inner and outer loops, as well as the way they communicate. The external loops were given in Equations (5.6)–(5.10). The inner loops will be position and velocity, both with Jacobian inverse and Jacobian transpose. For the position inner loop, cases of absolute and incremental positions will be considered. For each one, the steady-state error and stiffness matrix will be deduced.

The analysis of the inner loops allows to understand how they can affect the force response, and in this way, to deduce what inner loop should be applied in the robot to ensure better performance in the interaction task.

5.4.1. The stiffness matrix

In force control, the interaction forces may cause deviation of the end-effector from the nominal trajectory. There are two different reasons. First, the external forces produce mechanical deformation of the gears. Second, the external forces induce a deviation of the motors from their reference path. The first case depends on the mechanical robustness of the robot. The second case depends on the controller.

The mechanical deformations occur in joint space. Regarding the controller, it can be implemented in both joint and cartesian space. The effect on the error will be different in the two cases.

The joint stiffness matrix is defined as the relation between the deformation of the joints and the applied torque,

$$\boldsymbol{\tau} = \boldsymbol{K}_q \Delta \boldsymbol{q} \tag{5.11}$$

where $\boldsymbol{\tau}$ is the vector of motor torques, $\boldsymbol{K_q}$ is the diagonal stiffness matrix, and $\Delta\boldsymbol{q}$ is the vector of differences between actual joint and reference positions.

The force control tasks are programmed in the cartesian space. Thus, for a good performance, it is crucial that the robot deviates from the nominal cartesian trajectory as little as possible. The cartesian stiffness matrix describes the relationship between the deformations and the force in all the cartesian directions. It is highly recommended to have higher stiffness in order to avoid errors. The opposite phenomenon of stiffness is called compliance.

The robot cartesian stiffness matrix, $\boldsymbol{K_x}$, was first introduced in Salisbury, J. [36] as

$$\boldsymbol{K_x = J^{-T}(q)\left(K_q\right)J^{-1}(q)} \tag{5.12}$$

where $\boldsymbol{J(q)^{-T}}$ and $\boldsymbol{J(q)^{-1}}$ are the Jacobian transpose and Jacobian inverse, respectively.

Next equation relates the cartesian position deviations and the external force vector,

$$\boldsymbol{f = K_x \Delta x} \tag{5.13}$$

It should be noted that the Jacobian matrix of the robot depends on its position and, therefore, the cartesian stiffness matrix, too.

In reference [37], researchers introduced the conservative congruence transformation—Equation (5.14)—giving an improved version of the cartesian stiffness matrix,

$$\boldsymbol{K_x = J^{-T}(q)\left(K_q - K_g\right)J^{-1}(q)} \tag{5.14}$$

where $\boldsymbol{K_g = \left[\frac{\partial J^T}{\partial q_n} f\right]}$ is the additional stiffness term, caused by the variation of the Jacobian matrix and the external force vector.

The part of the stiffness due to the mechanical deformation of the gears is called passive stiffness. It is always expressed in cartesian space. In this study, it is referred as joint stiffness. The part due to the deviations of the motors is called active stiffness and can be modified by the adequate adjustment of the controller. It can be

expressed in cartesian or joint space, depending on the way the control is made. The works of Salisbury, J. [36] and Chen, S. and Kao, I. [37] were made for classical, rigid robots.

These robots usually have only one position sensor per motor. It is located on the motor side and not in the link because the measured position has a higher resolution. It is assumed that the position of the motor and the link are equivalent. It is considered that there is no deformation of the gears, which may be corrected by the position control. However, in force control tasks, the deformations cannot be neglected.

On the other hand, the robots with elastic joints usually have two position sensors (encoders) [38].

The first encoder is on the motor side, and the second one is on the link side, as shown in Figure 5.3.

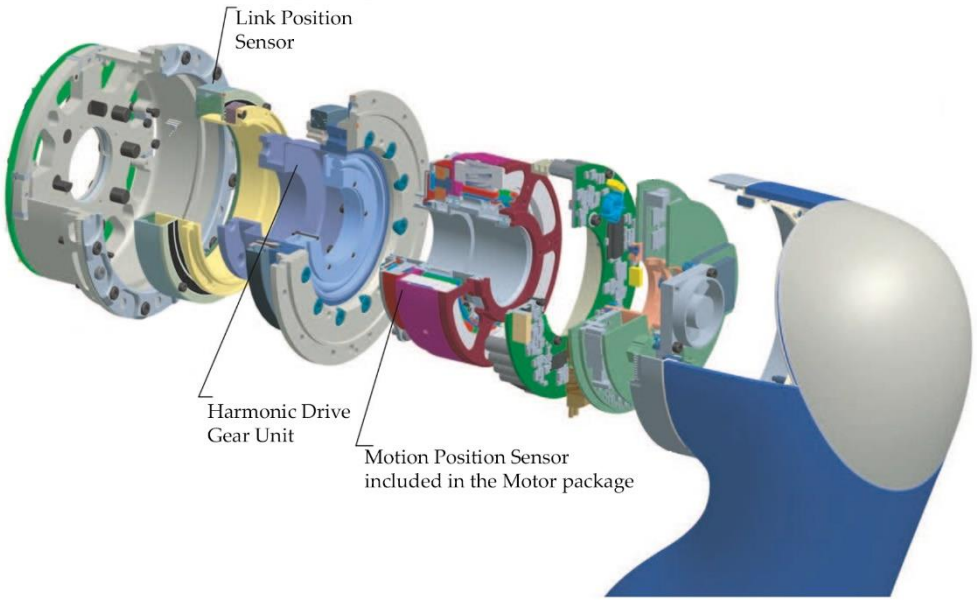

Figure 5.3. The joint module of the Light WeigthRobot III, adapted from Institute of Robotics and Mechatronics of German Aerospace Centre (Deutsches Zentrum für Luft-und Raumfahrt-DLR) [38].

This way, it is possible to control as feedback the position of the motor or the position of the link. Besides, the motor or the link velocities can be controlled, too.

Thus, there are several possibilities: motor position control, motor velocity control, link position control, link velocity control, or a combination of them.

5.4.1.1. Motor Position

Considering the robot dynamics, Equations (5.1) and (5.2) in a steady-state and an input control in the motor side, we have

$$\boldsymbol{K}(\boldsymbol{q}-\boldsymbol{\theta}) = -\boldsymbol{J}^{\boldsymbol{T}}\boldsymbol{f} \tag{5.15}$$

$$\boldsymbol{K}(\boldsymbol{\theta}-\boldsymbol{q}) = \boldsymbol{\tau} = \boldsymbol{K}_{\boldsymbol{p\theta}}(\boldsymbol{\theta}_{\boldsymbol{d}}-\boldsymbol{\theta}) \tag{5.16}$$

where $\boldsymbol{\theta}_{\boldsymbol{d}}$ is the desired motor position, and $\boldsymbol{K}_{\boldsymbol{p\theta}}$ is the proportional gain matrix of the motor position control. Solving for $\boldsymbol{\theta}$ from Equation (5.16),

$$\boldsymbol{\theta} = \boldsymbol{\theta}_{\boldsymbol{d}} - \boldsymbol{K}_{\boldsymbol{p\theta}}^{-\mathbf{1}}\boldsymbol{\tau} = \boldsymbol{\theta}_{\boldsymbol{d}} - \boldsymbol{K}_{\boldsymbol{p\theta}}^{-\mathbf{1}}\boldsymbol{J}^{\boldsymbol{T}}\boldsymbol{f} \tag{517.}$$

Replacing (5.17) in (5.15) and solving for $\boldsymbol{q}$, we have

$$\boldsymbol{q} = \boldsymbol{\theta} - \boldsymbol{K}^{-\mathbf{1}}\boldsymbol{J}^{\boldsymbol{T}}\boldsymbol{f} = \boldsymbol{\theta}_{\boldsymbol{d}} - \left(\boldsymbol{K}_{\boldsymbol{p\theta}}^{-\mathbf{1}} + \boldsymbol{K}^{-\mathbf{1}}\right)\boldsymbol{J}^{\boldsymbol{T}}\boldsymbol{f} \tag{5.18}$$

Therefore, the link positions will be affected by an equivalent stiffness that is influenced by the passive stiffness, $\boldsymbol{K}^{-\mathbf{1}}$, and the active stiffness of the motion control, $\boldsymbol{K}_{\boldsymbol{p\theta}}^{-\mathbf{1}}$. Since the motor and link positions are equivalent and assuming the reduction factor $N = 1$, we can consider that $\boldsymbol{\theta}_{\boldsymbol{d}} = \boldsymbol{q}_{\boldsymbol{d}}$. For small deformations, $\Delta\boldsymbol{x}$ and $\Delta\boldsymbol{q}$ can be related,

$$\Delta\boldsymbol{x} \approx \boldsymbol{J}(\boldsymbol{q})\Delta\boldsymbol{q} = \boldsymbol{J}(\boldsymbol{q})(\boldsymbol{\theta}_{\boldsymbol{d}} - \boldsymbol{q}) \tag{5.19}$$

Then, the cartesian stiffness matrix is

$$\boldsymbol{K}_{\boldsymbol{x}} = \frac{\boldsymbol{f}}{\Delta\boldsymbol{x}} = \boldsymbol{J}^{-\boldsymbol{T}}\left(\boldsymbol{K}_{\boldsymbol{p\theta}}^{-\mathbf{1}} + \boldsymbol{K}^{-\mathbf{1}}\right)^{-\mathbf{1}}\boldsymbol{J}^{-\mathbf{1}} \tag{5.20}$$

Hence, in this case, the active and passive stiffnesses are equivalent.

5.4.1.2. Link Position

Considering the robot in a steady-state and input control (position sensor) in the link side, we have

$$\boldsymbol{K(q-\theta)=-J^{T}f} \tag{5.21}$$

$$\boldsymbol{K(\theta-q)=\tau=K_{pq}(q_{d}-q)} \tag{5.22}$$

where $\boldsymbol{q_d}$ is the desired link position, and $\boldsymbol{K_{pq}}$ is the proportional gain matrix of the link position control. Solving for $\boldsymbol{q}$ from Equation (5.22),

$$\boldsymbol{q=q_{d}-K_{pq}^{-1}\tau=q_{d}-K_{pq}^{-1}J^{T}f} \tag{5.23}$$

therefore, the link positions will be affected only by the active stiffness of the joint motion control, $\boldsymbol{K_{pq}^{-1}}$. The stiffness matrix will be

$$\boldsymbol{K_{x}=\frac{f}{\Delta x}=J^{-T}K_{pq}J^{-1}} \tag{5.24}$$

5.4.1.3. Link velocities

In the case of link velocity control, there is a possibility of finding stiffness effects depending on the type of control. Considering the control input, $\boldsymbol{\tau}$, as a proportional-integral with gravity compensation, $\boldsymbol{G(q)}$,

$$\boldsymbol{\tau=K_{p\dot{q}}(\dot{q}_{d}-\dot{q})\ +\ K_{i\dot{q}}\int(\dot{q}_{d}-\dot{q})dt\ +\ G(q)} \tag{5.25}$$

where $\boldsymbol{\dot{q}_d}$ is the desired link velocity, $\boldsymbol{K_{p\dot{q}}}$ is the proportional gain matrix, and $\boldsymbol{K_{i\dot{q}}}$ is the integral gain matrix of the velocity control.

The integral term can be analysed as a proportional term regarding the position.

$$\boldsymbol{\tau=K_{p\dot{q}}(\dot{q}_{d}-\dot{q})\ +\ K_{i\dot{q}}(q_{d}-q)} \tag{5.26}$$

Considering the robot dynamics, Equations (5.1) and (5.2) and the input in a steady state, we have

$$\boldsymbol{K}(\boldsymbol{q}-\boldsymbol{\theta})=-\boldsymbol{J}^{\boldsymbol{T}}\boldsymbol{f} \tag{5.27}$$

$$\boldsymbol{K}(\boldsymbol{\theta}-\boldsymbol{q})=\boldsymbol{\tau} \tag{5.28}$$

$$\boldsymbol{\tau}=\boldsymbol{K}_{\boldsymbol{pq}}\dot{\boldsymbol{q}}_{\boldsymbol{d}}+\boldsymbol{K}_{\boldsymbol{iq}}(\boldsymbol{q}_{\boldsymbol{d}}-\boldsymbol{q}) \tag{5.29}$$

Solving for $\boldsymbol{q}$ from Equation (5.29)

$$\boldsymbol{q}=\boldsymbol{q}_{\boldsymbol{d}}+\boldsymbol{K}_{\boldsymbol{iq}}^{-\mathbf{1}}\left(\boldsymbol{K}_{\boldsymbol{pq}}\dot{\boldsymbol{q}}_{\boldsymbol{d}}-\boldsymbol{\tau}\right)=\boldsymbol{q}_{\boldsymbol{d}}+\boldsymbol{K}_{\boldsymbol{iq}}^{-\mathbf{1}}\left(\boldsymbol{K}_{\boldsymbol{pq}}\dot{\boldsymbol{q}}_{\boldsymbol{d}}-\boldsymbol{J}^{\boldsymbol{T}}\boldsymbol{f}\right) \tag{5.30}$$

Ordering the equation,

$$\boldsymbol{f}=\boldsymbol{J}^{-\boldsymbol{T}}(\boldsymbol{K}_{\boldsymbol{iq}}(\boldsymbol{q}_{\boldsymbol{d}}-\boldsymbol{q})+\boldsymbol{K}_{\boldsymbol{pq}}\dot{\boldsymbol{q}}_{\boldsymbol{d}})\approx\boldsymbol{J}^{-\boldsymbol{T}}(\boldsymbol{K}_{\boldsymbol{iq}}\boldsymbol{J}^{-\mathbf{1}}(\boldsymbol{x}_{\boldsymbol{d}}-x)+\boldsymbol{K}_{\boldsymbol{pq}}\dot{\boldsymbol{q}}_{\boldsymbol{d}}) \tag{5.31}$$

Hence, the cartesian stiffness matrix of the robot will be,

$$\boldsymbol{K}_{\boldsymbol{x}}=\boldsymbol{J}^{-\boldsymbol{T}}\boldsymbol{K}_{\boldsymbol{iq}}\boldsymbol{J}^{-\mathbf{1}} \tag{5.32}$$

The term $\boldsymbol{J}^{-\boldsymbol{T}}\boldsymbol{K}_{\boldsymbol{pq}}\dot{\boldsymbol{q}}_{\boldsymbol{d}}$ acts like a bias. It means, for zero external force $\boldsymbol{f}$, the robot will have some deformation. Therefore, the integral control acts like active stiffness and the proportional control as a bias. If the velocity loop does not have an integrator, just like a proportional control, the control action will be.

$$\boldsymbol{\tau}=\boldsymbol{K}_{\boldsymbol{pq}}(\dot{\boldsymbol{q}}_{\boldsymbol{d}}-\dot{\boldsymbol{q}}) \tag{5.33}$$

$$\boldsymbol{f}=\boldsymbol{J}^{-\boldsymbol{T}}\boldsymbol{K}_{\boldsymbol{pq}}(\dot{\boldsymbol{q}}_{\boldsymbol{d}}-\dot{\boldsymbol{q}})=\boldsymbol{J}^{-\boldsymbol{T}}\boldsymbol{K}_{\boldsymbol{pq}}\dot{\boldsymbol{q}}_{\boldsymbol{d}}-\boldsymbol{J}^{-\boldsymbol{T}}\boldsymbol{K}_{\boldsymbol{pq}}\dot{\boldsymbol{q}} \tag{5.34}$$

The first term acts like bias and the second one as damping. Thus, there is no active stiffness. The system will behave like a mass-damper under an external force. The final state will be achieved when the robot stops ($\dot{\boldsymbol{q}}=\mathbf{0}$).

$$\boldsymbol{f}=-\boldsymbol{J}^{-\boldsymbol{T}}\boldsymbol{K}_{\boldsymbol{pq}}\dot{\boldsymbol{q}}_{\boldsymbol{d}} \tag{5.35}$$

which means, that the reference velocities, $\dot{\boldsymbol{q}}_{\boldsymbol{d}}$, should be

$$\dot{\boldsymbol{q}}_{\boldsymbol{d}} = -\boldsymbol{J}^{\boldsymbol{T}}\boldsymbol{K}_{\boldsymbol{pq}}^{-\boldsymbol{1}}\boldsymbol{f} \tag{5.36}$$

This corresponds to an open control loop, theoretically without force error.

In summary, if the velocity loop has an integrator, the integrator acts like active stiffness in the joint space and the proportional control as bias. In the case, it does not contain an integrator; if no stiffness term appears, then the exerted force is proportional to the reference velocity.

5.4.2. Absolute cartesian position inner loop

In the following subsection, we will make the convergence analysis of the force for the case when the external loop sends the absolute reference position to the controller. In the deduction, we will use the proportional-derivative and the proportional-derivative with feedforward as external loops. The proportional-integral-derivative will not be studied since it guarantees zero error if the system is stable.

Regarding the inner loops, both possibilities—Jacobian inverse and Jacobian transpose—will be contemplated. Every combination of inner and outer loop will be studied. The deductions of the formulae will be omitted for briefness. Only the final results will be presented.

5.4.2.1. Jacobian Transpose

Considering the motion control as PV with gravity compensation. In this case, the error is in cartesian coordinates. Thus, the input torque is

$$\boldsymbol{\tau} = \boldsymbol{J}^{\boldsymbol{T}}\boldsymbol{K}_{\boldsymbol{px}}(\boldsymbol{x}_{\boldsymbol{d}} - \boldsymbol{x}) \; + \; \boldsymbol{G}(\boldsymbol{q}) \tag{5.37}$$

where $\boldsymbol{K}_{\boldsymbol{px}}$ is the proportional gain matrix in cartesian space.

Replacing Equation (5.37) in dynamics, Equations (5.1) and (5.2), and resolving for steady-state force $\boldsymbol{f}_{\infty}$, the following expression is obtained:

$$\boldsymbol{f}_{\infty} = \left(\boldsymbol{I} \; + \; \boldsymbol{K}_{\boldsymbol{px}}\boldsymbol{K}_{\boldsymbol{e}}^{-\boldsymbol{1}}\right)^{-\boldsymbol{1}}\left(\boldsymbol{K}_{\boldsymbol{px}}\boldsymbol{x}_{\boldsymbol{d}} - \boldsymbol{K}_{\boldsymbol{px}}\boldsymbol{x}_{\boldsymbol{e}}\right) \tag{5.38}$$

The force will be influenced by the passive stiffness of the environment, $\boldsymbol{K}_{\boldsymbol{e}}^{-\boldsymbol{1}}$, and the active stiffness of the motion control, $\boldsymbol{K}_{\boldsymbol{px}}$, as well as the position of the

environment, $\boldsymbol{x_e}$. Typically, these values are unknown. However, the value of $\boldsymbol{K_{px}}$ is uniform in all the working range of the robot.

5.4.2.2. *Jacobian inverse*

In this case, the error is in joint coordinates. Therefore, the inner control torque input is

$$\boldsymbol{\tau = K_{pq}(q_d - q) + G(q)} \tag{5.39}$$

where $\boldsymbol{K_{pq}}$ is the gains matrix of the proportional control in the joint space.

Replacing Equation (5.39) in dynamics and resolving for steady-state force, we have

$$\boldsymbol{f_\infty = \left(I + \widetilde{K}_{px}K_e^{-1}\right)^{-1}\left(\widetilde{K}_{px}x_d - \widetilde{K}_{px}x_e\right)} \tag{5.40}$$

where $\boldsymbol{\widetilde{K}_{px} = J^{-T}K_{pq}J^{-1}}$ is the active stiffness in cartesian space, which is calculated through the coordinate transformation expressed in Equation (5.12).

The force will be influenced by the passive stiffness of the environment, $\boldsymbol{K_e^{-1}}$, and the active stiffness of the motion control, $\boldsymbol{\widetilde{K}_{px}}$, as well as the position of the environment, $\boldsymbol{x_e}$. Typically, these values are unknown. However, the value of $\boldsymbol{\widetilde{K}_{px}}$ is not uniform in all the working range of the robot.

5.4.2.3. *Implications*

The main difference in these methods is that the Jacobian inverse matrix, $\boldsymbol{J^{-1}}$, and Jacobian transpose matrix, $\boldsymbol{J^{-T}}$, appear in the term $\boldsymbol{\widetilde{K}_{px}}$ due to the transformation of the active joint stiffness into the cartesian space. This transformation of coordinates implies that the Cartesian stiffness depends on the actual position where the robot is, so it will not be constant during a given trajectory.

It should be noted that the force also depends on the $\boldsymbol{x_d}$ input reference coming from the possible outer loops. Therefore, in Table 5.2, the final value of the steady-state force, $\boldsymbol{f_\infty}$, in both cases, is obtained by replacing $\boldsymbol{x_d}$ with one of the outer algorithms already exposed in Table 5.1.

Table 5.2. Response force of the control force with absolute position inner loop

Jacobian Case	Outer Algorithm	Steady-State Force	
J^T	PV	$\boldsymbol{f}_\infty = \left(\boldsymbol{I} + \boldsymbol{K_{px}S_fK_{pf}} + \boldsymbol{K_{px}S_fK_e^{-1}}\right)^{-1}\left(\boldsymbol{K_{px}S_fK_{pf}f_d} - \boldsymbol{K_{px}S_fx_e}\right),$	**(5.41)**
J^T	P + FF	$\boldsymbol{f}_\infty = \left(\boldsymbol{I} + \boldsymbol{K_{Px}S_fK_{Pf}} + \boldsymbol{K_{Px}S_fK_e^{-1}}\right)^{-1}\left(\boldsymbol{K_{Px}S_fK_{Pf}f_d} + \boldsymbol{K_{Px}FF} - \boldsymbol{K_{Px}S_fx_e}\right),$	**(5.42)**
J^{-1}	PV	$\boldsymbol{f}_\infty = \left(\boldsymbol{I} + \boldsymbol{\widetilde{K}_{px}S_fK_{pf}} + \boldsymbol{\widetilde{K}_{px}S_fK_e^{-1}}\right)^{-1}\left(\boldsymbol{\widetilde{K}_{px}S_fK_{pf}f_d} - \boldsymbol{\widetilde{K}_{px}S_fx_e}\right),$	**(5.43)**
J^{-1}	P + FF	$\boldsymbol{f}_\infty = \left(\boldsymbol{I} + \boldsymbol{\widetilde{K}_{px}S_fK_{pf}} + \boldsymbol{\widetilde{K}_{px}S_fK_e^{-1}}\right)^{-1}\left(\boldsymbol{\widetilde{K}_{px}S_fK_{pf}f_d} + \boldsymbol{\widetilde{K}_{px}FF} - \boldsymbol{\widetilde{K}_{px}S_fx_e}\right),$	**(5.44)**

Here, $\boldsymbol{S_f}$ is the selection matrix of the force direction, $\boldsymbol{K_{pf}}$ is the compliance matrix of the force control, and $\boldsymbol{I}$ is the identity matrix.

The feedforward of the reference force eliminates the error in rigid robots, which have the possibility to access directly to the motor torques. However, the elasticity of the environment and the inner loop introduce an error. For the case of Jacobian transpose, to obtain zero error, the feedforward should be

$$\boldsymbol{f}_\infty = \boldsymbol{f_d} \iff \boldsymbol{FF} = \left(\boldsymbol{S_fK_e^{-1}} + \boldsymbol{K_{px}^{-1}}\right)\boldsymbol{f_d} + \boldsymbol{S_fx_e} \tag{5.45}$$

and for the case of the Jacobian inverse,

$$\boldsymbol{f}_\infty = \boldsymbol{f_d} \iff \boldsymbol{FF} = \left(\boldsymbol{S_fK_e^{-1}} + \boldsymbol{\widetilde{K}_{px}^{-1}}\right)\boldsymbol{f_d} + \boldsymbol{S_fx_e} \tag{5.46}$$

In Table 5.2, the final value for the steady-state force depends on the characteristics of the environment, as its position ($\boldsymbol{x_e}$) and stiffness ($\boldsymbol{K_e^{-1}}$). Thus, there will be a force error in steady state, unless those values are known with exactitude to be compensated.

It is crucial to notice that, in outer loops with feedforward action, it is possible to obtain a zero-force error. To achieve this, the reference force must have the value given by $\boldsymbol{FF}$ term. In the case of Jacobian transpose, the feedforward action depends on the environment and the proportional gain of the cartesian position control. In the other case (Jacobian inverse), the control action depends on the environment,

and the proportional gain of the joint control transformed into cartesian space. Therefore, it is necessary to know the Jacobian matrix to calculate the stiffness in each sampling period. In summary, in all the versions of the absolute cartesian position control, the characteristics of the environment (stiffness and position) appear. To achieve good tracking, these magnitudes must be known. Moreover, for the inner loop with Jacobian transpose, the force control is uniform in all the working range. For the Jacobian inverse, it is not.

5.4.3. Incremental cartesian position inner loop

In the case of cartesian position control, we have another alternative to give a reference to the control. We can give the incremental difference $\Delta \boldsymbol{x_d}$ instead of $\boldsymbol{x_d}$.

5.4.3.1. Jacobian transpose

The calculated steady-state force depends on the product of the gain matrix of the cartesian proportional control and the desired incremental position.

$$\boldsymbol{f}_\infty = \boldsymbol{K_{px}} \Delta \boldsymbol{x_d} \tag{5.47}$$

5.4.3.2. Jacobian inverse

In this case, the calculated steady-state force depends on the product of the gain matrix of the joint proportional control transformed into cartesian space and the desired incremental position.

$$\boldsymbol{f}_\infty = \widetilde{\boldsymbol{K}}_{\boldsymbol{px}} \Delta \boldsymbol{x_d} \tag{5.48}$$

5.4.3.3. Implications

As in the case of absolute position loop, in the Jacobian inverse method, the stiffness matrix must be determined through the transformation of the proportional gain from the space of the articulations into the cartesian space of the end effector. However, it should be noted that, in an incremental position loop, the force will not be affected by environmental conditions. Table 5.3 shows the steady-state force obtained by replacing $\Delta \boldsymbol{x_d}$ by the algorithms exposed in Table 5.1.

Table 5.3. Response force of the control force with incremental position inner loop.

Jacobian Type	Outer Algorithm	Steady-State Force	
J^T	PV	$\boldsymbol{f}_\infty = \left(\boldsymbol{I} + \boldsymbol{K_{px}S_fK_{pf}}\right)^{-1}\left(\boldsymbol{K_{px}S_fK_{pf}f_d}\right),$	**(5.49)**
J^T	PV + FF	$\boldsymbol{f}_\infty = \left(\boldsymbol{I} + \boldsymbol{K_{px}S_fK_{pf}}\right)^{-1}\left(\boldsymbol{K_{px}S_fK_{pf}f_d} + \boldsymbol{K_{px}FF}\right),$	**(5.50)**
J^{-1}	PV	$\boldsymbol{f}_\infty = \left(\boldsymbol{I} + \widetilde{\boldsymbol{K}}_{\boldsymbol{px}}\boldsymbol{S_fK_{pf}}\right)^{-1}\left(\widetilde{\boldsymbol{K}}_{\boldsymbol{px}}\boldsymbol{S_fK_{pf}f_d}\right),$	**(5.51)**
J^{-1}	PV + FF	$\boldsymbol{f}_\infty = \left(\boldsymbol{I} + \widetilde{\boldsymbol{K}}_{\boldsymbol{px}}\boldsymbol{S_fK_{pf}}\right)^{-1}\left(\widetilde{\boldsymbol{K}}_{\boldsymbol{px}}\boldsymbol{S_fK_{pf}f_d} + \widetilde{\boldsymbol{K}}_{\boldsymbol{px}}\boldsymbol{FF}\right),$	**(5.52)**

Here, $\boldsymbol{S_f}$ is the selection matrix of the force direction and $\boldsymbol{K_{pf}}$ is the active compliance matrix of the force control.

The force control with incremental position loop depends only on the active stiffness of the position control, $\boldsymbol{K_{px}}$ or $\widetilde{\boldsymbol{K}}_{\boldsymbol{px}}$, and the active stiffness of the force control, $\boldsymbol{K_{pf}}$. Besides, the feedforward action is easier to implement because it only depends on the gains of the position controls. For the case of Jacobian transpose, to obtain zero error, the feedforward should be

$$\boldsymbol{f}_\infty = \boldsymbol{f_d} \iff \boldsymbol{FF} = \boldsymbol{K_{px}^{-1}f_d} \tag{5.53}$$

and for the case of the Jacobian inverse,

$$\boldsymbol{f}_\infty = \boldsymbol{f_d} \iff \boldsymbol{FF} = \widetilde{\boldsymbol{K}}_{\boldsymbol{px}}^{\boldsymbol{-1}}\boldsymbol{f_d} \tag{5.54}$$

In summary, the incremental position control has an important advantage over the absolute position control; it does not depend on characteristics of the environment.

5.4.4. Cartesian Velocity inner loop

In the case of the inner velocity loop, the input is considered as a proportional control with gravity compensation.

5.4.4.1. Jacobian transpose

In this case, the input of the inner loop in the cartesian space is

$$\boldsymbol{\tau} = \boldsymbol{J^TK_{p\dot{x}}}(\dot{\boldsymbol{x}}_{\boldsymbol{d}} - \dot{\boldsymbol{x}}) + \boldsymbol{G}(\boldsymbol{q}) \tag{5.55}$$

where $\boldsymbol{K_{p\dot{x}}}$ is the proportional gain matrix of the velocity cartesian control.

Replacing Equation (5.55) in dynamics and resolving it for steady state, we can calculate the force as the product of the proportional gain matrix and the desired velocity as

$$\boldsymbol{f_\infty = K_{p\dot{x}} \dot{x}_d} \tag{5.56}$$

5.4.4.2. Jacobian inverse

In this case, the input in the inner control is expressed in joint space. Thus, the input is

$$\boldsymbol{\tau = K_{p\dot{q}}(\dot{q}_d - \dot{q}) + G(q)} \tag{5.57}$$

where $\boldsymbol{K_{p\dot{q}}}$ is the proportional gain matrix of the velocity joint control.

Replacing Equation (5.57) in dynamics and resolving it for steady state, we can calculate the force $\boldsymbol{f_\infty}$ as the product of the proportional gain matrix of the joint control (transformed into cartesian space) and the desired velocity,

$$\boldsymbol{f_\infty = \widetilde{K}_{p\dot{x}} \dot{x}_d} \tag{5.58}$$

As can be seen in the Equations (5.56) and (5.58), the force in steady state depends only on the active stiffness of the velocity control. In Equation (5.56) depends on the cartesian stiffness, $\boldsymbol{K_{p\dot{x}}}$, and in Equation (5.58) depends on the joint stiffness and the position of the robot due to the Jacobian term $\boldsymbol{\widetilde{K}_{p\dot{x}}}$.

5.4.4.3. Implications

The results of the force obtained replacing $\boldsymbol{\Delta x_d}$ by the algorithms exposed in Table 5.1 are shown in Table 5.4.

Table 5.4. Response force of the control force with inner velocity loop

Jacobian Type	Algorithm	Steady-State Force	
J^T	PV	$\boldsymbol{f_\infty = \left(I + K_{p\dot{x}} S_f K_{pf}\right)^{-1} K_{p\dot{x}} S_f K_{pf} f_d,}$	**(5.59)**
J^T	PV + FF	$\boldsymbol{f_\infty = \left(I + K_{p\dot{x}} S_f K_{pf}\right)^{-1} K_{p\dot{x}} S_f K_{pf} f_d + K_{p\dot{x}} FF,}$	**(5.60)**
J^{-1}	PV	$\boldsymbol{f_\infty = \left(I + \widetilde{K}_{p\dot{x}} S_f K_{pf}\right)^{-1} \widetilde{K}_{p\dot{x}} S_f K_{pf} f_d,}$	**(5.61)**
J^{-1}	PV + FF	$\boldsymbol{f_\infty = \left(I + \widetilde{K}_{p\dot{x}} S_f K_{pf}\right)^{-1} \widetilde{K}_{p\dot{x}} S_f K_{pf} f_d + \widetilde{K}_{p\dot{x}} FF,}$	**(5.62)**

Here, $\boldsymbol{S_f}$ is the selection matrix of the force direction and $\boldsymbol{K_{pf}}$ is the compliance matrix of the force control.

In both cases, incremental position and velocity loop, it is possible to observe that control with feedforward action $\boldsymbol{FF}$ will only depend on the gain of the controller and will not depend on the position and stiffness of the environment. For the case of Jacobian transpose, to obtain zero error, the feedforward should be

$$\boldsymbol{f}_\infty = \boldsymbol{f_d} \iff \boldsymbol{FF} = \boldsymbol{K_{px}^{-1} f_d} \tag{5.63}$$

and for the case of the Jacobian inverse,

$$\boldsymbol{f}_\infty = \boldsymbol{f_d} \iff \boldsymbol{FF} = \widetilde{\boldsymbol{K}}_{\boldsymbol{px}}^{\boldsymbol{-1}} \boldsymbol{f_d} \tag{5.64}$$

Moreover, if the velocity control is a proportional-integral control, the force error in steady state will be zero.

Summarizing, the incremental position control and the velocity control are very similar. However, in real robots, they may behave in different ways. There are two main reasons for this. In one case, the inner loop uses the position proportional constants, while in the other case, it uses the velocity proportional constants. There is no reason why they should be equal. Thus, the active stiffness in one case will be higher than in the other. The other reason is that one of the inner loops (position or velocity) may use Jacobian transpose, while the other applies Jacobian inverse.

5.5. Methodology

The previous deductions have been verified experimentally. Different control methods have been tested and compared in practice. With these results, the best combination of inner and outer loop has been identified. These experiments were carried out through polishing operations.

5.5.1. Experimental setup

The physical system employed in this study is shown in Figure 5.4. The robot used for the experiments is a UR3 (Universal Robots A/S, Odense, Denmark). This robot arm has a six-revolute-joints anthropomorphic geometry. The joints are

actuated by servo motors via harmonics drive reduction; two encoders are used in each joint. A magnetic encoder monitors the motor position, and an optical encoder monitors the link position. A force sensor is mounted on the end effector of the robot.

The robot has a sampling frequency of 125 Hz or, in other words, a sampling period of 0.008 s. The force/torque sensor is type HEX-EB165 (OnRobot A/S, Odense, Denmark), with a force range from 0 N to 200 N and a torque range from 0 Nm to 10 Nm. The sensor has a maximum sampling frequency of 500 Hz and is directly connected with the robot controller. All the variables, such as position, velocity, torques, and forces, are sent via ethernet to a computer, where the data are received every sampling period by an acquisition software implemented in LabVIEW (version 2017, National Instruments, Austin, TX, USA). Afterward, these data are processed with MATLAB (version 2019, MathWorks Inc., Natick, MA, USA).

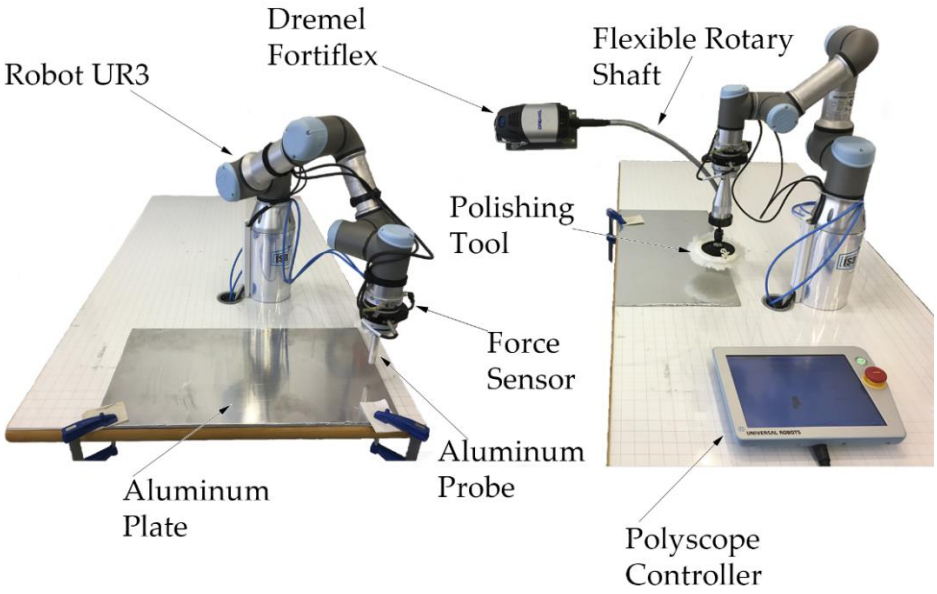

Figure 5.4. Experimental setup.

The preliminary experiments were made using an aluminium probe with a spherical tip attached directly to the force sensor to avoid vibrations. The definitive experiments were made with a common polishing tool.

Two materials were considered as workpiece—aluminium and a polymer plate—with the aim to evaluate the force control with different stiffness of the environment.

The tool chuck was driven by a Dremel model FortiFlex 9100 (Dremel Europe, Breda, The Netherlands) with a flexible rotary shaft. It was installed in the end-effector of the robot through a custom machined coupling. The final tool was a commercial polishing tool of 130 mm of diameter. It was composed of a rubber base and a buffing pad.

5.5.2. Method

To avoid the experimental comparisons of all the combinations of inner and outer loops, in the first step, we identified the internal loop with the best performance. For these experiments, we used a proportional force controller for the external loop. As demonstrated later in this paper, the best results were obtained with an inner velocity loop. In the following step, the behaviours of several external regulators were compared. The best inner loop identified in the first step was applied.

Regarding the identification of the optimal inner loop, in this work were considered the position and velocity loops in cartesian space. In the case of the position, both proposals, absolute and incremental, were treated. Also, in all the cases, the stiffness was evaluated.

Next, we explain the commands used to implement the inner loops. In the case of position loops, we used the command script movel,

$$movel(x\ vector, a, v, t, r)$$

where *x vector* represents the cartesian position to be reached by the end-effector, *a* is the acceleration, *v* is the velocity, *t* is the time, and *radius* is the blend radius. This command controls the position in the cartesian space in each sampling period. If the variable time is specified, the command will ignore the velocity and acceleration values. In our case, it was necessary to specify a time of 8 ms as a sampling period. Also, it was necessary to implement an external trapezoidal trajectory generator to specify the velocity and acceleration of the movement on the Y-axis. This trajectory generator was implemented with script commands.

In the case of the velocity loop, we used the command script speedl,

speedl(v vector, a, t).

where *v vector* represents the cartesian velocity to be reached by the end-effector, *a* is the acceleration, and *t* is the time. This command controls the velocity in the cartesian space. We can indicate a specific cartesian velocity in each degree of freedom. However, we only can indicate a global acceleration. In this case, it was not necessary to specify the time because the command was applied in each sampling period.

Then, the inner loop with the best performance was used with different outer force loops. A comparison between PD and PV algorithm is shown to study the effect of the damping action in the interaction task. In addition, the integral control action is compared with the feedforward action, in order to study which alternative is more appropriate in practical applications. All these results were obtained using the aluminium probe tool to avoid the vibrations of a real polishing tool.

Finally, a real application is shown. A polishing task was performed with the polishing tool and with the best force control obtained. The task was performed with and without the force control to compare results. The gains, applied in the different control algorithms, were determined experimentally. These values were found after several experiments and analysis of the force response. The best values of these gains are exposed in this work.

5.5.3. Task planning

The trajectory of the task used in the experiments had initially a free movement in the minus Z direction with constant speed, switching to force control in the Z direction when the measured force surpassed a threshold of 1 N. The impact control consisted of a proportional gain of less value until reaching the reference force (5 N or 10 N). When the force reference was reached, the robot started a controlled movement on the Y direction, maintaining the pressure force over the workpiece surface. A scheme of the experiments is shown in Figure 5.5.

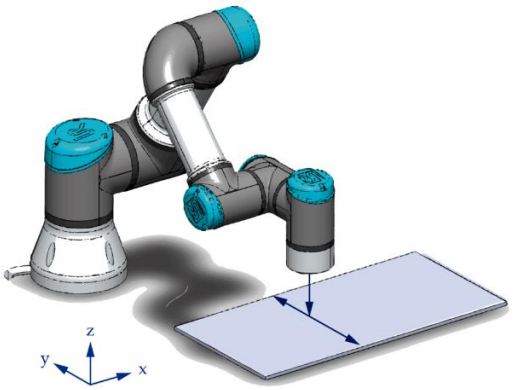

Figure 5.5. Scheme of experiments.

5.5.4. Stiffness parameters identification

The stiffnesses of the joints were identified experimentally. The robot was stopped while the controller was working. Then different weights of 2 kg, 2.5 kg, and 3 kg were applied on the joints of the robot. The joint torques and joint positions were measured in the robot. The stiffness of each joint was calculated through Equation (5.65). The stiffness values k_i of the joints are shown in Table 5.5.

$$k_i = \frac{\Delta\tau_i}{\Delta q_i} \tag{5.65}$$

where, for each joint, $\Delta\tau_i$ was the change in the torque value due to the added weights and Δq_i was the change in the position value. As the joints of the UR3 robot have only three sizes [39], it was not necessary to measure the six joints. Base joint and shoulder joint have the same size, the elbow joint has the other size, and the three wrist joints have another same size. Then, it was only necessary to identify joint 5 (wrist), joint 3 (elbow), and joint 2 (shoulder). The three weights were applied to each joint and the stiffness values were obtained through the mean of the measurements.

Table 5.5. Stiffness joint parameters.

Joint	k1	k2	k3	k4	k5	k6
Stiffness (N/m)	13323	13323	4412	2729	2729	2729

5.6. Results and discussions

5.6.1. The inner loop

5.6.1.1. Absolute position loop

In Section 5.4, it was demonstrated that the performance of the absolute position loop depends on the characteristics of the environment much more than the others. The worst results were expected from this loop. This hypothesis was confirmed by the experiments.

The output of the external loop corresponds to the reference position of the robot. In some cases, this position was not in contact with the environment, which provoked bouncing. High accelerations were reached. Sometimes, the robot had hard impacts against the piece, and the security measures were activated, causing an emergency stop. After several experiments, this type of inner loop was discarded. It was the worst of three.

The plots resulting from these experiments have not been shown in the article. However, we included this method since we consider that our experience, albeit negative, may be useful to other people that work in force control.

5.6.1.2. Incremental position loop

Figure 5.6 shows the force control with an inner position loop applied over two materials: a polymer (orange lines) and aluminium (blue lines).

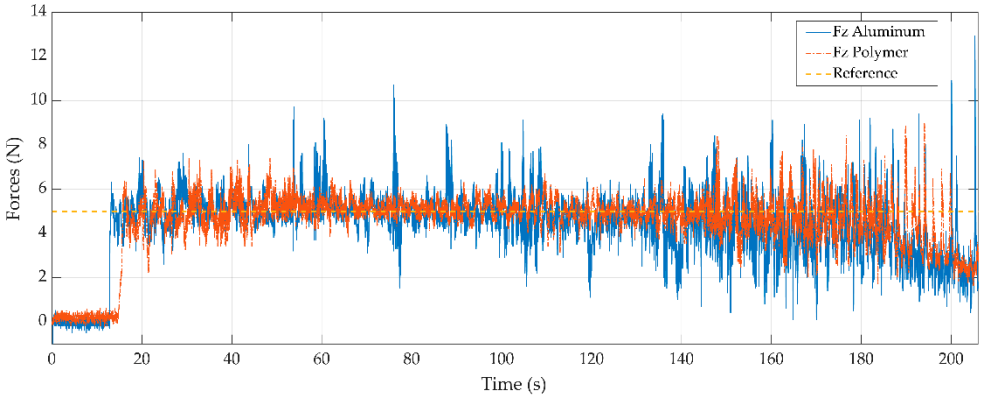

Figure 5.6. Force control with inner position loop.

As can be seen, the force response remains around the reference force of 5 N for the first 150 s. Concerning the material in contact, the force shows higher deviations in the aluminium as a result of seizing between same materials.

The force error at the end of the stroke (from 150 s) is mainly due to the changes produced in the cartesian stiffness. This suggests that the position loop is made with the Jacobian inverse method; therefore, the stiffness changes due to the change in position and the use of the Jacobian matrix.

A representation of the cartesian stiffness during the trajectory is shown in Figure 5.7. It was calculated using the coordinate transformation in Equation (5.12). In the figure, the force and stiffness in the Z direction, $\boldsymbol{K_z}$, are shown. As can be seen, during the time that the end effector is within the stable force path, at 5 N, the stiffness $\boldsymbol{K_z}$ has the maximum value. However, when the robot is near the end of the trajectory, the stiffness decreases, generating errors in the force response. If the internal control gains were known, this effect would be compensated in the control action to avoid the observed deviations.

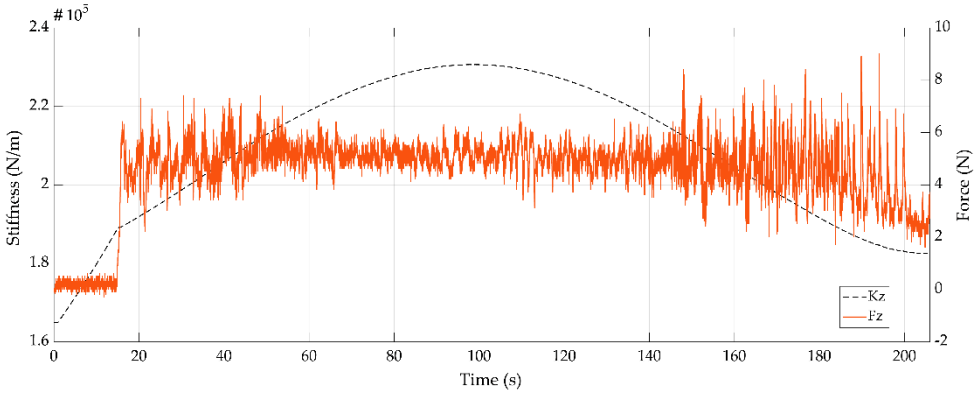

Figure 5.7. Stiffness analysis in the inner position loop.

5.6.1.3. Velocity loop

Figure 5.8 shows the force control with the inner velocity loop applied over the polymer (orange line) and aluminium (blue line).

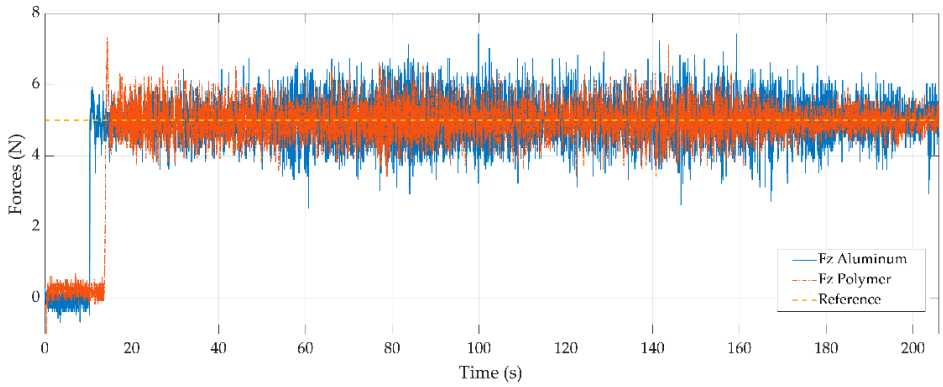

Figure 5.8. Force control with inner velocity loop.

As can be seen, unlike the position loop, in the speed loop, the force is maintained around the reference value throughout the trajectory. Furthermore, it should be noted that there is no significant difference in the force error between materials. This coincides with stated in Equation (5.57), which indicates that the force response does not depend on the environment stiffness.

In addition, the velocity loop is not affected by the position in the trajectory of the robot. This allows to obtain better results, independently of the position of the robot in the workspace. This suggests that the velocity loop is implemented with the Jacobian transpose.

5.6.2. The outer loops

This subsection describes the experimental comparative analysis of the several external loops explained previously. The internal loop used in all the cases was the velocity loop, which demonstrated the best results.

In force control is not only important tracking the reference force. The oscillations and peaks of the applied force cause not only uneven polishing but also, a gradual deterioration in the robot mechanics. For these reasons, this work presents the average force tracking error, standard deviation, number of peaks, and maximal/minimal value to compare the different external loops.

5.6.2.1. Proportional Derivative (PD) vs. Proportional with Velocity Feedback (PV)

In Figure 5.9, we can observe the function of the force derivative (blue lines) and the velocity feedback term (yellow lines).

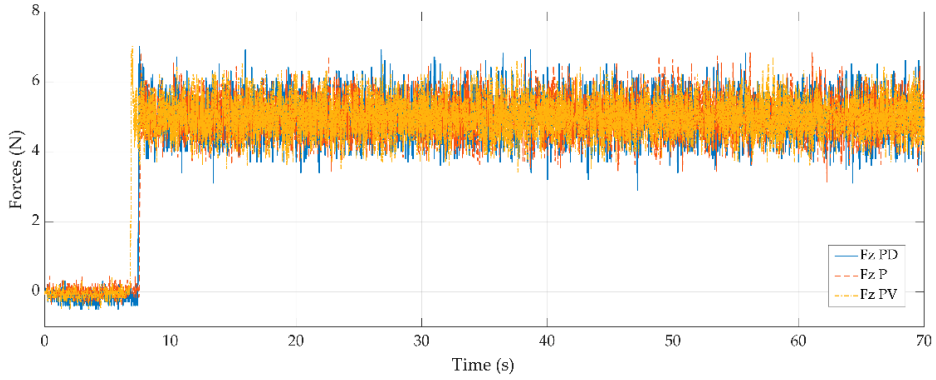

Figure 5.9. Proportional derivative (PD) vs. proportional with velocity feedback (PV) comparison.

The proportional algorithm P (orange lines) is used as a reference to compare the performance of the other algorithms. Regarding the response, the classic derivative action of the force control does not present good results due to the noise in the sensor, which worsens the numerical derivation, generating peaks up to 34% higher (highlighted as circles) than the pure proportional controller. This is due to the noise of the sensor and the long sampling period. Thus, the force derivative may change substantially during a sampling period.

Through the numerical results associated with the graph, the derivative control action employing the velocity feedback (PV) shows a slight improvement in damping peak force by 30%, and the PD peaks have a smaller size than in PV and P controls. However, the velocity changes faster than the sampling period, so its effect is not so observable.

5.6.2.2. Integral Action (PI) vs. Feedforward Action (P + FF)

In Figure 5.10, we can observe the function of the integral action and the feedforward of the force to reduce the error of the system.

Although theoretically, the integral action guarantees a null error, it is not very popular, because it can have stability problems, wind-up, and slower convergence than a feedforward action.

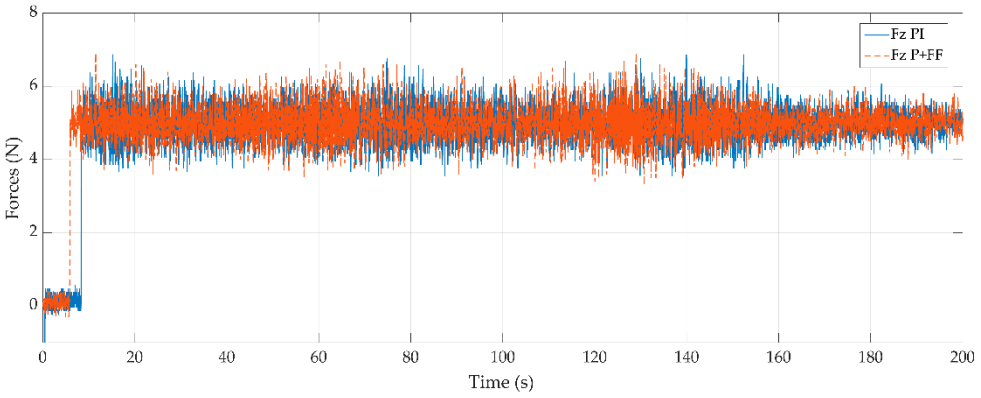

Figure 5.10. Integral action (PI) vs. feedforward action (P + FF) comparison.

On the other hand, control with feedforward is challenging to implement since it requires knowledge of the active stiffness matrix of the position control. In this case, we consider a constant $\boldsymbol{FF}$ gain for the feedforward action.

Due to the low sampling period and the fast dynamics of the interaction, both the integral action and the feedforward action do not guarantee a zero error. However, even using a constant feedforward, like the one used in Figure 5.10, P + FF allows to reduce the error from 0.11% to 0.02%.

5.6.2.3. Global Results

Table 5.6 contains the results of force control with velocity inner loop and with various types of outer loops. It should be noted that $\boldsymbol{FF}$, $\boldsymbol{K_{pf}}$, $\boldsymbol{K_{if}}$, and $\boldsymbol{K_{vf}}$ are the gains of the outer force loops. The table shows the mean, standard deviation, and the error respect to the reference value of 5 N. Also, it incorporates the maximum and minimum values reached by the force control. Finally, the quantity of picks outside the range of ±1 N are shown.

Table 5.6. Comparison of outer loops.

Outer	$\boldsymbol{FF}$	$\boldsymbol{K_{pf}}$	$\boldsymbol{K_{if}}$	$\boldsymbol{K_{vf}}$	Mean	Standard	Error	Max	Min	N° Picks	N° Picks

Loop					Deviation					<4 N	>6 N
P		.001			4.993	.444	.13%	6.972	3.272	324	392
PV		.001		.03	4.989	.450	.21%	6.878	3.178	231	420
PD		.001		.03	4.985	.609	.29%	6.908	2.908	297	456
PI		.001	.0001		4.994	.448	.10%	6.863	3.563	320	324
PIV		.001	.0001	.03	4.994	.434	.11%	7.128	3.428	204	355
P+FF	10^{-6}	.001			4.999	.453	.02%	6.898	3.298	389	341

Table 5.6 represents the value of the best experiments for every regulator (outer loop). It may be appreciated that the error is very small for all the outer loops.

According to the theory, PV should be more damped than a simple proportional, albeit it is slower to converge. According to the experiments, PV control has a slightly worse average error and standard deviation. However, it has fewer peaks, and they are lower. In the same way, a PD algorithm is applied. The results show as the derivative action in the force is worse than the feedback velocity action.

The smallest average error is obtained with P + FF control. However, PI and PIV have better standard deviation and fewer peaks outside the range of ±1 N. It should be emphasized that the feedforward term was constant in these experiments. The results can be improved by adjusting the feedforward gain based on the stiffness matrix.

Due to the number of criteria that determine the performance of force control, a prioritization matrix has been made. The aim of this matrix is determining the most suitable algorithm for the outer loop. The criteria for evaluating the algorithms are

- A mean close to the reference force;
- A minimum standard deviation;
- Fewer peaks above and below the reference force;
- Lower value of maximum and minimum force.

Furthermore, it is preferable to use algorithms where the adjustment of the gains of the force control is not dependent on the knowledge of the features of the inner loop.

Table 5.7 presents a prioritization matrix where the different algorithms are evaluated according to the criteria above. The weights of the criteria were previously determined, these weights should be decided according to the final application (in

this case, a polishing task). The options were evaluated with a score from 1 to 5, with 5 being the best score.

Table 5.7. Prioritization matrix of outer loops.

	Mean (46%)		Std. Deviation (19%)		N° Picks >6 N (11%)		N° Picks <4 N (11%)		Max Pick (4%)		Min Pick (4%)		Adjusting Gain (6%)		Total
	Pt	%	Pt	%	Pt	%	Pt	%	Pt	%	Pt	%	Pt	%	
P	4	1.82	5	.96	4	.43	4	.43	4	.16	4	.16	5	.29	4.25
PV	3	1.37	4	.77	3	.32	5	.54	4	.16	4	.16	5	.29	3.60
PD	3	1.37	4	.77	3	.32	4	.43	4	.16	3	.12	5	.29	3.46
PI	4	1.82	5	.96	5	.54	3	.32	5	.20	5	.20	5	.29	4.33
PIV	4	1.82	5	.96	4	.43	5	.54	4	.16	5	.20	5	.29	4.40
P + FF	5	2.28	5	.96	4	.43	2	.21	5	.20	3	.12	3	.18	4.37

The total scores indicate that the use of a PIV algorithm is the most suitable option for this example. However, the P + FF algorithm is also a good option if the inner loop structure is known.

5.6.3. Polishing application

A polishing task was performed to demonstrate the effectiveness of the force control. In Figures 5.11 and 5.12, the force measurements for polishing with a reference force of 5 N and 10 N, are presented. For these experiments, we used an inner velocity loop with an outer PIV force loop. The figures display the measured cartesian forces, the reference force, and the force in Z—direction without force control.

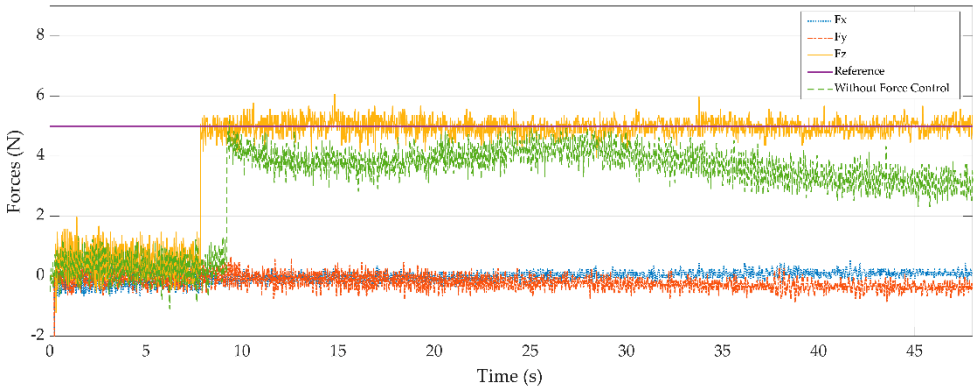

Figure 5.11. Polishing with force control with reference force 5 N.

In both cases, the force F_z remains stable in both experiments. Forces F_x and F_y are shown. The force F_y was produced by the friction along the trajectory. The force F_x was produced by the radial force due to the polishing tool. It can be seen as the force F_x and F_y increase if the force F_z increases.

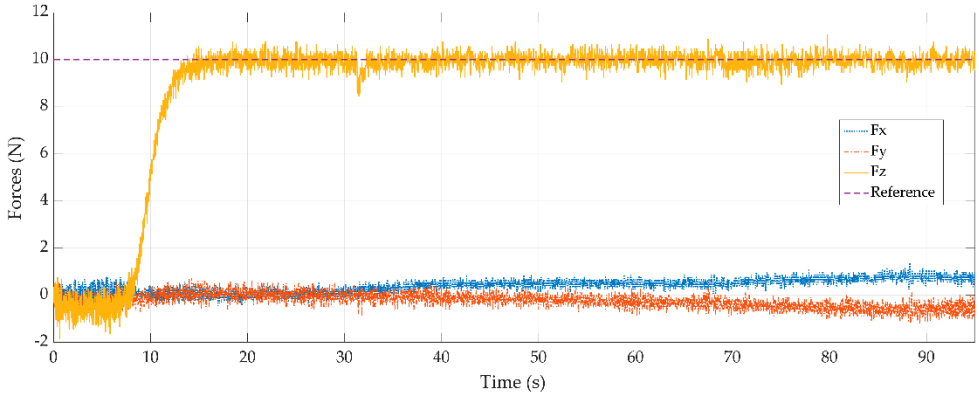

Figure 5.12. Polishing with Force control with reference force 10 N.

As can be observed, the force response is better with the polishing tool than with the probe. This proves that the inner velocity loop is affected by the stiffness of the tool. Further, in Figure 5.11, it is possible to observe the polishing task without force control (green line). This demonstrates that without external force control is not possible to maintain the reference force. Thus, we obtain a poor surface polish. Table 5.8 shows the result of the polishing task.

Table 5.8. Results for polishing task.

Reference Force	Mean	Standard Deviation	Error	Max	Min	N° Picks <4/9 N	N° Picks >6/11 N
5	4.9525	0.2591	0.95%	5.6617	3.9617	1	0
10	9.9666	0.2975	0.33%	11.056	8.4562	33	4
w/o	3.4416	0.5915	31.26%	4.9181	1.6181	8460	0

Table 5.8 includes values of mean, standard deviation, and error of the force control. Also, since the polishing tool is more flexible, it allows to obtain smaller measurement errors than the reference. This effect is reflected in the fewer number of observed picks.

5.7. Conclusions

In summary, the main goals have been achieved. An analysis of inner and outer control loops has been made, working with equations oriented to collaborative robots, unlike the proposals made for rigid robots [18–21]. The study was made with a practical approach to identify the inner loops when their characteristics are unknown. This is easier to implement than the works in Ma, Z. et al. [16] and Huang, L. et al. [17] because they measured all the variables of the robot, like torques, motor position, etc. The article also explains how that information may be used to define the external loop in order to obtain better results. The importance of the concept of the stiffness matrix, applied to robot control, has been proved in theory and practice.

After completing the previous steps and making experiments, the absolute position inner loop obtains the worse results. Theoretically, the incremental position loop and the velocity loops are equivalent. However, in practice, this equivalence depends on the way the internal loop is implemented and the gains of the inner control.

According to the way of the coordinate transformation is made by the robot controller (Jacobian transpose vs. Jacobian inverse), the stiffness matrix changes considerably. The Jacobian transpose gives a constant stiffness matrix, which causes stable contact force in all the working area of the robot, while the Jacobian inverse method gives a cartesian stiffness matrix that depends on the joint stiffness and the position of the robot.

As a rule, the user does not have the information on the way the inner loop was implemented. However, it can be deduced experimentally. To prove this, an experimental verification was made with a UR3 CB3 robot. Despite the limitations of this robot (as slow sampling frequency and low joint stiffness), the theoretical results have been mostly verified.

Summarizing, the results on the UR3 robot show that the variations in the performance of the different external controllers are small. Using a PV over a proportional (P) in the outer loop improves the impacts, while the PD action confirms a worse performance in force control, as observed in the paper of Neranon, P and Bicker, P. [21]. A feedforward term (FF) achieves better force tracking than an integrator (PI)—in this case, it is an improvement compared to the methods exposed in the book Siciliano, B. et al. [33]. However, it has more peaks. It may be enhanced

if the stiffness matrix is introduced. Regarding the inner control, the inner velocity loop gives the best results, probably because it is implemented using the Jacobian transpose in the UR3.

The force control is affected by the stiffness of the tool, as is the case with the polishing tool, where its more flexible material lets reducing the number of oscillations obtained during the execution of the task. This fact decreases the effect of the problem explained in Iglesias, I. et al. [3].

Several problems remain for future works, and three stand out. Experiments should be repeated with a robot with better performance, such as increased joint stiffness and a faster sampling period, to prove their influence in the improvement of the force control. The feedforward term should be implemented considering the stiffness matrix; in this way, the force error can be cancelled. On the other hand, for outer loops, other types of algorithms could be used, like adaptive control or the sliding mode.

Author Contributions: Conceptualization, R.Z.-S., R.P.-U., and S.C.G.; methodology, R.Z.-S., R.P.-U., and S.C.G.; software, R.P.-U.; validation, R.Z.-S., R.P.-U., and S.C.G.; formal analysis, R.Z.-S., and R.P.-U.; investigation, R.P.-U.; resources, R.Z.-S. and S.C.G.; data curation, R.P.-U.; writing—original draft preparation, R.P.-U.; writing—review and editing, R.Z.-S., R.P.-U., and S.C.G.; visualization, R.Z.-S., R.P.-U., and S.C.G.; supervision, R.Z.-S. and S.C.G.; project administration, R.Z.-S., and S.C.G.; funding acquisition, R.P.-U. and R.Z.-S. All authors have read and agreed to the published version of the manuscript.

Funding: The authors are grateful for the financial support of the Spanish Ministry of Economy and European Union, grant DPI2016-81002-R (AEI/FEDER, UE), to the research work here published. Rodrigo Pérez-Ubeda is grateful to the Ph.D. Grant CONICYT PFCHA/DOCTORADO BECAS CHILE/2017–72180157).

Conflicts of Interest: The authors declare no conflict of interest.

5.8. References

1. Top Trends Robotics 2020—International Federation of Robotics. Available online: https://ifr.org/ifr-press- releases/news/top-trends-robotics-2020 (accessed on 16 May 2020).
2. Gaz, C.; Magrini, E.; De Luca, A. A model-based residual approach for human-robot collaboration during manual polishing operations. *Mechatronics* **2018**, 55, 234–247.
3. Iglesias, I.; Sebastián, M.A.; Ares, J.E. Overview of the State of Robotic Machining: Current Situation and Future Potential. *Procedia Eng*. **2015**, 132, 911–917.
4. Perez, R.; Gutierrez Rubert, S.C.; Zotovic, R. A Study on Robot Arm Machining: Advance and Future Challenges. In Proceedings of the 29th Daaam International Symposium on Intelligent Manufacturing and Automation, Zadar, Croatia, 24–27 October 2018; pp. 0931–0940.
5. Perez-Ubeda, R.; Gutierrez, S.C.; Zotovic, R.; Lluch-Cerezo, J. Study of the application of a collaborative robot for machining tasks. *Procedia Manuf*. **2019**, 41, 867–874.
6. Spong, M.W. On the Force Control Problem for Flexible Joint Manipulators. *IEEE Trans. Automat. Contr*. **1989**, 34, 107–111.
7. Ren, T.; Dong, Y.; Wu, D.; Chen, K. Impedance control of collaborative robots based on joint torque servo with active disturbance rejection. *Ind. Rob.* **2018**, 4, 518–528.
8. Ajoudani, A.; Tsagarakis, N.G.; Bicchi, A. Choosing poses for force and stiffness control. *IEEE Trans. Robot*. **2017**, 33, 1483–1490.
9. Magrini, E.; De Luca, A. Hybrid force/velocity control for physical human-robot collaboration tasks. In Proceedings of the 2016 IEEE/RSJ International Conference on Intelligent Robots and Systems (IROS), Daejeon, Korea, 9–14 October 2016; pp. 857–863.
10. Ahmad, S. Constrained Motion (Force/Position) Control of Flexible Joint Robots. *IEEE Trans. Syst. Man Cybern*. **1993**, 23, 374–381.
11. Goldsmith, P.B.; Francis, B.A.; Goldenberg, A.A. Stability of hybrid position/force control applied to manipulators with flexible joints. *Int. J. Robot. Autom*. **1999**, 14, 146–160.

12. Rafik, A.; Farid, F.; Redouane, T. Hybrid force/position approach for flexible-joint robot with Fuzzy-Sliding mode control. In Proceedings of the 2018 International Conference on Applied Smart Systems, ICASS 2018, Médéa, Algeria, 24–25 November 2018; IEEE: New York City, NY, USA, 2018; pp. 1–6.
13. Calanca, A.; Fiorini, P. Understanding environment-Adaptive force control of series elastic actuators. *IEEE/ASME Trans. Mechatron*. **2018**, 23, 413–423.
14. Oh, S.; Kong, K. High-Precision Robust Force Control of a Series Elastic Actuator. *IEEE/ASME Trans. Mechatron*. **2017**, 22, 71–80.
15. Yin, H.; Li, S.; Wang, H. Sliding mode position/force control for motion synchronization of a flexible-joint manipulator system with time delay. In Proceedings of the Chinese Control Conference CCC, Chengdu, China, 27–29 July 2016; pp. 6195–6200.
16. Ma, Z.; Hong, G.S.; Ang, M.H.; Poo, A.N.; Lin, W. A force control method with positive feedback for industrial finishing applications. In Proceedings of the 2018 IEEE/ASME International Conference on Advanced Intelligent Mechatronics (AIM), Auckland, New Zealand, 9–12 July 2018; pp. 810–815.
17. Huang, L.; Ge, S.S.; Lee, T.H. Position/force control of uncertain constrained flexible joint robots. *Mechatronics*. **2006**, 16, 111–120.
18. Chiaverini, S.; Siciliano, B.; Villani, L. A survey of robot interaction control schemes with experimental comparison. *IEEE/ASME Trans. Mechatron*. **1999**, 4, 273–285.
19. Winkler, A.; Suchy, J. Explicit and implicit force control of an industrial manipulator—An experimental summary. In Proceedings of the 2016 21st International Conference on Methods and Models in Automation and Robotics (MMAR), Miedzyzdroje, Poland, 29 August–1 September 2016; IEEE: New York City, NY, USA, 2016; pp. 19–24.
20. De Schutter, J.; Bruyninckx, H.; Zhu, W.-H.; Spong, M.W. Force control: A bird's eye view. In Control of Fluid Flow; Springer Science and Business Media LLC: Berlin, Germany, 1998; Volume 230, pp. 1–17, ISBN 978-3-540-40913-7.
21. Neranon, P.; Bicker, R. Force/position control of a robot manipulator for human-robot interaction. *Therm. Sci.* **2016**, 20, 537–548.
22. Chen, S.Y.; Zhang, T.; Zou, Y.B. Fuzzy-Sliding Mode Force Control Research on Robotic Machining. *J. Robot*. **2017**, 2017.

23. Lin, H.-I.; Dubey, V. Design of an Adaptive Force Controlled Robotic Polishing System Using Adaptive Fuzzy-PID. In Advances in Intelligent Systems and Computing; Springer Science and Business Media LLC: Berlin, Germany, 2018; Volume 867, pp. 825–836.
24. Perez-Vidal, C.; Gracia, L.; Sanchez-Caballero, S.; Solanes, J.E.; Saccon, A.; Tornero, J. Design of a polishing tool for collaborative robotics using minimum viable product approach. *Int. J. Comput. Integr. Manuf.* **2019**, 32, 848–857.
25. Chen, F.; Zhao, H.; Li, D.; Chen, L.; Tan, C.; Ding, H. Contact force control and vibration suppression in robotic polishing with a smart end effector. *Robot. Comput. Integr. Manuf.* **2019**, 57, 391–403.
26. Mohammad, A.E.K.; Hong, J.; Wang, D. Design of a force-controlled end-effector with low-inertia effect for robotic polishing using macro-mini robot approach. *Robot. Comput. Integr. Manuf.* **2018**, 49, 54–65.
27. Xiao, C.; Wang, Q.; Zhou, X.; Xu, Z.; Lao, X.; Chen, Y. Hybrid force/position control strategy for electromagnetic based robotic polishing systems. In Proceedings of the Chinese Control Conference CCC, Guangzhou, China, 27–30 July 2019; pp. 7010–7015.
28. Li, J.; Zhang, T.; Liu, X.; Guan, Y.; Wang, D. A Survey of Robotic Polishing. In Proceedings of the 2018 IEEE International Conference on Robotics and Biomimetics (ROBIO), Kuala Lumpur, Malaysia, 12–15 December 2018; pp. 2125–2132.
29. Zollo, L.; Siciliano, B.; De Luca, A.; Guglielmelli, E.; Dario, P. Compliance Control for an Anthropomorphic Robot with Elastic Joints: Theory and Experiments. *J. Dyn. Syst. Meas. Control* **2005**, 127, 321.
30. Han, D.; Duan, X.; Li, M.; Cui, T.; Ma, A.; Ma, X. Interaction Control for Manipulator with compliant end-effector based on hybrid position-force control. In Proceedings of the 2017 IEEE International Conference on Mechatronics and Automation (ICMA), Takamatsu, Japan, 6–9 August 2017; pp. 863–868.
31. Schindlbeck, C.; Haddadin, S. Unified passivity-based Cartesian force/impedance control for rigid and flexible joint robots via task-energy tanks. In Proceedings of the 2015 IEEE International Conference on Robotics and Automation (ICRA), Seattle, WA, USA, 26–30 May 2015; pp. 440–447.

32. Zotovic Stanisic, R.; Valera Fernández, Á. Simultaneous velocity, impact and force control. *Robotica* **2009**, 27, 1039–1048.
33. Siciliano, B.; Sciavicco, L.; Villani, L.; Oriolo, G. Robotics: Modelling, Planning and Control, 2nd ed.; Springer-Verlag: London, UK, 2009; ISBN 9781846286414.
34. Volpe, R.; Khosla, P. A theoretical and experimental investigation of explicit force control strategies for manipulators. *IEEE Trans. Automat. Contr*. **1993**, 38, 1634–1650.
35. Zeng, G.; Hemami, A. An overview of robot force control. *Robotica* **1997**, 15, 473–482.
36. Salisbury, J. Active stiffness control of a manipulator in cartesian coordinates. In Proceedings of the 1980 19th IEEE Conference on Decision and Control including the Symposium on Adaptive Processes, Albuquerque, NM, USA, 10–12 December 1980; IEEE: New York City, NY, USA, 1980; pp. 95–100.
37. Chen, S.F.; Kao, I. Conservative congruence transformation for joint and Cartesian stiffness matrices of robotic hands and fingers. *Int. J. Rob. Res*. **2000**, 19, 835–847.
38. Institute of Robotics and Mechatronics DLR Light Weight Robot III. Available online: https://www.dlr.de/rm/en/desktopdefault.aspx/tabid-12464/#gallery/29165 (accessed on 7 April 2020).
39. Universal, Robots. Service Manual UR3; Universal Robots: Odense, Denmark, 2003.

Capítulo 6

Behavioural study of the force control loop used in a collaborative robot for sanding materials

materials

MDPI

Article

Behavioural Study of the Force Control Loop Used in a Collaborative Robot for Sanding Materials

Rodrigo Pérez Ubeda [1,*], Santiago C. Gutiérrez Rubert [1], Ranko Zotovic Stanisic [2] and Ángel Perles Ivars [3]

Received: 7 November 2020
Accepted: 22 December 2020
Published: 25 December 2020

[1] Department of Mechanical and Materials Engineering, Universitat Politècnica de València, 46022 Valencia, Spain; scgutier@mcm.upv.es
[2] Institute of Industrial Control Systems and Computing, Universitat Politècnica de València, 46022 Valencia, Spain; rzotovic@isa.upv.es
[3] ITACA Institute, Universitat Politècnica de València, 46022 Valencia, Spain; aperles@disca.upv.es
* Correspondence: rodpeub@doctor.upv.es; Tel.: +34-96-3877622

Pérez-Ubeda, R.; Gutiérrez Rubert, S.C.; Stanisic, R.Z.; Perles Ivars, Á. Behavioural Study of the Force Control Loop Used in a Collaborative Robot for Sanding Materials. Materials 2021, 14, 67. https://dx.doi.org/10.3390/ma14010067

Behavioural study of the force control loop used in a collaborative robot for sanding materials

Rodrigo Pérez-Ubeda [1]*, Santiago C. Gutiérrez Rubert [1], Ranko Zotovic-Stanisic [2] and Ángel Perles Ivars [3]

[1] Department of Mechanical and Materials Engineering, Universitat Politècnica de València, 46022 Valencia, Spain

[2] Institute of Industrial Control Systems and Computing, Universitat Politècnica de València, 46022 Valencia, Spain

[3] ITACA Institute, Universitat Politècnica de València, 46022 Valencia, Spain

* Correspondence: rodpeub@doctor.upv.es.

Abstract

The rise of collaborative robots urges the consideration of them for different industrial tasks such as sanding. In this context, the purpose of this article is to demonstrate the feasibility of using collaborative robots in processing operations, such as orbital sanding. For the demonstration, the tools and working conditions have been adjusted to the capacity of the robot. Materials with different characteristics have been selected, such as aluminium, steel, brass, wood, and plastic. An inner/outer control loop strategy has been used, complementing the robot's motion control with an outer force control loop. After carrying out an explanatory design of experiments, it was observed that it is possible to perform the operation in all materials, without destabilising the control, with a mean force error of 0.32%. Compared with industrial robots, collaborative ones can perform the same sanding task with similar results. An important outcome is that unlike what might be thought, an increase in the applied force does not guarantee a better finish. In fact, an increase in the feed rate does not produce significant variation in the finish—less than 0.02 μm; therefore, the process is in a "saturation state" and it is possible to increase the feed rate to increase productivity.

Keywords: robot sanding; robot finishing; inner/outer control loop; force control; collaborative robot

6.1. Introduction

Surface finishing operations such as polishing and sanding play an important role within industry. These operations are not only performed with an aesthetic purpose but also for functional reasons. The main objective is to obtain a specified surface roughness. On the other hand, the main drawback of these operations is that they have been commonly carried out manually, which makes them expensive and dependent on operator skill. They are time-consuming and prone to errors [1,2]. In manual operations, the time for polishing pieces represents up to 50% of the total production and costs can reach 15% of the total amount. Therefore, improvements in time efficiency and surface quality are the main objectives for this process [3].

Industrial robots have appeared as an alternative to operators, since, due to their competitive cost, flexibility, programmability, and a large volume of work, they are potentially better suited to automate finishing operations [4,5].

In the last decade, collaborative robots (cobots) have gained popularity within the industry because, in addition to the advantages already mentioned, these robots allow for safe work in conjunction with a human operator [6]. Cobots are an important part in the physical systems of the Smart Manufacturing Systems of Industry 4.0 [7]. These robots are commonly used in applications such as assembly, pick and place, inspection, and welding operations, among others [8]. Research in [9] shows an initial focus on the use of collaborative robots in mould polishing, where automatic polishing by the robot without force control is performed in parallel with manual operation. Polishing a flat surface, the authors demonstrated that a cobot presents a similar result that a 3-axis CNC machine (Hardinge Corporate Headquarters, Westlakes, Berwyn, PA, USA).

In the case of surface finishing applications, it is crucial to control the necessary contact force to ensure the same quality throughout the treated part. To solve this problem, some studies offer several solutions for industrial robots (non-collaborative), where the force control is accomplished passively through a tool with a specific design [10]. In this case, we can find studies where a force control is not used, but only a single position control is used. However, it is necessary to know the whole geometry of the part and to have a computer-aided design and manufacturing software to generate the right trajectory. It is also necessary to use a tool that absorbs vibrations due to the contact force [11]. Another example can be found in [12], where

researchers develop a specific end effector for grinding applications. In this study, an abrasive belt and a force-controlled grinding tool mounted in the end effector are used to improve finishing in welding seams. The application of a specific end effector is useful when the workpiece is large. However, a specific device reduces the stiffness and increases the weight in the end effector.

Otherwise, force control can also be carried out actively through feedback with the measured force. This method requires a modification of the control algorithm gains to adapt them to the environmental conditions [13–15]. In the case of collaborative robots, some studies have developed sanding applications, but they are based on controlling the torques of the motors [16], which is not usually possible in commercial robots. Other studies, such as [17], combine a force sensor with a laser position sensor. The laser is responsible for keeping the tool in the normal direction to the workpiece, independently of the changing geometric shape. However, this task can also be performed by the force controller. End effector torques or tilt angle can be controlled through machine learning, allowing the user to teach the desired route with significant precision [18].

In [19], the authors presented a complete analysis of the use of an inner/outer loop force control in collaborative robots, from which it is extracted that the best results will be obtained for an inner velocity loop and an outer force loop with a Proportional-Integral with Velocity feedback algorithm (PIV), or a Proportional with Feedforward algorithm (P + FF). Under the conditions of this study, one of the main contributions of this work is that the force control does not depend on the environment. This allows obtaining of the reference value without the need to change the gains of the control algorithm when the task is performed on different materials. These are the algorithms that are going to be used and tested in the present work.

In addition to force control, productivity is an important feature to be improved with the automation of these processes. The most basic way to measure the material removal rate (MRR) is through the Preston equation (Equation (6.1)).

$$MRR = k \cdot P \cdot V \tag{6.1}$$

where P is the contact pressure, V is the feed rate of the tool, and k is the Preston coefficient, which is determined experimentally and depends on the material,

abrasive and lubrication, among other factors [20]. However, other works provide more complex mathematical models that allow obtaining the minimum number of passes and the characteristics of the abrasive material that should be used to obtain the desired roughness [11,21]. An experimental investigation was developed in [22], from which the parameters that affect the surface quality in an industrial robot (no collaborative) polishing could be obtained. From this work, it was concluded that the geometry of the workpiece and the cutting speed do not contribute significantly to the roughness response. However, an increase in the feed rate will generate an increase in the surface roughness value.

Another important aspect in Smart Manufacturing Systems is the determination and optimization of the process parameters to eliminate wastage of resources, especially materials and energy. In [23], the authors used teaching–learning-based optimization and bacterial foraging optimization methods. They obtained the optimum values of cutting speed, feed rate, and depth-of-cut to achieve the lowest surface roughness parameters and cutting temperature.

In a similar way, the authors in [24] used a factorial procedure to characterize the experimental robotic system, predicting the attainable manufacturing tolerances, and allowing the study of the main constraints in the machining of relatively soft materials.

Despite the advances in productivity and optimization of parameters in sanding tasks, it is necessary to study the capacity of collaborative robots in these applications. For this reason, this article is dedicated not only to demonstrating that it is possible to perform operations that imply additional efforts with cobots, but that these operations can be improved with a study that includes the control loops used and the main characteristics of the process and the environment.

One of the situations that this study has revealed is what we have colloquially called "the process saturation concept". This concept is directly related to the conditions of execution of the operation. In this case, it is an orbital sanding process, where effort is being applied between the sandpaper tool and the part, while movement is carried out on the work surface (cut feed) at the same time as the sandpaper rotates around its axis (cutting movement). Once these three parameters (force, cutting speed, and feed rate) have been set, the grain size is the decisive element that ultimately determines the surface quality achieved. In other words,

once the surface has been completely sanded, improving the finish using the same grain size would hardly imply any improvement (beyond the almost negligible effect that the wear of the grains themselves could have). This means that, once a cutting speed is set (orbital sanding usually employs motors without speed variation), it is possible to:

- Adjust the applied force, as long as it is sufficient for the grains to remove the material, looking for the best selection for the combined, control algorithm—characteristics of the robot (e.g., taking into account the sampling frequency);
- Increase the feed rate to improve productivity.

The minimum force required together with the maximum cut feed rate would be the "optimal" values. Any variation on them that does not prevent reaching the quality provided by the selected grain size would mean "saturating the process". That is, reprocessing the same area without any improvement.

This article is structured as follows. Section 6.2 describes the materials, experimental bench, and the design of experiments used. Section 6.3 shows the results and discussion of the experiments developed with the collaborative robot. Finally, Section 6.4 presents conclusions and future work.

6.2. Materials and Methods

6.2.1. Experimental setup

The sanding operation to be performed consists of a straight movement on the XY plane, travelling 189 mm along the +Y direction of the robot. The experimental bench can be seen in Figure 6.1. A collaborative robot from the company "Universal Robots", UR3 (Universal Robots A/S, Odense, Denmark), is used, with a maximum load of 30 N. A force sensor "OnRobot HEX-EB165" (OnRobot A/S, Odense, Denmark) with 6 degrees of freedom is docked at the end effector of the robot. The data received from the sensor measurements have an accuracy of 0.001 N and a signal noise of 0.2 N in Z, according to its data sheet. The measurement of variables such as positions, speeds, forces, and torques is carried out through the robot controller. These are sent in real-time to the computer via ethernet with a sampling

period of 8 ms. Data acquisition is made through the "LabVIEW" software (version 2017, National Instruments, Austin, TX, USA), to be later processed using the "MATLAB" software (version 2019, MathWorks Inc., Natick, MA, USA).

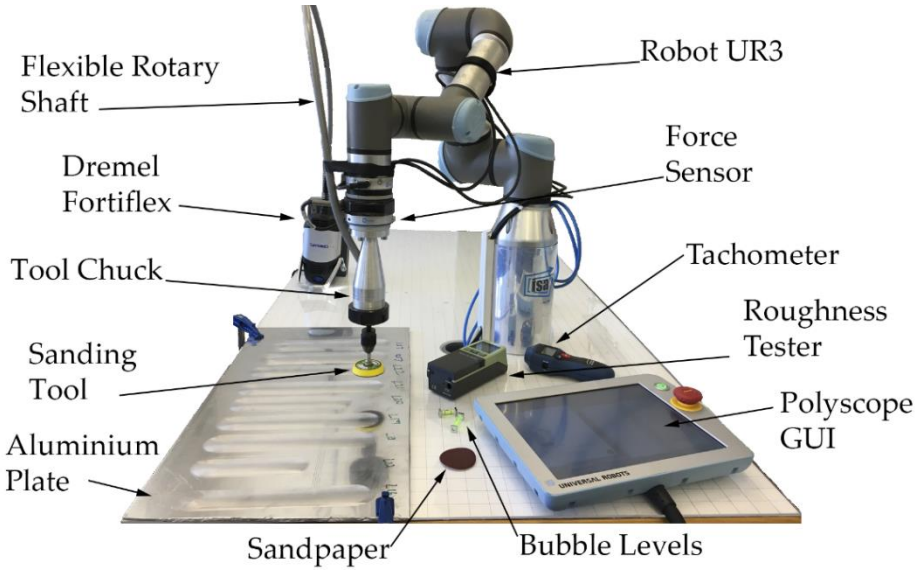

Figure 6.1. Experimental setup.

The sanding tool consists of a commercial 50 mm diameter disc with an adherent surface at its bottom, which allows the exchange of sandpaper for each experiment. The sanding tool is driven by a "Dremel" with a flexible shaft. To expand the range of tool diameters that can be clamped and cutting power, the flexible shaft was replaced by one from the German company Wolfcraft (Wolfcraft GmbH, Kempenich, Germany). Wolfcraft limits the revolutions for their flexible shafts to 3500 rpm. However, to couple the new shaft to the Dremel and to mount an industrial tool clamping system on the UR3, with some common parts with a BT30-ER11 tool holder (Ferretería UNCETA S.A, Elgoibar, Spain), new self-made parts were necessary.

The final system planned forced a reduction in revolutions to values below 1500 rpm. The self-made tool chuck that holds and allows the rotation of the sanding tool can be seen in Figure 6.1. This tool chuck is screwed to the interchangeable base of the robot tip.

6.2.2. Design of experiments

The input variables of the design of experiments planned for this study are shown in Table 6.1. Two possibilities are allowed for the control algorithm, PIV and P+FF. The magnitudes for the reference force used are 2.5 N and 5 N. The materials on which the sanding operation is executed are steel, brass, aluminium, wood, and PVC (Polyvinyl chloride). Materials with very different properties. These are commercial materials, and they are supplied pre-treated. This means that the initial roughness in some of them, see Table 6.1, is better than what can be achieved with a P600 grain size. This research aims to prove that collaborative robots can be used in operations that imply additional efforts, maintaining a constant $\boldsymbol{R_a}$ value under the selected working conditions. The final industrial function for the processed surface, and whether the roughness for that purpose should be greater or less than the original one, remains outside of this study.

In order to reduce the number of experiments, the cutting speed is set to 1070 rpm (bellow 1500 rpm), and feed rate is set to 5 mm/s (300mm/min), this last value was decided consistently with the cutting speed and with the sampling period. The grain size selected for the sandpaper is P600. It should be noted that the diameter of the tool, the grain size and the magnitude of the reference force significantly affect the set of forces required in the process, which is why their values are in concordance with the limitations of the collaborative robot used.

The algorithms and their control gains have been previously determined in the research referred in [19]. These algorithms let obtaining the best results in the UR3 robot when an inner velocity loop is used. During the trajectory, the force is controlled in the Z direction, while the movement is controlled in X and Y direction employing the velocity loop. Being active the feed rate (300 mm/min) in the Y direction and a zero velocity in the X-direction. Due to the type of tests, one single path on a flat surface, and the results of preliminary tests, the velocity loop in the UR3 keeps very low the variations in the feed rate. Once completed, all the tests showed in point 3 'Results and discussions' the calculated mean for the feed rate was around 304 mm/min, less than 1.3% of variation. These variations are not considered in this study.

Table 6.1. Design of the experiments.

Control Algorithm	Reference Force	Materials	Initial R_a (μm)	Feed Rate	Cut Feed	Sandpaper Grain
PIV P+FF	2.5 N 5 N	Steel Brass Aluminium Wood PVC	1.30 0.38 0.18 2.10 0.17	300 mm/min	1070 rpm	P600

For the selected variables, it is necessary to perform 20 experiments. Two repetitions were made with a total of 40 experiments. In each experiment a new path is made in the corresponding material, using a new sanding disc each time. Before executing the sanding operations and with the sanding tool stopped, a couple of bubble levels are used, one in the direction of the X-axis and the other in the direction of the Y-axis, to leave the sanding disc parallel to the work surface in each test. Due to the type of machining performed in the tests, a considerable inclination of the sanding disc could cause decompensation on the resultant of the cutting forces between the area that works in accordance and the area that works in opposition. This would accentuate the different surface finish between both areas, the wear of the tool [25], and most importantly, it would cause an imbalance in the tool increasing oscillations and even causing the UR3 to overstress devices of security. However, in our case, the support for the sandpaper is not rigid, then, small parallelism deviations between the sandpaper and the surface are easily absorbed by this support.

If the robot is used in production, the arrangement of the tool axis normal to the work surface can be automated by software. In this case, it is necessary to incorporate an orientation correction in the control loop, either by a measurement in real-time or by planning the trajectories to be executed.

Because the cutting speed is set without load, this must be measured in each test. Through a digital tachometer 'PCE-DY-65', it is possible to check the speed differences between the theoretical and the real value once the tool contacts with each different material. After the execution of the tests, the surface roughness, $\boldsymbol{R_a}$, arithmetic mean roughness (ISO 4287) is measured at three different points in the machined area: close to the beginning, middle, and the end of the path. The tests only have one travel, the overlap between cutting paths, needed to guarantee the

same roughness over the entire surface, was not included in this study. Based on this criterion, the roughness measurements have been made in the central area to avoid the effect that takes place on the sides of the trajectory due to the variation of the contact force. This effect is caused by the slightly flexible disc that holds the sandpapers. The value of $\boldsymbol{R_a}$ finally shown, corresponds to the average of the three measurements taken. In the measurements, the 'Mitutoyo SJ-201' roughness tester is used. From the data acquired through the force sensor mounted on the robot's wrist, the variables calculated, for each test are:

- The mean of the force measurements on the Z-axis, $\overline{\boldsymbol{F}}_{\boldsymbol{z}}$.
- The standard deviation of the measured force, $\boldsymbol{S_z}$.
- The maximum percentage deviation, $\Delta \boldsymbol{max_z}$, from the reference.
- The minimum percentage deviation, $\Delta \boldsymbol{min_z}$, from the reference.
- The number of upper peaks, $\boldsymbol{N_{upp}}$ (>3.5/6 N) represents the number of deviations that exceed the value of the reference force by + 1 Newton.
- The number of lower peaks, $\boldsymbol{N_{low}}$ (<1.5/4 N) represents the number of deviations that exceed the value of the reference force by -1 Newton.
- The force error, $\boldsymbol{e_f}$, between the reference value and the mean $\overline{\boldsymbol{F}}_{\boldsymbol{z}}$. This relative error is obtained by subtracting the mean of the force measurements to the reference force value divided by the reference force value.

The limit of 1 N to measure the upper and lower peaks was decided after performing several prior experiments with the OnRobot HEX-EB165 force sensor and the UR3. The experiments covered different tasks (machining on soft materials, polished and sanding) and all the measures indicated that 1 N was a perfectly demandable value for the system. Like the roughness measurements, in each experiment, the force measurements are divided into three equal intervals, so that for each dependent variable, there is a total of six samples.

6.2.3. Analysis of variance

Finally, a three-way analysis of variance (ANOVA) is performed to evaluate the effect of the variables on roughness and the results of the force control. The variables measured by the force sensor were taken as dependent variables, and as fixed factors, the parameters, type of control, reference force and material were used. The

Shapiro-Wilk test was used to determine if data were normally distributed before analysis. Besides, the Levene's test was used to assess the homogeneity of variance in each factor groups. Both assumptions are corroborated for each combination of groups of the independent variables. Once it has been determined that there are general differences between the means, post hoc tests are performed to determine which variables in each group differ from each other, that is, the tests allow a pairwise comparison. Tukey's test was used in the paper. The results of the ANOVA are represented by a 95% confidence level ($p<0.05$).

6.3. Results and discussions

6.3.1. Effect of the parameters

The results of the experiments can be seen in Table 6.2. These values are the means of six samples, three for each repetition. The values between parentheses indicate the standard deviation of the six measurements. Most of them present a good outcome regarding compliance with the reference force. In general, many peaks due to overshoots are also observed in the results. However, the number of lower peaks is greater than the number of upper peaks; this is related to the measured values of the force since their mean values are less than the value of the reference force. It is important to highlight that the measurements shown correspond to the data obtained during the entire time that the tool is in contact with the workpiece, allowing a total amount of approximately 9000 data read.

The results of the multivariate analysis are shown in Table 6.3 and Table 6.4. The F-ratio is a test used to evaluate the explanatory power of a group of independent variables on the variation of the dependent variable. If that ratio is large enough, it can be concluded that not all means are equal. To be concise, only groups of variables that had a significant p-value (<0.05) are shown.

It is observed that the 'Control type' factor no produces significant differences in the variables of the study. The 'Material' factor produces significant differences in the variables, arithmetic mean roughness ($\boldsymbol{R_a}$), the standard deviation of the force ($\boldsymbol{S_z}$), the maximum percentage deviation ($\Delta\boldsymbol{max_z}$), the minimum percentage deviation ($\Delta\boldsymbol{min_z}$), the number of upper peaks ($\boldsymbol{N_{upp}}$), and the number of lower peaks ($\boldsymbol{N_{low}}$). The 'Reference force' factor produces significant differences in the

variables, arithmetic mean roughness ($\boldsymbol{R_a}$), mean of the contact force ($\boldsymbol{\overline{F}_z}$), the standard deviation of the force ($\boldsymbol{S_z}$), minimum percentage deviation ($\boldsymbol{\Delta min_z}$), the number of upper peaks ($\boldsymbol{N_{upp}}$), and the number of lower peaks ($\boldsymbol{N_{low}}$).

Table 6.2. Experimental results.

N° Exp	Control	Ref. Force (N)	Material	R_a (μm)	Mean $\overline{F}_z$ (N)	Std. Dev. S_z (N)	Δmax_z (%)	Δmin_z (%)	N_{upp} >3.5/6 (N)	N_{low} <1.5/4 (N)	e_f (%)
E1	P+FF	2.5	Alum.	0.95^{a}	2.488^{a1}	0.495^{a}	60^{a11}	-53^{a11}	209^{a1}	186^{a1}	0.48^{a}
				(0.34)	(0.021)	(0.230)	(25)	(12)	(129)	(111)	(0.008)
E2	P+FF	5	Alum.	1.38^{a}	4.979^{a1}	1.000^{a}	59^{a11}	-61^{a11}	836^{a1}	973^{a1}	0.41^{a}
				(0.36)	(0.027)	(0.283)	(16)	(17)	(222)	(213)	(0.005)
E3	PIV	2.5	Alum.	0.99^{a}	2.477^{a1}	0.458^{a}	57^{a11}	-50^{a11}	53^{a1}	591^{a1}	0.90^{a}
				(0.21)	(0.017)	(0.160)	(13)	(13)	(46)	(101)	(0.007)
E4	PIV	5	Alum.	1.30^{a}	4.968^{a1}	1.402^{a}	71^{a11}	-67^{a11}	483^{a1}	515^{a1}	0.64^{a}
				(0.17)	(0.039)	(0.485)	(23)	(23)	(297)	(284)	(0.008)
E5	P+FF	2.5	Steel	0.53^{b}	2.500^{a2}	0.389^{a}	40^{a2}	-46^{a2}	45^{a2}	455^{a2}	0.02^{a}
				(0.12)	(0.023)	(0.453)	(20)	(21)	(85)	(74)	(0.009)
E6	P+FF	5	Steel	0.56^{b}	5.001^{a2}	0.453^{a}	23^{a2}	-29^{a2}	27^{a2}	480^{a2}	-0.04^{a}
				(0.09)	(0.019)	(0.160)	(6)	(11)	(31)	(188)	(0.004)
E7	PIV	2.5	Steel	0.76^{b}	2.471^{a2}	0.324^{a}	42^{a2}	-41^{a2}	21^{a2}	725^{a2}	1.18^{a}
				(0.15)	(0.037)	(0.171)	(19)	(17)	(46)	(153)	(0.015)
E8	PIV	5	Steel	0.58^{b}	4.994^{a2}	0.395^{a}	26^{a2}	-25^{a2}	22^{a2}	48^{a2}	0.12^{a}
				(0.20)	(0.018)	(0.079)	(6)	(3)	(22)	(21)	(0.004)
E9	P+FF	2.5	Brass	0.37^{b}	2.494^{a}	0.504^{a}	52^{a12}	-50^{a12}	102^{a}	1037^{a}	0.29^{a}
				(0.05)	(0.044)	(0.215)	(35)	(9)	(176)	(174)	(0.018)
E10	P+FF	5	Brass	0.36^{b}	4.991^{a}	0.627^{a}	35^{a12}	-34^{a12}	159^{a}	915^{a}	0.17^{a}
				(0.08)	(0.024)	(0.103)	(4)	(2)	(103)	(142)	(0.005)
E11	PIV	2.5	Brass	0.39^{b}	2.486^{a}	0.513^{a}	50^{a12}	-60^{a12}	68^{a}	937^{a}	0.74^{a}
				(0.07)	(0.046)	(0.170)	(13)	(6)	(117)	(128)	(0.018)
E12	PIV	5	Brass	0.35^{b}	4.987^{a}	0.942^{a}	47^{a12}	-40^{a12}	379^{a}	888^{a}	0.27^{a}
				(0.10)	(0.033)	(0.399)	(20)	(11)	(279)	(271)	(0.007)
E13	P+FF	2.5	Wood	1.77^{c}	2.490^{a1}	0.527^{a}	57^{a1}	-53^{a1}	208^{a}	145^{a1}	0.39^{a}
				(0.29)	(0.010)	(0.304)	(28)	(15)	(245)	(162)	(0.004)
E14	P+FF	5	Wood	1.71^{c}	4.989^{a1}	0.890^{a}	43^{a1}	-42^{a1}	303^{a1}	349^{a1}	0.21^{a}
				(0.49)	(0.017)	(0.430)	(14)	(10)	(296)	(269)	(0.003)
E15	PIV	2.5	Wood	1.21^{c}	2.495^{a1}	0.471^{a}	49^{a1}	-53^{a1}	61^{a1}	114^{a1}	0.19^{a}
				(0.15)	(0.019)	(0.223)	(17)	(20)	(111)	(148)	(0.007)
E16	PIV	5	Wood	1.74^{c}	4.985^{a1}	1.073^{a}	53^{a1}	-49^{a1}	502^{a1}	479^{a1}	0.30^{a}
				(0.43)	(0.022)	(0.515)	(18)	(20)	(383)	(413)	(0.004)
E17	P+FF	2.5	PVC	1.00^{a}	2.496^{a}	0.432^{a}	42^{a12}	-43^{a12}	32^{a}	1011^{a1}	0.18^{a}
				(0.26)	(0.021)	(0.226)	(16)	(16)	(36)	(117)	(0.009)
E18	P+FF	5	PVC	1.10^{a}	5.009^{a}	0.938^{a}	44^{a12}	-37^{a12}	407^{a}	723^{a1}	-0.18^{a}
				(0.25)	(0.029)	(0.558)	(23)	(17)	(428)	(467)	(0.006)
E19	PIV	2.5	PVC	0.91^{a}	2.500^{a}	0.415^{a}	45^{a12}	-43^{a12}	57^{a}	842^{a1}	0.02^{a}
				(0.07)	(0.021)	(0.205)	(16)	(16)	(69)	(50)	(0.009)
E20	PIV	5	PVC	0.96^{a}	4.995^{a}	0.736^{a}	40^{a12}	-36^{a12}	255^{a}	265^{a1}	0.11^{a}
				(0.18)	(0.023)	(0.386)	(16)	(14)	(284)	(284)	(0.005)

* Same superscript letters = no statistically significant difference. $a \neq b \neq c$ in the same columns indicate significant differences according to Tukey's test ($p < 0.05$). Same superscript numbers = no significant difference, $1 \neq 2$ means a significant difference between them, but not with the others in the same column.

Besides, it should be noted that there is no significant effect due to the interaction between control type with reference force and control type with material. The interaction between reference force and material produces significant differences in the variables, arithmetic mean roughness ($\boldsymbol{R_a}$), the standard deviation of the force ($\boldsymbol{S_z}$), minimum percentage deviation ($\boldsymbol{\Delta min_z}$), the number of upper peaks ($\boldsymbol{N_{upp}}$), and the number of lower peaks ($\boldsymbol{N_{low}}$). Finally, triple interactions between factors only produce significant differences in the arithmetic mean roughness ($\boldsymbol{R_a}$)

Table 6.3. ANOVA results (part one).

Source of Variation	Variable	Sum of Squares	df	Mean Square	F-ratio	p-value
Control Type	R_a	0.094	1	0.094	1.677	0.198
	$\bar{F}_z$	0.002	1	0.002	2.951	0.089
	S_z	0.054	1	0.054	0.568	0.453
	Δmax_z	112.937	1	112.937	0.374	0.542
	Δmin_z	234.799	1	234.799	0.970	0.327
	N_{upp}	1491.075	1	1491.075	0.034	0.853
	N_{low}	69.008	1	69.008	0.002	0.969
	e_f	1.927	1	1.927	2.498	0.117
Reference Force	R_a	0.411	1	0.411	7.320	0.008
	$\bar{F}_z$	187.630	1	187.630	256585.617	0.000
	S_z	4.453	1	4.453	47.012	0.000
	Δmax_z	1004.402	1	1004.402	3.325	0.071
	Δmin_z	949.822	1	949.822	3.922	0.050
	N_{upp}	1474305.008	1	1474305.008	34.087	0.000
	N_{low}	1620990.075	1	1620990.075	35.571	0.000
	e_f	1.674	1	1.674	2.169	0.144
Material	R_a	22.432	4	5.608	99.956	0.000
	$\bar{F}_z$	0.006	4	0.001	1.944	0.109
	S_z	2.629	4	0.657	6.938	0.000
	Δmax_z	10264.652	4	2566.163	8.496	0.000
	Δmin_z	9325.331	4	2331.333	9.627	0.000
	N_{upp}	932522.883	4	233130.721	5.390	0.001
	N_{low}	922109.617	4	230527.404	5.059	0.001
	e_f	4.102	4	1.025	1.329	0.264
Control Type * Reference Force	R_a	0.010	1	0.010	0.180	0.673

Table 6.4. ANOVA results (part two).

Source of Variation	Variable	Sum of Squares	df	Mean Square	F-ratio	p-value
Control Type * Reference Force	$\bar{F}_z$	2.828E-07	1	2.828E-07	0.000	0.984
	Sz	0.172	1	0.172	1.814	0.181
	Δmax_z	397.822	1	397.822	1.317	0.254
	$\Delta minz$	171.097	1	171.097	0.707	0.403
	N_{upp}	90036.408	1	90036.408	2.082	0.152
	$Nlow$	21253.408	1	21253.408	0.466	0.496
	e_f	0.201	1	0.201	0.261	0.611
Control Type * Material	R_a	0.504	4	0.126	2.244	0.070
	$\bar{F}_z$	0.001	4	0.000	0.397	0.810
	S_z	0.390	4	0.098	1.030	0.396
	Δmax_z	98.097	4	24.524	0.081	0.988
	Δmin_z	731.837	4	182.959	0.755	0.557
	N_{upp}	79586.883	4	19896.721	0.460	0.765
	N_{low}	138840.950	4	34710.238	0.762	0.553
	e_f	1.807	4	0.452	0.585	0.674
Reference Force * Material	R_a	0.824	4	0.206	3.673	0.008
	$\bar{F}_z$	0.002	4	0.000	0.616	0.652
	S_z	1.434	4	0.359	3.785	0.007
	Δmax_z	1613.502	4	403.375	1.335	0.262
	Δmin_z	5328.349	4	1332.087	5.501	0.000
	N_{upp}	510518.617	4	127629.654	2.951	0.024
	N_{low}	495118.383	4	123779.596	2.716	0.034
	e_f	0.995	4	0.249	0.322	0.862
Control Type * Reference Force * Material	R_a	0.593	4	0.148	2.642	0.038
	$\bar{F}_z$	0.001	4	0.000	0.469	0.758
	S_z	0.369	4	0.092	0.975	0.425
	Δmax_z	684.011	4	171.003	0.566	0.688
	Δmin_z	693.957	4	173.489	0.716	0.583
	N_{upp}	250338.217	4	62584.554	1.447	0.224
	N_{low}	88352.050	4	22088.013	0.485	0.747
	e_f	1.975	4	0.494	0.640	0.635

In Figure 6.2, the marginal means of the analysed variables can be observed. Plots show how these variables vary according to the type of material, control type and reference force.

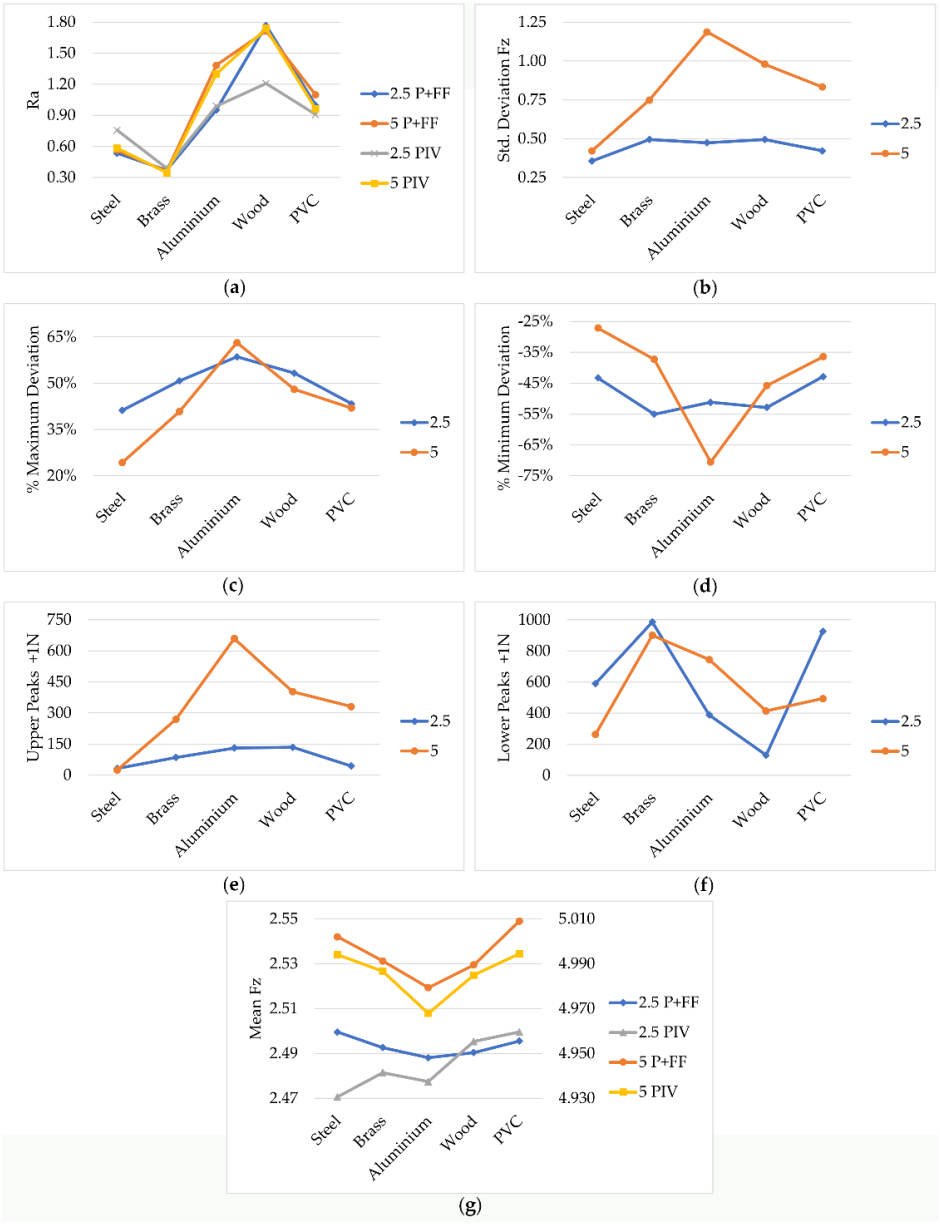

Figure 6.2. Marginal means. (a) Surface roughness, (b) Standard deviation, (c) Maximum deviation, (d) Minimum deviation, (e) Number of upper peaks, (f) Number of lower peaks, (g) Mean of contact force.

The marginal means have been calculated in order to visualise in a better way, the factors that influence the variable plotted in ordinates. This implies that in the case of Figure 6.2 (a), (b), (c) and (d) the means obtained represent four data, two for the P + FF controller and two for the PIV controller. This can be made because the variables shown in ordinates are not affected by the control type.

In the plot of Figure 6.2 (a), something already known become evident, such as the direct influence of the type of material on the roughness achieved, when the working conditions remain constant. However, it is interesting to note how in softer materials, according to Young's modulus (aluminium, wood, and PVC), the application of a greater force on the sandpaper does not significantly improve the finish. This is mainly due to the rapid dulling of the sandpaper, as can be seen in Figure 6.3, where the surface appearance of the sandpaper discs, selected as example for each material, can be compared.

Figure 6.3. The surface appearance of sanding discs.

Continuing with the observation of Figure 6.2 (a), it shows how all materials maintain a trend and very similar values, in the two reference forces, which reinforces the hypothesis that the operation is in a 'state of saturation'. With the chosen cutting conditions and grain size, an increase in force does not cause significant improvements. In this variable, $\boldsymbol{R_a}$, the Tukey's test for post hoc analysis (pair comparison) indicated significative differences between surface roughness obtained in all materials except for steel with brass (p=0.137) and PVC with aluminium (p=0.122).

Another interesting aspect is the higher standard deviation in the softer materials (aluminium, wood, PVC), Figure 6.2 (b), when a force of 5 N is applied. The dulling effect, mentioned above, contributes to increasing friction, which causes

a greater separation concerning the reference force that must be continuously compensated. In this variable, the Tukey's test for post hoc analysis (pair comparison) indicated significative differences between standard deviation obtained in steel with aluminium (p=0.000) and steel with wood (p=0.001).

In Figure 6.2 (c) and 6.2 (d), we can observe the maximum and minimum deviations regarding the reference force. In general, it is detected that the worst behaviour is when a force of 2.5 N is applied, regardless of the control algorithm used: P+FF or PIV. It is important to highlight the high deviations obtained in aluminium. This behaviour has a direct relationship with the working conditions, cutting speed and feed rate. When the right conditions required by the material deviate further from those used in the tests, greater the minimum deviations are. In this variable, the post hoc test indicates significative differences between minimum deviations obtained in steel and aluminium (p=0.041). In these variables, the Tukey's test for post hoc analysis (pair comparison) shown significative differences between maximum deviations obtained in steel with aluminium (p=0.000), steel with wood (p=0.005), aluminium with brass (p=0.027), and aluminium with PVC (p=0.004). The significative differences between minimum deviations were obtained in steel with aluminium (p=0.000), steel with wood (p=0.018), aluminium with brass (p=0.012), and aluminium with PVC (p=0.000).

In Figure 6.2 (e) and 6.2 (f), the number of upper peaks is bigger in soft materials when a force of 5 N is used. In contrast, the number of lower peaks is bigger for a force of 2.5 N in the most rigid materials. This is directly related to the stiffnesses of these materials. If the material is soft, it affects the dynamics of the process, so that a greater amount of oscillations will be obtained at a lower frequency. On the other hand, in hard materials, there will be a lower number of oscillations, but at a higher frequency. In these variables, the Tukey's test for post hoc analysis revealed significative differences between the number of upper peaks obtained in steel with aluminium (p=0.001) and steel with wood (p=0.001). The significative differences between the number of lower peaks were found in steel with aluminium (p=0.001) and steel with wood (p=0.003).

Finally, in Figure 6.2 (g), the fact that the material does not affect the mean force ($\bar{\boldsymbol{F}}_{\boldsymbol{z}}$) corroborates the results obtained in work [19]. In that work, it was deduced that when using an inner velocity loop, the value of the force in the steady-state does not

depend on the material stiffness. However, it does affect the dynamics of the process. On the other hand, the reference force, and the type of control influence in the mean of the contact force. In general, if P+FF control is used, the mean is closer to the reference value. This effect is more evident with a reference force of 5 N.

6.3.2. Graphs of force response and surface aspects

For this section, the most significant response graphs have been selected. Full results can be found in supplementary materials. It is important to mention that the empty entry times are different in each test since they are influenced by the thickness of the material and by the speed of the first impact, which is a function of the reference force. Additionally, the noise at the input is a product of the no-load noise (0.2 N) of the sensor plus the vibrations produced by the revolution of the tool. The noise due to the vibrations is important because it affects all the measures; it behaves like a systematic error. To decrease these vibrations, the Dremel and/or the method used to transmit the torque (flexible shaft) should be changed.

In Figure 6.4 (a), the test that showed the best behaviour of the force Fz is shown (yellow colour). This was obtained working on steel, using a P+FF control and with a reference force of 5 N (black line). A green curve within the force/time graph of the mean force Fz is shown, to visualise the control method effects better. Figure 6.4 (b) shows the appearance of the sandpaper used after processing the test. In Figure 4 (c), the trajectory followed by the sanding tool has been included, in parallel with the measured forces. This way, it is easy to relate the marks left by the tool on the material with the variation obtained in the forces. The vertical lines in black represent the start and endpoint of the toolpath.

It is interesting to notice how the transition at the end of the control algorithm (with a duration of less than one second) between the force control and velocity control (once contact is finished), makes the marks left less intense, even incomplete. To solve this, it would be necessary to keep the tool in this area longer when the trajectory has finished.

Queried the specific numerical values for this test in Table 2, we can see that this experiment is one of the most stable, since it presents the minimum upper and lower peaks, in addition to achieving one of the smallest force errors. This

corroborates the effect of material stiffness on the process dynamics. The minimum values of the oscillations are related to the noise of the force sensor.

For the case of the forces *Fx* and *Fy*, a greater number of oscillations are observed, being greater for the direction in X-axis. The value of the force in Y-axis is due to the process friction. However, in the case of the X-axis, this happens due to the tangential forces acting on the sanding process. According to the spatial configuration used in the robot, the force *Fx* is only supported by one of the robot joints with less capacity. Therefore, as it is a more flexible joint, it generates a great number of oscillations.

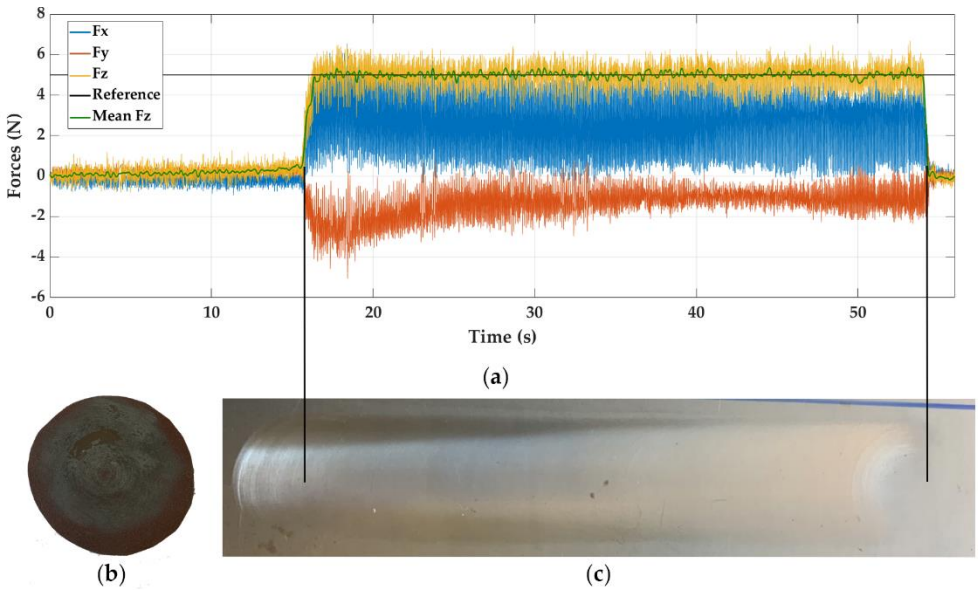

Figure 6.4. Experiment E6, sanding steel with P+FF control and reference force of 5 N. (a) Force response, (b) sandpaper aspect and (c) visual surface finish.

Figure 6.5 (a) shows the force response graph for E2. In Figure 6.5 (c) you can see the surface result for the aluminium sanding test using a P+FF controller and a reference force of 5 N. Figure 6.5 (b) evidences the state of the sandpaper after the operation.

In general, the force response between steel and aluminium are very similar; however, in aluminium, more oscillations are observed in the final part of the

trajectory. Which is supported with the previous results of the ANOVA analysis in which aluminium had the highest maximum and minimum percentage deviation from the reference value. It can also be seen that, due to the lower stiffness of the material, the dynamics are different, so greater amplitude oscillations appear, but with a lower frequency (closer peaks).

Besides, the forces *Fx* and *Fy* are of greater magnitude than in the case of sanding steel, being the responsible, the dulling of aluminium that induces a greater friction force. This was also ratified by the amount of powdered chips left on the treated surface.

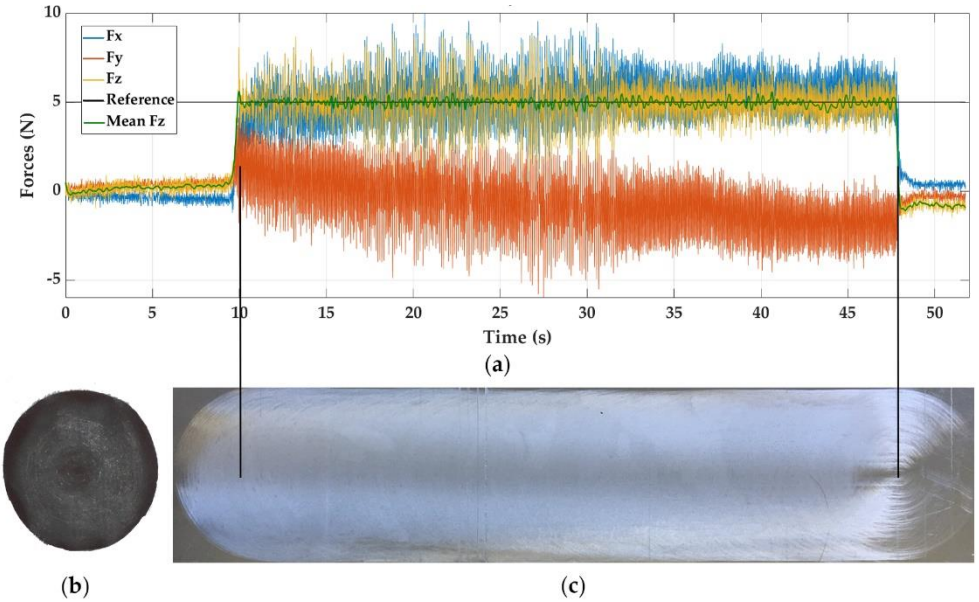

Figure 6.5. Experiment E2, sanding aluminium with P+FF control and reference force of 5 N. (a) Force response, (b) sandpaper aspect and (c) visual surface finish.

In the case of sanding brass, Figure 6.6 (a), shows the response graph and Figure 6.6 (c) the surface appearance obtained after using a PIV controller with a reference force of 5 N.

In E12, it can be noticed that force *Fz* presents an average value of oscillations between the steel and aluminium, which is in accordance with the material rigidity.

Besides, it can be observed how in brass the overshoots are of less intensity than those in aluminium.

Regarding the appearance of the sandpaper, it contains a greater amount of residual material. This is because sanding on brass produces a residue, powder type, that dye sandpaper.

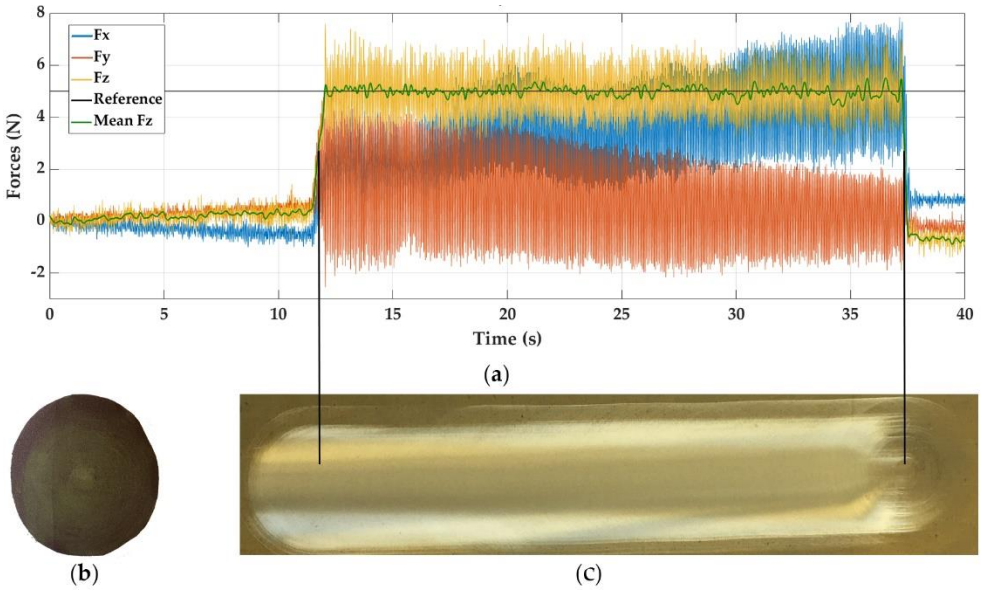

Figure 6.6. Experiment E12, sanding brass with PIV control and reference force of 5 N. (a) Force response, (b) sandpaper aspect and (c) visual surface finish.

Continuing with the softer materials, in Figure 6.7 can be seen the response graph (a), the aspect of PVC surface after sanding it with a PIV controller and 5 N as reference force (c), and the final condition of the sandpaper (b). On the other hand, Figure 6.8 (a) shows the response graph for sanding wood with a P + FF controller and 5 N as reference force too. Figures 6.8 (b) and 6.8 (c) show the wear produced in the sandpaper and the surface appearance left, respectively.

The response graphs of PVC and wood are very similar, they present great stability in the force in Z-axis, and the oscillations keep constant around the reference force, but of greater amplitude than in the case of steel. It can be confirmed that regardless of the type of control (P+FF or PIV) the behaviour is similar.

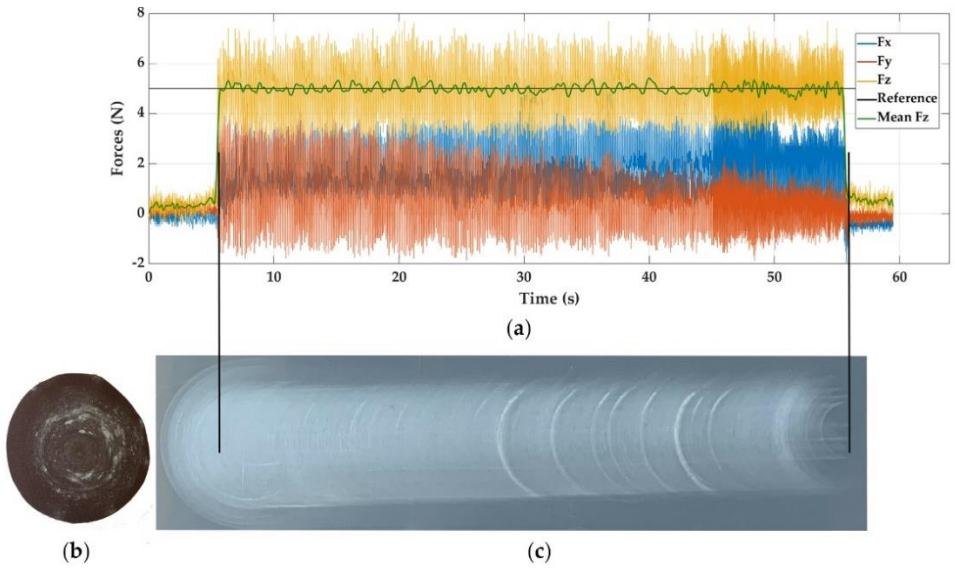

Figure 6.7. Experiment E20, sanding PVC with PIV control and reference force of 5 N. (a) Force response, (b) sandpaper aspect and (c) visual surface finish.

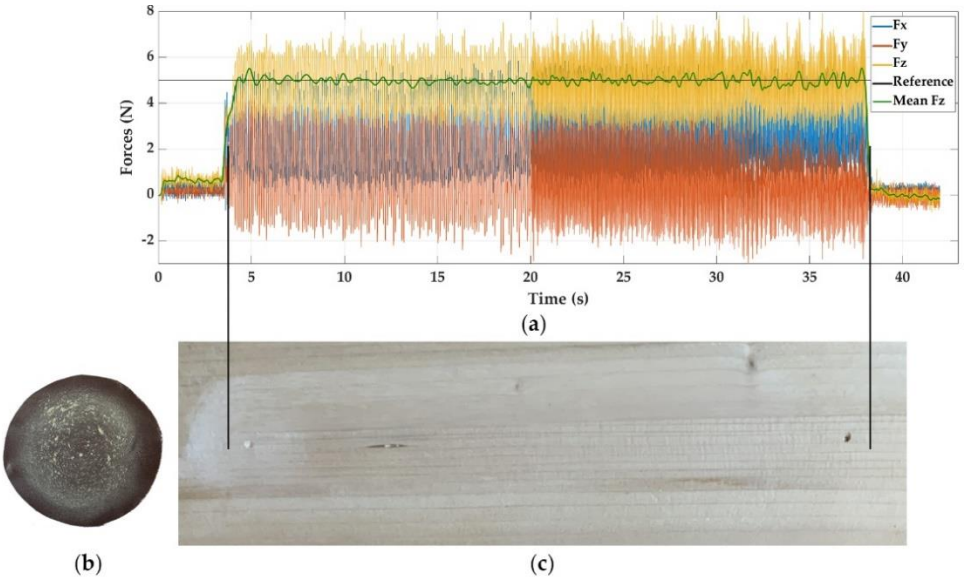

Figure 6.8. Experiment E14, sanding wood with P+FF control and reference force of 5 N. (a) Force response, (b) sandpaper aspect and (c) visual surface finish.

The remarkable thing, according to the selected cutting conditions for the PVC, is the dulling that the sandpaper suffers, which generates marks on the sanded surface until the stuck material come loose. This is due to softening of the material by heat. It should be noted that both examples are for a reference force of 5 N. In the case of reference forces of 2.5 N, the dulling exists, but it is lower.

6.3.3. Effect of feed rate

Since the reference force does not have a significant effect on the surface roughness, it is interesting to test what effects the feed speed will produce. This way, the sanding process can be optimised without overloading the contact forces with the robot. Table 6.5 shows the experiments carried out on brass with a PIV control and a reference force of 2.5 N. In these tests the cut feed is varied in four levels, 300 (repeating E11), 450, 600 and 900 mm / min.

As explained in the Introduction under the name of 'process saturation concept', it can be noticed how a change in the cut feed does not generate a significant change in the surface roughness on the brass. Additionally, it can be verified that the results of the force measurements in E21 are similar to the previous experiment, E11.

Table 6.5. Test results for the cut feed variations

N° Exp	Feed Rate (mm/min)	Ra (μm)	Mean $\bar{F}_z$ (N)	Std. Deviation S_z (N)	Δmax_z (%)	Δmin_z (%)	N_{upp} >3.5/6 (N)	N_{Low} <1.5/4 (N)	e_f (%)
E21	300	0.44	2.4836	0.4302	56	-56	92	5264	0.66
E22	450	0.42	2.4893	0.5834	84	-69	202	2211	0.43
E23	600	0.42	2.4824	0.5646	70	-58	151	7570	0.70
E24	900	0.44	2.4790	0.5140	59	-57	52	2240	0.84

In Figure 6.9, the surface appearance of the experiments with speed variation is shown. It should be noted that the pictures have been taken separately, with a different position and orientation of the camera, hence the changes in brightness that are appreciated. However, what is really important are the values obtained, shown in the table above.

Given the value of $\boldsymbol{R_a}$ measured, practically the same for E21, E22, E23 and E24 tests, it allows us to select a higher feed rate for the same reference force, type of control, cutting speed and tool diameter. This way, it is possible to increase the productivity of the process.

Comparing the most extreme values of the tests in Figure 6.9, the cut feed in E24 is tripled with respect to E21, achieving the same value of $\boldsymbol{R_a}$, 0.44 μm. The rest of the parameters hardly change, according to what they represent. The standard deviation of the measured force, $\boldsymbol{S_z}$, remains at similar levels, as do the maximum and minimum percentage changes, $\Delta\boldsymbol{max_z}$, $\Delta\boldsymbol{min_z}$. The most significant difference is found in the number of upper peaks $\boldsymbol{N_{upp}}$ (> 3.5 / 6 N) and lower peaks $\boldsymbol{N_{low}}$ (<1.5 / 4 N), where a considerable improvement is observed in the case of E24, with higher cutting speed. As can be noticed in the different tests shown, the noise in the force sensor and the intrinsic characteristics of the process itself (where forces are mixed with cycloid movements) generate many oscillations, as well as, lower and upper peaks. However, the improvement in E24 is considerable, due to the inertia of the robot during the cut feed and the influence of dynamic friction speed, among other things.

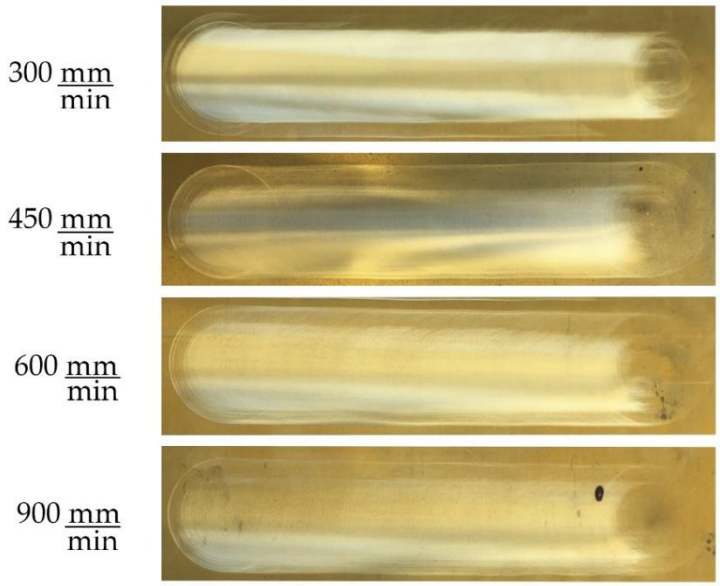

Figure 6.9. Results for cut feed variation on brass.

Following the comparison between E21 and E24, if we apply the Preston formula, Equation (6.1), maintaining the same pressure in the two tests (P), as well as, the same material, and same abrasive (K), the material removal rate (MMR) in the E24 assay triples the rate achieved in E21.

6.3.4. Comparison with a standard industrial robot

Industrial robots are widely used in grinding and sanding processes with excellent performance. In order to have reference values, it is interesting to contrast the results of the collaborative robot UR3 with standard industrial ones, working with similar process conditions.

Chen C. et al. [26] used a Kuka KR60-3 to perform several experiments on carbon fibre composite material with different cutting conditions.

Among these conditions, they used a rotational speed of 3000 rpm, cut feed of 30 mm/s (1800 mm/min.), Z force of 10 N, sandpaper grain of P600 and an inclination of the tool axis of 10º, obtaining a final $\boldsymbol{R_a}$ of 1.77 μm.

Chen C. et al. sand the outer layer of the composite material. The type of resin is not named in the article, but we can make a reasonable comparison between plastic materials. The UR3 has been used to sand PVC with the same Z force, same size grain and adapting the cutting speed to 1000 rpm and the consequent feed rate to 600 mm/min. to keep the same proportion as them. However, taking into account the low rigidity of the UR3 and the increase of Z force and feed rate, the tool axis tilt angle used to avoid instability is 7°. The control algorithm used is P+FF.

The value of the $\boldsymbol{R_a}$ parameter achieved is 0.45 μm, being $\boldsymbol{e_f}$ = 0.07%, $\overline{\boldsymbol{F}}_{\boldsymbol{z}}$ = 10.007, $\boldsymbol{N_{upp}}$ = 243 and $\boldsymbol{N_{low}}$ = 320. For sure, the main reason for the differences between the $\boldsymbol{R_a}$ values are the characteristics of the plastics, but the results of the experiment confirm the feasibility of the operation with a cobot.

Nagata F. et al. [13] with a Kawasaki FS20N robot for sanding wood (oak), employed in their last pass a Z force of 10 N, a feed rate of 30 mm/s (1800 mm/min.) and a size grain of 400. The UR3 has been used with a PIV control algorithm, the same Z force, the same size of grain and a feed rate adapted of 600 mm/min. In these conditions the $\boldsymbol{R_a}$ achieved has been of 1.64 μm, with a $\boldsymbol{e_f}$ = 0.13%, $\overline{\boldsymbol{F}}_{\boldsymbol{z}}$ = 10.013, $\boldsymbol{N_{upp}}$ = 489 and $\boldsymbol{N_{low}}$ = 687. Once again, the type of wood is not the same and Nagata F. et al. apply three passes with 80, 220 and finally 400 size of grain to obtain the final

result of 1 μm. However, the process can be made with the collaborative robot, and the force response is acceptable, as can be seen in Figure 6.10.

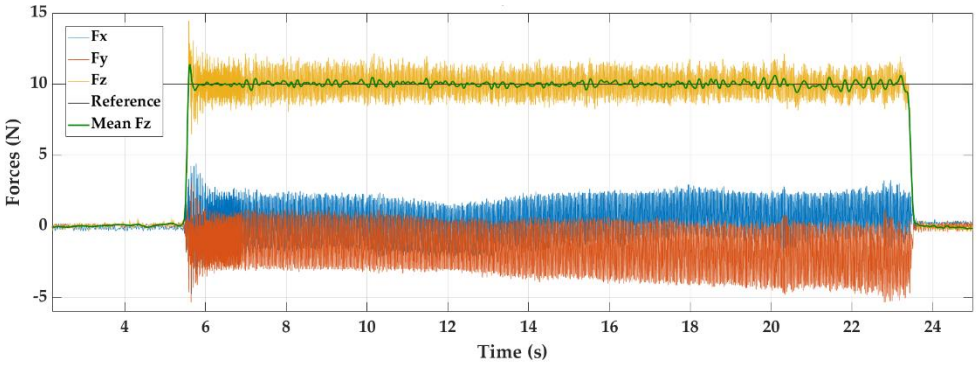

Figure 6.10. Force response for UR3 sanding wood with a sandpaper grain size of 400.

Nevertheless, the main differences between the cobots and the standard industrial robots are the much smaller torque and the low rigidity that collaborative robots have. These differences limit the achievable performances, decreasing productivity significantly. A clear example of the repercussion of these differences is the weight and dimensions of the tool (sandpaper disc diameter, e.g.) that the cobot can bear.

6.4. Conclusions

The capability to perform a sanding process with a collaborative robot has been demonstrated through various experiments on different materials. What has also been confirmed is the importance of knowing what the best type of control in the combination is: inner control loop for robot movements and outer loop to control force in the robot. It should be noted that the force control with an inner velocity loop allows obtaining of good results in contact force control tracking, since, as it has been seen, this type of control in the UR3 robot is not affected by the rigidity of the processed material [19].

On the other hand, there has been an opportunity to test how the stiffness of the material (hardness) only influences the dynamics of the process, generating a

greater or lesser number of peaks with respect the reference force, as indicated by the ANOVA results.

From the analysis of variance, it follows that the type of force control algorithm—PIV or P + FF—does not have significant effects on the performance of the sanding process using a collaborative robot like the UR3. The effective difference would be found with more complex cutting paths. In these cases, both algorithms will be valid, but work conditions (especially feed rate) should be fitted to achieve the desired roughness. These adjustments will have a direct impact on the productivity reached.

Furthermore, increasing the force does not have a significant effect on the surface finish either. That means the surface finish is determined by the type of material and the grain size of the sandpaper only, as long as the force is enough for the right application of sanding. However, a triple interaction between the factors—control type, reference force, and material—produces a significative difference in the arithmetic mean roughness. The worst values are obtained in soft materials with a P+FF control and a reference force of 5 N. Due to the low effect (almost null) of the reference force value, it was decided to perform an analysis to check the effect of the feed rate according to what was stated in the Introduction under the name of the "process saturation concept". This analysis allowed us to corroborate that the process was in a "state of saturation", with which a productivity improvement could be sought simply by adjusting the cutting conditions. As a demonstration, it was decided to increase one of the cutting conditions, the cut feed. The results maintain the same value for the surface finish of brass, 0.44 μm, tripling productivity, and keeping the force level at its minimum value. Unlike the study in [22], the level of roughness obtained with the sanding process is not affected by an increase in the feed rate, in a "saturated state". This is the main outcome from this work because it will allow optimizing of the process parameters in future sanding tasks with a collaborative robot.

A comparison between industrial and collaborative robots showed that the latter can perform the same sanding operation with similar results of surface roughness. Therefore, these experiments confirm the feasibility of these operations with a cobot. However, the main limitation will be the payload capacity of the cobots.

As future works, it would be interesting to study in depth what parameters can be modified in the force control and what types of impact control algorithms can be used to minimise the effect caused by the sanding tool on the entry and exit of the trajectory. In addition, the controller might require additional variables such as the vibration effects introduced by the dynamic components. Another important aspect of developing would be to analyse the stability of the sanding process when it also has the option to vary the cutting speed. Finally, it is important to include optimization methods to determine the process parameters that allow for obtaining the best roughness surface results.

Supplementary Materials: The following are available online at https://www.mdpi.com/1996-1 944/14/1/67/s1, Table S1: ANOVA results, Figure S1: Experiment E1, sanding aluminium with P + FF control and reference force of 2.5 N, Figure S2: Experiment E3, sanding aluminium with PIV control and reference force of 2.5 N, Figure S3: Experiment E4, sanding aluminium with PIV control and reference force of 5 N, Figure S4: Experiment E5, sanding steel with P + FF control and reference force of 2.5 N, Figure S5: Experiment E7, sanding steel with PIV control and reference force of 2.5 N, Figure S6: Experiment E8, sanding steel with PIV control and reference force of 5 N, Figure S7: Experiment E9, sanding brass with P + FF control and reference force of 2.5 N, Figure S8: Experiment E10, sanding brass with P + FF control and reference force of 5 N, Figure S9: Experiment E11, sanding brass with PIV control and reference force of 2.5 N, Figure S10: Experiment E13, sanding wood with P + FF control and reference force of 2.5 N, Figure S11: Experiment E15, sanding wood with PIV control and reference force of 2.5 N, Figure S12: Experiment E16, sanding wood with PIV control and reference force of 5 N, Figure S13: Experiment E17, sanding PVC with P + FF control and reference force of 2.5 N, Figure S14: Experiment E18, sanding PVC with P + FF control and reference force of 5 N, Figure S15: Experiment E19, sanding PVC with PIV control and reference force of 2.5 N.

Author Contributions: Conceptualisation, S.C.G.R., R.P.U., R.Z.S. and Á.P.I.; methodology, S.C.G.R., R.P.U., R.Z.S. and Á.P.I.; software, R.P.U.; validation, S.C.G.R., R.P.U., and R.Z.S.; formal analysis, S.C.G.R. and R.P.U.; investigation, R.P.U.; resources, S.C.G.R., R.Z.S. and Á.P.I.; data curation, R.P.U.; writing—original

draft preparation, R.P.U. and S.C.G.R.; writing—review and editing, S.C.G.R., R.P.U., and R.Z.S.; visualisation, S.C.G.R., R.P.U., and R.Z.S.; supervision, S.C.G.R., R.Z.S. and Á.P.I.; project administration, S.C.G.R., and R.Z.S.; funding acquisition, R.P.U. All authors have read and agreed to the published version of the manuscript.

Funding: Rodrigo Pérez-Ubeda is grateful to the Ph.D. Grant CONICYT PFCHA/Doctorado Becas Chile/2017–72180157 and the University of Antofagasta, Chile.

Institutional Review Board Statement: Not applicable.

Informed Consent Statement: Not applicable.

Data Availability Statement: Data is contained within the article or Supplementary Materials.

Conflicts of Interest: The authors declare no conflict of interest.

6.5. References

1. Kalt, E.; Monfared, R.P.; Jackson, M.R. Development of an intelligent automated polishing system. In Proceedings of the 16th International Conference of the European Society for Precision Engineering and Nanotechnology, EUSPEN 2016, Nottingham, UK, 30 May–3 June 2016.
2. Walker, D.D.; Yu, G.; Bibby, M.; Dunn, C.; Li, H.; Wu, H.Y.; Zheng, X.; Zhang, P. Robotic automation in computer controlled polishing. *J. Eur. Opt. Soc. Rapid Publ.* **2016**, 11, 16005.
3. Hahnel, S.; Pini, F.; Leali, F.; Dambon, O.; Bergs, T.; Bletek, T. Reconfigurable Robotic Solution for Effective Finishing of Complex Surfaces. In Proceedings of the 2018 IEEE 23rd International Conference on Emerging Technologies and Factory Automation (ETFA), Turin, Italy, 4–7 September 2018; Volume 2018, pp. 1285–1290.
4. Tam, H.Y.; Lui, O.C.H.; Mok, A.C. Robotic polishing of free-form surfaces using scanning paths. *J. Mater. Process. Technol.* **1999**, 95, 191–200.
5. Dieste, J.A.; Fernández-Cuello, A.; Javierre, C.; Santolaria, J. Conformal polishing approach: Tool footprint analysis. *Adv. Mech. Eng*. **2016**, 8, 1–14.

6. Perez-Ubeda, R.; Gutierrez, S.C.; Zotovic, R.; Lluch-Cerezo, J. Study of the application of a collaborative robot for machining tasks. *Procedia Manuf.* **2019**, 41, 867–874.
7. Qu, Y.J.; Ming, X.G.; Liu, Z.W.; Zhang, X.Y.; Hou, Z.T. Smart manufacturing systems: State of the art and future trends. *Int. J. Adv. Manuf. Technol*. **2019**, 103, 3751–3768.
8. El Zaatari, S.; Marei, M.; Li, W.; Usman, Z. Cobot programming for collaborative industrial tasks: An overview. *Rob. Auton. Syst*. **2019**, 116, 162–180.
9. Wang, K.; Dailami, F.; Matthews, J. Towards collaborative robotic polishing of mould and die sets. *Procedia Manuf*. **2019**, 38, 1499–1507.
10. Huang, H.; Gong, Z.; Chen, X.; Zhou, L. Robotic grinding and polishing for turbine-vane overhaul. *J. Mater. Process. Technol*. **2002**, 127, 140–145.
11. Fernandez, A.; Jose Antonio, D.; Javierre, C.; Jorge, S. Surface Roughness Evolution Model for Finishing Using an Abrasive Tool on a Robot. *Int. J. Adv. Robot. Syst.* **2015**, 12.
12. Li, M.; Du, Z.; Ma, X.; Gao, K.; Dong, W.; Di, Y.; Gao, Y. System design and monitoring method of robot grinding for friction stir weld seam. *Appl. Sci.* **2020**, 10, 2903.
13. Nagata, F.; Kusumoto, Y.; Fujimoto, Y.; Watanabe, K. Robotic sanding system for new designed furniture with free-formed surface. *Robot. Comput. Integr. Manuf.* **2007**, 23, 371–379.
14. Maric, B.; Mutka, A.; Orsag, M. Collaborative Human-Robot Framework for Delicate Sanding of Complex Shape Surfaces. *IEEE Robot. Autom. Lett.* **2020**, 5, 2848–2855.
15. Liang, X.; Mohsin, I.; Xu, Y.; Yan, C.; He, K. Robotic Polishing of the Meat Grinder Blade under Path Planning and Controlled Force. *IOP Conf. Ser. Mater. Sci. Eng*. **2020**, 790, 012158.
16. Dong, Y.; Ren, T.; Hu, K.; Wu, D.; Chen, K. Contact force detection and control for robotic polishing based on joint torque sensors. *Int. J. Adv. Manuf. Technol*. **2020**, 107, 2745–2756.
17. Wen, Y.; Hu, J.; Pagilla, P.R. A Novel Robotic System for Finishing of Freeform Surfaces. In Proceedings of the 2019 International Conference on Robotics and

Automation (ICRA), Montreal, QC, Canada, 20–24 May 2019; Volume 2019, pp. 5571–5577.

18. Brito, T.; Queiroz, J.; Piardi, L.; Fernandes, L.A.; Lima, J.; Leitão, P. A Machine Learning Approach for Collaborative Robot Smart Manufacturing Inspection for Quality Control Systems. *Procedia Manuf.* **2020**, 51, 11–18.
19. Pérez-Ubeda, R.; Zotovic-Stanisic, R.; Gutiérrez, S.C. Force Control Improvement in Collaborative Robots through Theory Analysis and Experimental Endorsement. *Appl. Sci.* **2020**, 10, 4329.
20. Guiot, A.; Pattofatto, S.; Tournier, C.; Mathieu, L. Modeling of a Polishing Tool to Simulate Material Removal. *Adv. Mater. Res.* **2011**, 223, 754–763.
21. Márquez, J.J.; Pérez, J.M.; Ríos, J.; Vizán, A. Process modeling for robotic polishing. *J. Mater. Process. Technol.* **2005**, 159, 69–82.
22. Padmanabhan, S.N.; Halil, Z.; Sun, Y.; Vu, T.T.; Yeo, S.H.; Wee, A. Experimental investigation of Robotic Surface Finishing Using Abrasive Disc. *Int. J. Mater. Mech. Manuf.* **2018**, 6, 127–130.
23. Mia, M.; Królczyk, G.; Maruda, R.; Wojciechowski, S. Intelligent optimization of hard-turning parameters using evolutionary algorithms for smart manufacturing. *Materials* **2019**, 16, 879.
24. Iglesias Sánchez, I.; Ares, J.E.; González Gaya, C.; Rosales Prieto, V. A New Approach to the Consideration and Analysis of Critical Factors in Robotic Machining. *Appl. Sci.* **2020**, 10, 8885.
25. Zhang, S.; Zhou, K.; Ding, H.; Guo, J.; Liu, Q.; Wang, W. Effects of grinding passes and direction on material removal behaviours in the rail grinding process. *Materials* **2018**, 11, 2293.
26. Chen, C.-Y.; Li, J.; Zhu, Y.; Tu, L.; Weng, W. Automatic finishing system research for industrial robot. In Proceedings of the 2017 IEEE International Conference on Cybernetics and Intelligent Systems (CIS) and IEEE Conference on Robotics, Automation and Mechatronics (RAM), Ningbo, China, 19–21 November 2017; Volume 2018, pp. 266–271.

Capítulo 7
Discusión general de los resultados

En este capítulo se resumen los principales resultados obtenidos en las publicaciones presentadas anteriormente.

El objetivo de esta tesis doctoral consiste en realizar una propuesta de inclusión de esfuerzos en el control de un brazo robot, teniendo en cuenta la mejor adaptación a los algoritmos de control de su bucle interior, para asegurar el cumplimiento de la rugosidad superficial en operaciones de mecanizado, como es el lijado. La principal dificultad radica en estimar los parámetros de funcionamiento interno. Esta estimación se hace a través de comparaciones de su comportamiento experimental con los desarrollos teóricos que caracterizan las distintas formas de control.

En la **primera publicación** [29], capítulo 2, se mostraron los principales aspectos o características que afectan al mecanizado con un brazo robot. A pesar de las ventajas que presentan los robots frente a las máquinas de control numérico, las deflexiones producidas en el efector final debido a las fuerzas del proceso generan errores de posición, vibraciones y baja calidad en las piezas fabricadas. Estas desviaciones son producidas principalmente por la menor rigidez que presenta la cadena antropomórfica del robot y, en específico, la menor rigidez de sus articulaciones. Adicionalmente, el principal desafío con respecto al mecanizado con robots, fue la realización de un modelo matemático completo que considerara

adecuadamente las propiedades elásticas de las articulaciones en la dinámica del robot, además de tener en cuenta las propiedades dinámicas del mismo.

Del análisis del estado del arte se extrae que los principales métodos y avances para solucionar estos problemas son:

1. El control del proceso de mecanizado que se realiza por medio de la compensación estimada, *off-line*, para la cual se requiere un conocimiento total del modelo de rigidez, dinámica y fuerzas de corte, o bien, por medio de la compensación en tiempo real, *on-line*, la cual se implementa a través de bucles de fuerza, posición, o impedancia. La compensación en tiempo real es la más adecuada cuando no se conocen los parámetros dinámicos internos del robot, situación habitual en los robots comerciales.
2. El uso de softwares comerciales para la planificación y programación correcta de las trayectorias, especialmente cuando las geometrías son muy complejas o se considera compensar las desviaciones en la pieza fabricada. Sin embargo, tiene la desventaja de ser una solución que implica un coste extra.
3. El uso de la redundancia funcional (más grados de libertad) del robot frente a la tarea de mecanizado permite que existan múltiples configuraciones del robot para realizar lo mismo, lo cual posibilita encontrar las zonas más estables o de mayor rigidez y asegurar así una mayor precisión de la tarea. La desventaja es que no se consideran las fuerzas existentes en el proceso.
4. La optimización de la postura o configuración del robot, la cual busca determinar la configuración con mayor rigidez y así disminuir los errores en el mecanizado; sin embargo, al igual que el uso de la redundancia, no se consideran las fuerzas que actúan durante el proceso de mecanizado.
5. El análisis de las vibraciones ocurridas durante el proceso de mecanizado, que permite modificar las condiciones de corte o la postura de la herramienta para mejorar la ejecución de la tarea. La desventaja recae en la necesidad de disponer de elementos extras para medir las vibraciones durante el proceso.
6. El desarrollo de efectores finales con diseños específicos, que permitan mejorar el desempeño de la tarea. Una de las metodologías más utilizadas consiste en desarrollar un mini-manipulador en el efector final, el cual se

encarga de realizar las tareas de control de fuerza. Esto deja al robot como un macro-manipulador que se encarga solo de seguir la trayectoria de la tarea de mecanizado. El inconveniente radica en que el diseño de un efector final con esas características posee un alto coste, peso extra y una mayor complejidad en su diseño y fabricación.

Dentro de estas alternativas, en la presente Tesis se emplea la opción del control de procesos a través del uso de un control sensorizado de fuerza externo. En el caso de robots colaborativos, el sensor de torque es necesario para reaccionar frente al contacto del robot con otros objetos. En la **segunda publicación** [30], capítulo 3, se muestra el diseño y fabricación de un sensor de bajo coste. Los resultados exponen que un diseño de sensor del tipo *hub-sprocket* o de vigas cruzadas permite obtener una alta deformación si la pieza, en específico las vigas, son fabricadas de forma simple a través de operaciones de taladrado, obteniendo así un novedoso diseño de vigas cruzadas curvas. Un análisis por elementos finitos permitió optimizar las dimensiones de los agujeros para los diferentes tamaños de sensores requeridos, 1 Nm y 20 Nm. Estos tamaños fueron definidos de acuerdo con el rango de trabajo de un robot colaborativo. El análisis de coste indicó que el sensor fabricado por medio de operaciones de mecanizado sencillas, como el taladrado, presenta costes mínimos en comparación con otros diseños que requieren operaciones más complejas y, por tanto, máquinas más caras. Tras la calibración, los resultados indicaron que los sensores poseen muy buena linealidad, bajo error de medición y una sensibilidad de 4.9 y 1.09 mV/Nm para los tamaños de 1 y 20 Nm respectivamente.

A pesar de los buenos resultados respecto al sensor de torque desarrollado, el uso de estos no siempre es posible en robots comerciales, debido a que su estructura no está pensada para acceder o modificar las articulaciones.

En la **tercera publicación** [31], capítulo 4, es evaluada la caracterización del comportamiento de un brazo robot industrial y de un brazo robot colaborativo frente a una tarea de fresado. Sin un control de fuerza, el fresado sobre resina indica que, para las mismas condiciones de corte, el robot industrial Mitsubishi presenta menos errores de posición que el robot colaborativo UR3. Lo que se ve reflejado en los resultados de rugosidad y fuerzas de corte. Sin embargo, el robot colaborativo tiene muchas ventajas en relación con la implementación del control de fuerza, esto es

debido a las diferentes alternativas de bucles internos de control que pueden ser utilizados.

Tras los resultados obtenidos se decidió implementar un control de fuerza por bucle interior/exterior en el brazo colaborativo UR3, ya que, a pesar de que su control interno no es completamente abierto, permite el control de una mayor cantidad de variables comparado con el robot industrial Mitsubishi RV-2AJ.

En la **cuarta publicación** [32], capítulo 5, se analizó y evaluó, teórica y experimentalmente, el uso del control de fuerza por bucle interior/exterior en el robot colaborativo UR3. En concreto, se utilizaron los bucles interiores de control por posición absoluta, por posición incremental y por velocidad. Debido al desconocimiento del método de control interno por parte del robot (los fabricantes son reacios a proporcionar esta información). Los bucles interiores fueron analizados, tanto por el método de la jacobiana inversa como por el método de la jacobiana transpuesta. Los resultados experimentales mostraron que el bucle interno de control por posición absoluta es el que peores resultados presenta. En el caso de bucle de posición incremental, los resultados indicaron una mayor desviación de la fuerza, respecto de la fuerza de referencia cuando se trabaja con aluminio o con polímero. Adicionalmente, al final de la trayectoria se apreció una desviación para ambos materiales, lo que indicó que este bucle esta implementado a través del método de la jacobiana inversa, ya que se produce un cambio en la rigidez calculada. El bucle interno por velocidad presentó los mejores resultados. El error fue insignificante entre ambos materiales, lo que coincide con la teoría desarrollada, ya que este bucle no se ve afectado por la rigidez del entorno. Además, no se presenta la desviación del bucle incremental, lo que indica que el bucle por velocidad esta implementado con el método de la jacobiana transpuesta.

En el caso del bucle de fuerza exterior se comparó el funcionamiento de varios algoritmos, entre los cuales está, el proporcional (P), proporcional-derivativo (PD), proporcional con retroalimentación de velocidad (PV), proporcional-integral (PI), proporcional-integral con retroalimentación de velocidad (PIV) y proporcional con pre-alimentación (P+FF). Los resultados indicaron que la acción derivativa no presenta buenos resultados debido al ruido del sensor, lo que empeoró la desviación, generando un 34% de picos más altos. Aunque la acción derivativa mediante la retroalimentación de velocidad mejora levemente los resultados, los rápidos

cambios de velocidad del proceso y el bajo periodo de muestreo, producen que el efecto no sea tan evidente. Dado el periodo de muestreo que posee el robot, la acción integral tampoco garantiza un error de fuerza igual a cero. Sin embargo, con el algoritmo proporcional con pre-alimentación de fuerza, se reduce el error de 0.11% a 0.02%.

Por medio de una matriz de decisión se determinó que los algoritmos PIV y P+FF presentaban los mejores resultados.

Por último, los resultados obtenidos en una aplicación real de pulido, con un bucle interno por velocidad y un bucle externo PIV, constataron que se alcanzaba un error del 0.95% y del 0.33% con una fuerza de referencia de 5 y 10 N. Estos valores son muy pequeños en comparación con el error de 31.26% que se obtiene al no utilizar un control de fuerza. Cabe destacar que, con el control PIV, se obtiene un número de picos en la fuerza menor.

Tras optimizar el modelo de control de fuerza, se realizó un análisis más profundo para estudiar el comportamiento de este modelo con el robot colaborativo UR3 en el lijado sobre diferentes materiales. Como se puede observar en la **quinta publicación** [33], capítulo 6, se realizó un diseño de experimentos completo de la operación de lijado, teniendo como factores, el tipo de material, donde se utilizó acero, bronce, aluminio, PVC y madera. De acuerdo con los resultados de la publicación anterior, y la capacidad del robot, se eligieron y definieron los dos tipos de control de fuerza a utilizar para el bucle exterior, PIV y P+FF, y los dos niveles de fuerza de referencia, 2.5 y 5 N. Los parámetros en el proceso de lijado como, el diámetro de 50 mm del disco de lijar, un tamaño de grano P600, la velocidad de avance de 300 mm/min y la velocidad de giro de 1070 rpm, se mantuvieron constantes. Como variables de salida se tuvieron en consideración la media en la fuerza aplicada, la desviación estándar, el porcentaje máximo y el mínimo de desviación respecto a la fuerza de referencia y el número de picos superiores e inferiores de la fuerza de contacto, además, como variable de salida importante se midió la rugosidad superficial. Un análisis de varianza (ANOVA) realizado en los 40 experimentos ejecutados, indicó que el factor tipo de control de fuerza, PIV o P+FF no tiene un efecto significativo sobre las variables de salida. El factor material produce diferencias significativas en las variables, rugosidad superficial, desviación estándar de la fuerza, porcentaje máximo y mínimo de desviación y número de picos

superiores e inferiores. Por su parte, el factor nivel de fuerza de referencia produce diferencias significativas en la rugosidad superficial, la media de la fuerza, la desviación estándar de la fuerza, la desviación porcentual mínima y el número de picos superiores e inferiores.

Los únicos efectos producidos por la interacción entre factores se obtienen de la combinación del factor fuerza de referencia y el factor material, la cual produce diferencias significativas en la rugosidad superficial, la desviación estándar, la desviación porcentual mínima y el número de picos superiores e inferiores.

La triple interacción de los factores (fuerza de referencia, material y tipo de control) solo genera efectos significativos en la rugosidad superficial.

Dentro de los resultados más destacables se observaron valores similares en todos los materiales para ambos niveles de fuerza. Esto refuerza la hipótesis de que esta operación estaba en "estado de saturación", lo cual implica que, con las condiciones de corte seleccionadas, un aumento del nivel de fuerza no generará mejoras significativas. Por otra parte, a pesar de utilizar un bucle interno por velocidad, el número de picos superiores es mayor en los materiales menos duros cuando la fuerza aplicada es de 5 N. Esto estaría directamente relacionado con la rigidez de los materiales. Un material menos duro afecta a la dinámica del proceso, por lo que se obtendrán picos mayores a bajas frecuencias de oscilaciones. En cambio, en materiales más duros habrá un menor número de oscilaciones, pero a una mayor frecuencia de oscilación. Este efecto no contradice los resultados del artículo anterior, ya que se determinó que con un bucle de control por velocidad la rigidez del entorno no afecta a la fuerza deseada en estado estable. Lo que se corrobora con los resultados obtenidos, a la vista de la media de la fuerza en las gráficas de respuesta de los diferentes materiales.

Debido a que la operación está en estado de saturación respecto al nivel de fuerza, se puede optimizar la productividad sin sobrecargar la capacidad del robot, aumentando la velocidad de avance. Se utilizaron 4 niveles de prueba en el avance, 300, 450, 600 y 900 mm/min. Los resultados indican que la operación también se encuentra en estado de saturación respecto a los cambios en la velocidad de avance. El valor de la rugosidad superficial es prácticamente el mismo para todos los experimentos, por lo que se puede aumentar la velocidad y así poder aumentar la productividad del proceso hasta en un 300%.

Por último, en este trabajo se realizó la comparación de los resultados experimentales obtenidos con los presentados por otros investigadores para brazos robots industriales (no colaborativos). El análisis de las comparaciones confirma la capacidad de realizar operaciones de lijado que poseen los robots colaborativos.

Capítulo 8
Conclusiones

En el capítulo de conclusiones se analiza el nivel de cumplimento de los objetivos de investigación planteados en la introducción. También se recopilan las principales conclusiones alcanzadas, se exponen cuáles son las aportaciones más relevantes del trabajo y se proponen las líneas futuras de investigación.

8.1. Cumplimiento de los objetivos

De acuerdo con lo mostrado en los capítulos anteriores, es posible señalar que, el objetivo principal de evaluar la capacidad y la factibilidad del uso de robots en operaciones de mecanizado, tipo lijado, tras proponer modificaciones en su control para mejorar el comportamiento, fue alcanzado.

En cuanto a los objetivos específicos que se plantearon: (1) Comprender los procesos de mecanizado al utilizar un brazo robot industrial y colaborativo. (2) Estudiar la dinámica y control de brazos robot industriales/colaborativos y proponer las modificaciones adecuadas para aplicar un control de fuerza factible y (3) Evaluar, técnica y económicamente, la aplicación de elementos sensores y métodos de control para ser integrados en los procesos de mecanizado con brazos robóticos. Se puede observar que la primera y la tercera publicación, capítulos 2 y 4 respectivamente, se corresponden al primero de los objetivos mencionados, es decir a desarrollar el

estado del arte y las experiencias en las que se analizan, caracterizan y compara la utilización de los robots industriales y colaborativos en aplicaciones de mecanizado.

Por su parte, la cuarta y la quinta publicación, capítulos 5 y 6 respectivamente, describen el estudio de la dinámica y el control de brazos robots para implementar bucles de control de fuerza, correspondiendo al cumplimento del segundo objetivo específico.

Y, finalmente, en la segunda publicación, capítulo 3, se expone el desarrollo de un sensor de bajo coste que permite evaluar técnica y económicamente la aplicación de sensores en un brazo robot. Además, la quinta publicación, capitulo 6, integra un sensor de fuerza-par de 6 grados de libertad en operaciones de lijado, analizando el desempeño del control y la calidad superficial de la pieza fabricada. Por tanto, se dio cumplimiento satisfactoriamente a los tres objetivos específicos.

8.2. Aportaciones realizadas

Como se ha detallado en la introducción y en el capítulo 1, la literatura existente en el campo del mecanizado robótico es bastante amplia. Sin embargo, su aplicación depende en gran medida de la disponibilidad del tipo de robot, del tipo de control interior y de los complementos externos como, sensores de fuerza, sensores de posición, etc. Los nuevos robots colaborativos e industriales, con sensores de fuerza integrados, son el primer paso para que el mecanizado robótico sea ampliamente utilizado.

Por otra parte, el diseño y la fabricación de un sensor de torque de bajo coste permite obtener un sensor funcional y de fabricación propia que puede ser aplicado a robots con estructura abierta. Además, cabe destacar que la metodología utilizada permite obtener potencialmente un sensor de 6 grados de libertad, a través del desarrollo de un sensor resultando del ensamblado de partes más simples. Esto permitiría reducir considerablemente los costes, en comparación con los sensores sólidos con geometrías complejas.

La comparación entre un robot clásico (rígido) y un robot colaborativo permite caracterizar de manera correcta las capacidades, ventajas y desventajas de cada uno al ser utilizado en operaciones de mecanizado. En ambos casos es necesario que el

control de posición sea complementado con un bucle de externo, donde las fuerzas de contacto sean medidas en tiempo real.

En el caso de robots con control interno cerrado, el uso de un modelo de control de fuerza por bucle interior/exterior es la metodología más factible para la implementación de un bucle de fuerza.

A partir del desarrollo teórico se logró estimar los parámetros que intervienen en el control interno para mejorar el comportamiento del proceso en combinación con el control externo de fuerza. En concreto, para el caso del robot colaborativo, el poder modificar algunos parámetros del bucle de posición interior, así como disponer de diferentes tipos de bucles interiores fue un plus para la implementación del control de fuerza.

El control de fuerza con bucle interior de velocidad y bucle exterior de fuerza con algoritmos PIV y P+FF, presenta los mejores resultados en el robot UR3. El bucle interno por velocidad no se ve afectado por la rigidez del entorno, pero sí afecta a la dinámica del proceso. Por su parte, el bucle externo de fuerza, con los algoritmos ya mencionados, permite obtener los menores errores respecto a la fuerza de referencia, además de generar un menor número de oscilaciones.

Queda demostrada la factibilidad del uso de robots colaborativos en tareas de mecanizado, tales como pulido y lijado en diversos materiales. El diseño de experimentos ha permitido concluir que los factores que más influyen en el proceso son el material y la fuerza de referencia. Sin embargo, esta última solo afecta significativamente a las variables relacionadas con la fuerza de contacto y no tiene efecto sobre la rugosidad superficial obtenida. En el caso de la rugosidad superficial el proceso se encuentra en un "estado de saturación", tanto si se modifica el valor de la fuerza de referencia o el valor de la velocidad de avance. Esto permite aumentar considerablemente la productividad del proceso sin sobrecargar la capacidad del robot. Siendo la capacidad del robot, la principal limitante del tipo de operación y de las condiciones de trabajo a utilizar.

8.3. Líneas de investigación futuras

El propósito de este trabajo ha sido plantear una propuesta real de control de esfuerzos sobre un brazo robot para realizar operaciones de mecanizado del tipo

lijado. A medida que se ha avanzado en el estudio se han detectado otras líneas de investigación que serían interesantes para ser desarrolladas.

Como líneas de investigación futura se proponen:

- Desarrollar un sensor de fuerza integrado de 6 grados de libertad, con un buen comportamiento y de bajo coste.
- Ampliar el control de fuerza en brazos robots, a través del uso de metodologías adaptativas como *gain scheduling* y *model-reference adaptive control*.
- Combinar la propuesta de inclusión del control de fuerzas con otros tipos de alternativas para el mecanizado robótico, como son el control de vibraciones, el análisis de redundancia y la optimización de la postura del robot.
- Comparar el desarrollo del control de fuerza dentro de un robot, con el implementado mediante el diseño de un efector final con control de fuerza propio.
- Explorar los resultados de mecanizado robótico al ampliar el rango de condiciones de corte y materiales. Esto permite comprobar el funcionamiento del mecanizado robótico en rangos más amplios de trabajo.
- Analizar el desempeño del control de fuerza cuando los robots colaborativos trabajan al nivel de exigencia (fuerza) máximo.

Capítulo 9
Referencias bibliográficas

En este apartado se muestran las referencias utilizadas en la presente tesis. A excepción de las referencias bibliográficas utilizadas en los capítulos de los artículos publicados, capítulos del 2 al 6, ya que cada artículo posee sus propias referencias.

1. International Federation of Robotics, I. Executive Summary World Robotics 2020 Industrial Robots. *World Robot. Rep.* **2020**, 15–24.
2. International Federation of Robotics IFR forecast: 1.7 million new robots to transform the world´s factories by 2020 Available online: https://ifr.org/ifr-press-releases/news/ifr-forecast-1.7-million-new-robots-to-transform-the-worlds-factories-by-20 (accessed on Feb 15, 2019).
3. Top Trends Robotics 2020 - International Federation of Robotics Available online: https://ifr.org/ifr-press-releases/news/top-trends-robotics-2020 (accessed on May 16, 2020).
4. Janez, G.; Timi, K.; Karl, G.; Miran, B. Accuracy improvement of robotic machining based on robot's structural properties. *Int. J. Adv. Manuf. Technol.* **2020**, *108*, 1309–1329, doi:10.1007/s00170-020-05438-z.
5. Iglesias, I.; Sebastián, M. a.; Ares, J.E. Overview of the State of Robotic Machining: Current Situation and Future Potential. *Procedia Eng.* **2015**, *132*, 911–917, doi:10.1016/j.proeng.2015.12.577.

6. Chen, Y.; Dong, F. Robot machining: recent development and future research issues. *Int. J. Adv. Manuf. Technol.* **2013**, *66*, 1489–1497, doi:10.1007/s00170-012-4433-4.
7. Klimchik, A.; Ambiehl, A.; Garnier, S.; Furet, B.; Pashkevich, A. Efficiency evaluation of robots in machining applications using industrial performance measure. *Robot. Comput. Integr. Manuf.* **2017**, *48*, 12–29, doi:10.1016/j.rcim.2016.12.005.
8. Hui Zhang; Jianjun Wang; Zhang, G.; Zhongxue Gan; Zengxi Pan; Hongliang Cui; Zhenqi Zhu Machining with flexible manipulator: toward improving robotic machining performance. In Proceedings of the Proceedings, 2005 IEEE/ASME International Conference on Advanced Intelligent Mechatronics.; IEEE, 2005; pp. 1127–1132.
9. Cen, L.; Melkote, S.N. Effect of Robot Dynamics on the Machining Forces in Robotic Milling. *Procedia Manuf.* **2017**, *10*, 486–496, doi:10.1016/j.promfg.2017.07.034.
10. Caro, S.; Dumas, C.; Garnier, S.; Furet, B. Workpiece placement optimization for machining operations with a KUKA KR270-2 robot. In Proceedings of the 2013 IEEE International Conference on Robotics and Automation; IEEE, 2013; pp. 2921–2926.
11. Pan, Z.; Zhang, H. Robotic machining from programming to process control: a complete solution by force control. *Ind. Robot An Int. J.* **2008**, *35*, 400–409, doi:10.1108/01439910810893572.
12. Guo, Y.; Dong, H.; Ke, Y. Stiffness-oriented posture optimization in robotic machining applications. *Robot. Comput. Integr. Manuf.* **2015**, *35*, 69–76, doi:10.1016/j.rcim.2015.02.006.
13. Huynh, H.N.; Assadi, H.; Rivière-Lorphèvre, E.; Verlinden, O.; Ahmadi, K. Modelling the dynamics of industrial robots for milling operations. *Robot. Comput. Integr. Manuf.* **2020**, *61*, 101852, doi:10.1016/j.rcim.2019.101852.
14. Sánchez, I.I.; Ares, J.E.; Gaya, C.G.; Prieto, V.R. A new approach to the consideration and analysis of critical factors in robotic machining. *Appl. Sci.* **2020**, *10*, 1–18, doi:10.3390/app10248885.
15. Brito, T.; Queiroz, J.; Piardi, L.; Fernandes, L.A.; Lima, J.; Leitão, P. A Machine Learning Approach for Collaborative Robot Smart Manufacturing Inspection

for Quality Control Systems. *Procedia Manuf.* **2020**, *51*, 11–18, doi:10.1016/j.promfg.2020.10.003.

16. Galin, R.; Meshcheryakov, R.; Kamesheva, S.; Samoshina, A. Cobots and the benefits of their implementation in intelligent manufacturing. *IOP Conf. Ser. Mater. Sci. Eng.* **2020**, *862*, doi:10.1088/1757-899X/862/3/032075.
17. El Zaatari, S.; Marei, M.; Li, W.; Usman, Z. Cobot programming for collaborative industrial tasks: An overview. *Rob. Auton. Syst.* **2019**, *116*, 162–180, doi:10.1016/j.robot.2019.03.003.
18. Sousa, V.; Silva, F.J.G.; Fecheira, J.S.; Lopes, H.M.; Martinho, R.P.; Casais, R.B. Accessing the cutting forces in machining processes: An overview. *Procedia Manuf.* **2020**, *51*, 787–794, doi:10.1016/j.promfg.2020.10.110.
19. Makris, S. *Cooperating robots for flexible manufacturing*; 2021; ISBN 9783030515904.
20. Cvitanic, T.; Nguyen, V.; Melkote, S.N. Pose optimization in robotic machining using static and dynamic stiffness models. *Robot. Comput. Integr. Manuf.* **2020**, *66*, 101992, doi:10.1016/j.rcim.2020.101992.
21. Wu, K.; Kuhlenkoetter, B. Experimental analysis of the dynamic stiffness in industrial robots. *Appl. Sci.* **2020**, *10*, 1–14, doi:10.3390/app10238332.
22. Mousavi, S.; Gagnol, V.; Bouzgarrou, B.C.; Ray, P. Stability optimization in robotic milling through the control of functional redundancies. *Robot. Comput. Integr. Manuf.* **2018**, *50*, 181–192, doi:10.1016/j.rcim.2017.09.004.
23. Leonesio, M.; Villagrossi, E.; Beschi, M.; Marini, A.; Bianchi, G.; Pedrocchi, N.; Tosatti, L.M.; Grechishnikov, V.; Ilyukhin, Y.; Isaev, A. Vibration Analysis of Robotic Milling Tasks. *Procedia CIRP* **2018**, *67*, 262–267, doi:10.1016/j.procir.2017.12.210.
24. Tyapin, I.; Hovland, G.; Kosonen, P.; Linna, T. Identification of a static tool force model for robotic face milling. In Proceedings of the 2014 IEEE/ASME 10th International Conference on Mechatronic and Embedded Systems and Applications (MESA); IEEE, 2014; pp. 1–6.
25. Lehmann, C.; Halbauer, M.; Euhus, D.; Overbeck, D. Milling with industrial robots: Strategies to reduce and compensate process force induced accuracy influences. In Proceedings of the Proceedings of 2012 IEEE 17th International

Conference on Emerging Technologies & Factory Automation (ETFA 2012); IEEE, 2012; pp. 1–4.

26. Zhu, D.; Feng, X.; Xu, X.; Yang, Z.; Li, W.; Yan, S.; Ding, H. Robotic grinding of complex components: A step towards efficient and intelligent machining – challenges, solutions, and applications. *Robot. Comput. Integr. Manuf.* **2020**, *65*, 101908, doi:10.1016/j.rcim.2019.101908.
27. Torres, R.; Gonzalez, S.; Elguea, I.; Aginaga, J.; Iriarte, X.; Agirre, N.; Inziarte, I. Robotic assisted thin-wall machining with a collaborative robot. *IEEE Int. Conf. Autom. Sci. Eng.* **2020**, *2020-Augus*, 1505–1508, doi:10.1109/CASE48305.2020.9216864.
28. Rosa, D.G.G.; Feiteira, J.F.S.; Lopes, A.M.; de Abreu, P.A.F. Analysis and implementation of a force control strategy for drilling operations with an industrial robot. *J. Brazilian Soc. Mech. Sci. Eng.* **2017**, *39*, 4749–4756, doi:10.1007/s40430-017-0913-7.
29. Perez, R.; Gutierrez Rubert, S.C.; Zotovic, R. A Study on Robot Arm Machining: Advance and Future Challenges. In *29TH DAAAM INTERNATIONAL SYMPOSIUM ON INTELLIGENT MANUFACTURING AND AUTOMATION*; 2018; pp. 0931–0940.
30. Pérez Ubeda, R.; Gutiérrez Rubert, S.C.; Zotovic Stanisic, R.; Perles Ivars, Á. Design and Manufacturing of an Ultra-Low-Cost Custom Torque Sensor for Robotics. *Sensors* **2018**, *18*, 1786, doi:10.3390/s18061786.
31. Perez-Ubeda, R.; Gutierrez, S.C.; Zotovic, R.; Lluch-Cerezo, J. Study of the application of a collaborative robot for machining tasks. *Procedia Manuf.* **2019**, *41*, 867–874, doi:10.1016/j.promfg.2019.10.009.
32. Pérez-Ubeda, R.; Zotovic-Stanisic, R.; Gutiérrez, S.C. Force Control Improvement in Collaborative Robots through Theory Analysis and Experimental Endorsement. *Appl. Sci.* **2020**, *10*, 4329, doi:10.3390/app10124329.
33. Ubeda, R.P.; Gutiérrez Rubert, S.C.; Stanisic, R.Z.; Perles Ivars, Á. Behavioural Study of the Force Control Loop Used in a Collaborative Robot for Sanding Materials. *Materials (Basel).* **2020**, *14*, 67, doi:10.3390/ma14010067.